PNL--7581

DE92 041231

SUMO--SYSTEM PERFORMANCE ASSESSMENT FOR A HIGH-LEVEL NUCLEAR WASTE REPOSITORY: MATHEMATICAL MODELS

P. W. Eslinger
T. B. Miley
D. W. Engel
P. J. Chamberlain II

September 1992

Prepared for
the U.S. Department of Energy
under Contract DE-AC06-76RLO 1830

Pacific Northwest Laboratory
Richland, Washington 99352

EXECUTIVE SUMMARY

Following completion of the preliminary risk assessment of the potential Yucca Mountain Site by Pacific Northwest Laboratory (PNL) in 1988, the Office of Civilian Radioactive Waste Management (OCRWM) of the U.S. Department of Energy (DOE) requested the Performance Assessment Scientific Support (PASS) Program at PNL to develop an integrated system model and computer code that provides performance and risk assessment analysis capabilities for a potential high-level nuclear waste repository. The system model that has been developed addresses the cumulative radionuclide release criteria established by the U.S. Environmental Protection Agency (EPA) and estimates population risks in terms of dose to humans. The system model embodied in the SUMO (System Unsaturated Model) code will also allow benchmarking of other models being developed for the Yucca Mountain Project.

The system model has three natural divisions: 1) source term, 2) far-field transport, and 3) dose to humans. This document gives a detailed description of the mathematics of each of these three divisions. Each of the governing equations employed is based on modeling assumptions that are widely accepted within the scientific community.

GLOSSARY

ADI	alternating direction implicit method
BNL	Brookhaven National Laboratory
CCDF	complementary cumulative distribution function
CDF	cumulative distribution function
DOE	U.S. Department of Energy
EBS	engineered barrier system
EPA	U.S. Environmental Protection Agency
FSR	feedback shift register
LWR	light water reactor
NPI	nodal point integration
NRC	U.S. Nuclear Regulatory Commission
NWPA	Nuclear Waste Policy Act of 1982
OCRWM	Office of Civilian Radioactive Waste Management
PASS	Performance Assessment Scientific Support
PDF	probability density function
PIT	probability integral transform
PNL	Pacific Northwest Laboratory
PSOR	point successive over-relaxation method
SCC	stress corrosion cracking
SUMO	System Unsaturated Model

CONTENTS

FIGURES

TABLES

1.0 INTRODUCTION

The commercial generation of nuclear power produces spent nuclear fuel that must be disposed of safely. In addition, the reprocessing of such spent fuel has resulted in some high-level nuclear waste. The placement of high-level radioactive wastes in mined repositories deep underground is considered to be a disposal method that would effectively isolate these wastes from the environment for long periods of time. In the United States, the U.S. Department of Energy (DOE) has been assigned the responsibility and, within certain limitations, the authority to implement the provisions of the Nuclear Waste Policy Act (NWPA) of 1982, as amended in 1987, which provides for the development of a mined geologic repository. Yucca Mountain, Nevada, is currently being evaluated as a potential repository site. However, before a repository can be used for the disposal of nuclear waste, it must be licensed by the U.S. Nuclear Regulatory Commission (NRC) and meet standards established by the U.S. Environmental Protection Agency (EPA).

The DOE, through the Office of Civilian Radioactive Waste Management (OCRWM), is responsible for implementing the repository requirements of the NWPA, as amended. Because NRC and EPA regulations base the final determination of a site's suitability on a calculational projection of its performance into the distant future, DOE must ensure that its recommendations and decisions are based on technically defensible predictions of the performance of any repository. The Performance Assessment Scientific Support (PASS) Program at Pacific Northwest Laboratory (PNL)[a] assists OCRWM in its performance-assessment-related responsibilities.

1.1 PURPOSE AND SCOPE

The PASS Program has developed an integrated system model and computer code (SUMO, for System Unsaturated MOdel) to conduct performance and risk assessment analyses, and to provide a benchmark for other system codes being

---

(a) The Pacific Northwest Laboratory is operated by Battelle Memorial Institute for the U.S. Department of Energy, under Contract DE-AC06-76RL0 1830.

developed for the Yucca Mountain Site Characterization Project. The SUMO code is an outgrowth of the preliminary Yucca Mountain risk assessment analysis that was completed by the PASS Program in 1988. The system model consists of a number of component models embedded in a stochastic (Monte Carlo) framework that allows probabilistic estimation of releases to the accessible environment and of dose and health effects in a form consistent with current EPA criteria expressed in terms of a complementary cumulative distribution function. This document describes the mathematical models chosen as components of the system model.

1.2 REPORT ORGANIZATION

This report is organized into six sections. This section contains background material and an introduction to the rest of the document. Section 2.0 presents the modeling philosophy behind the development of SUMO and identifies the performance measures that can be evaluated with SUMO. Among the major performance measures that can be evaluated with SUMO are the EPA criteria for cumulative releases to the accessible environment (40 CFR 191).

Models governing generation of a source term for radionuclide release from the repository's Engineered Barrier System (EBS) are described in Section 3.0. Processes considered include degradation and failure of waste containers and release of radionuclides from breached waste containers. The approach taken to get a release term for the entire EBS is to model individual waste containers in detail and then to add the releases from containers that fail at random times.

A far-field transport model is described in Section 4.0. The far-field transport model employs the integrated finite-difference solution method to compute a hydrologic flow field and the transport of radionuclides through the flow field. A special feature of the transport model is that the model domain can be defined in one, two, or three dimensions.

Section 5.0 presents a dose model tailored to handle long-term releases of radionuclides to the environment. Doses can be computed for either a maximally exposed individual or a distributed population and are presented in terms of the cumulative effective dose equivalent in units of person-rem.

Finally, Section 6.0 describes the statistical algorithms employed in the SUMO code. The SUMO code implements a Monte Carlo framework to provide probabilistic estimates of cumulative radionuclide releases to the accessible environment.

2.0 MODELING PHILOSOPHY

The SUMO code was designed to provide answers to many questions about repository performance. For instance, it can be used to investigate the performance of a proposed repository relative to the cumulative radionuclide release limits established by the EPA (40 CFR 191). It also can be used to predict the risk posed by the repository in terms of population health effects. The code can also address differences in conceptual models, such as dimensionality of the model domain and major geologic fracture networks.

2.1 SOLUTIONS PROVIDED BY THE SYSTEM MODEL

The following specific solutions are available from the SUMO code as a function of time:

- fractional release rate of radionuclides from the EBS
- radionuclide flux across a boundary
- cumulative radionuclide flux across a boundary
- radionuclide concentration at a location
- individual or population dose.

Modeling requirements to implement each of these solutions are discussed in subsequent sections of this document.

The EPA cumulative radionuclide release criteria form the basis of the requirement for the cumulative radionuclide flux solution. The radionuclide flux solution is included for two reasons: first, it is an intermediate step in numerically computing the cumulative flux and, second, the dose model can then use the radionuclide flux and water flow rate to compute concentrations for dose considerations. The EPA's criteria also require estimation of the probability that releases will not exceed specified levels. Running the SUMO code in a Monte Carlo mode provides the framework to allow the expression of cumulative radionuclide flux reaching the accessible environment as a complementary cumulative distribution function (CCDF).

The dose solution allows computation of estimates of health effects (i.e., risk of the repository) in the surrounding population caused by releases from the repository subsequent to waste emplacement. The dosimetry models chosen require concentrations of radioactive contaminants to evaluate health effects. This requirement couples nicely with the implementation of the mass transport model, which is based on a governing differential equation expressed in terms of concentration.

Federal regulations (10 CFR 60) have imposed a performance requirement in the form of an upper bound on the allowable radionuclide flux rate, on a nuclide-by-nuclide basis, from the EBS of a repository. The source-term model incorporated in the SUMO code is the model used in AREST code (Liebetrau et al. 1987), which was designed for comparison with the NRC release-rate criteria. Because of modeling complexity and computer code size, output from the EBS model in the SUMO code is not intended to be used for comparison with the regulatory criteria; instead, it is used as a source term for further modeling. Users are directed to the parent AREST code when considering only releases from the EBS.

2.2 MODEL SOURCES

The SUMO code was formed by integrating three existing computer codes. The three codes perform distinct functions: 1) estimating releases from the repository's EBS, 2) conducting hydrologic modeling and modeling of transport of radionuclides, and 3) calculating dose to humans.

The parent code of the module for estimating source-terms was AREST (Liebetrau et al. 1987), which was developed for DOE by PNL. The parent code of the hydrologic and mass transport module was PORFLO-3 (Runchal and Sagar 1989), which was developed for DOE by Westinghouse Hanford Company and further enhanced by PNL. Finally, the parent code of the dose estimation was DITTY (Napier et al. 1988), a submodel of the GENII software system, which was also developed for DOE by PNL.

Integrating the three stand-alone codes into the SUMO code required substantial modification of many routines to resolve conflicting names for variables, input structures, and so on. Because many of the original modules

were extensively modified, any verification issues must be addressed by the SUMO developers rather than the developers of the parent codes. Enhancements to the parent codes will not necessarily be included in the SUMO code.

2.3 STOCHASTIC FRAMEWORK

The SUMO code implements a Monte Carlo framework to provide probabilistic estimates of cumulative radionuclide releases to the accessible environment. The distribution of these release estimates can then be presented as a CCDF if desired. To achieve the ability to generate a CCDF for an output performance measure, many input variables can be declared to be stochastic, with values being generated from specified statistical distributions. The only general restriction is that no time-dependent variables can be declared stochastic. A functional flow diagram for the SUMO code is shown in Figure 2.1.

Random numbers are generated in the SUMO code to obtain information about the distribution of a function of one or more (random) elements. Consider, for example, the equation for the steady-state rate of release of a radionuclide from an individual waste package, assuming a diffusion-controlled transport model. The release rate can be written as

$$R_i = 4\pi D_i \epsilon r_o C_i \qquad (2.1)$$

where R_i is the release rate of the ith radionuclide. Random selection of one or more of the terms on the right-hand side of this equation will cause the release rate to be random. Assume that the diffusion coefficient D_i is a random variable that can be described by some statistical distribution. Assume also that fixed values can be obtained for the other terms in the equation for R_i. Statistical simulation of the release rate thus involves repeated random selection of a value for D_i from the specified distribution, each time computing the release rate at the fixed value of D_i obtained from the selection. The distribution of these outcomes can then be expressed as an "empirical" cumulative distribution function (CDF) and, given a sufficiently

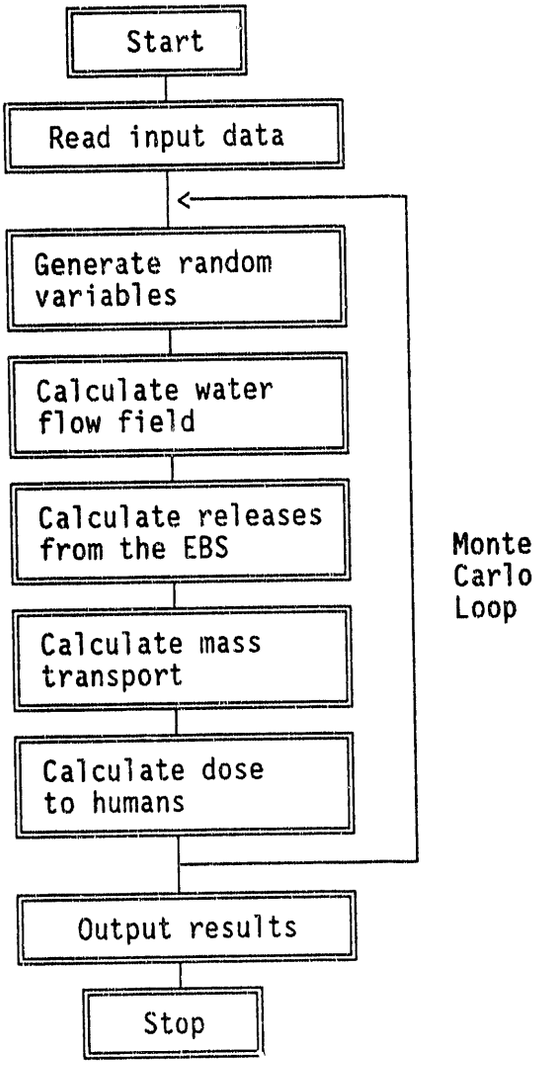

FIGURE 2.1. Functional Flow of the SUMO Computer Code

large number of replications, probability statements about the occurrence of the release rate in a given interval can be obtained. In addition, other terms in the release-rate equation may be randomized concurrently.

Probabilistic assignment of values to variables that are random increases the realism of a modeling effort. Section 6.0 of this report deals with implementation algorithms. It does not, however, address choosing appropriate statistical distributions based on field data or expert opinion. The reader is referred to statistical textbooks (e.g., Mood et al. 1974; Ferguson

1967) for techniques for choosing a statistical distribution given field data. A survey on the use of expert opinion to generate statistical distributions in relation to nuclear waste disposal has been done by Bonano et al. (1990).

3.0 SOURCE-TERM MODEL

The source-term model provides estimates of releases from the repository's EBS that are then used as source terms for the far-field transport model. Releases from the EBS depend on factors such as thermal loading, groundwater chemistry and fluxes, waste container material, and waste form; as a result, the SUMO code is necessarily complex.

The source-term model in the SUMO code starts with the simplifying assumption that waste packages can be treated independently, so that interactions among adjacent waste packages need not be modeled. Thus there are two major steps in the modeling of EBS releases: 1) determining when individual waste containers fail and 2) computing radionuclide releases from failed individual waste containers. All radionuclides released from the EBS are assumed to dissolve in groundwater and then move through the liquid phase. Even though recent studies of gas-phase releases of some nuclides have been published (e.g., Amter et al. 1988), the current version of the SUMO code does not consider gas-phase release and migration. However, in a regulatory setting, contaminants may move in the gas phase in concentrations sufficient to warrant future consideration.

The release models described in this section are approximate analytical solutions to the respective governing equations. Although these equations can be evaluated more quickly than numerical solutions, the equations relate only to very specific governing equations, and their usefulness is restricted accordingly. Alternatively, numerical solution procedures are often more number-intensive but they can easily accommodate modifications of governing equations, boundary conditions, and other model features. For this reason, the next version of the SUMO code will contain numerical rather than analytical solutions for release rates. The current release rate model considers chain decay only in the source-term inventory. Future versions of the SUMO code will reflect chain decays more generally.

3.1 WASTE FORM INVENTORY

On its removal from a nuclear reactor, spent fuel contains more than 100 radionuclides. Radionuclide half-life and inventory considerations mean that this number can be greatly reduced to a small set of key radionuclides that must be studied in detail. Nevertheless, the source-term model must be able to track the radionuclide inventories of the waste form as they change over time as a result of radioactive decay. To model such inventory changes in the waste form, the Bateman equations (Bateman 1910) are used. In addition, when all of the inventory of a radionuclide has been released from the waste package, the source-term contribution terminates. That is, when the sum of the releases at the host rock boundary exceeds the exhaustion inventory, the release rate is set to zero. (The exhaustion inventory is defined in the SUMO code as the inventory at 1000 years.)

3.2 WASTE-FORM RELEASE MODELS FOR SINGLE CONTAINERS

The EBS release model implemented in the SUMO code is a simplified version of the model implemented in the parent code, AREST (Liebetrau et al. 1987; Reimus et al. 1988). The implementation in the SUMO code allows a choice of three possible EBS release models: 1) a steady-state advective model, 2) a steady-state diffusive model, and 3) a transient diffusive model. In addition, either congruent or incongruent release of radionuclides from the waste form can be accommodated. Except for diffusion-limited release at very early times and at locations close to the surface of the waste form, the steady-state release rates are greater than the transient release rates and therefore more conservative. The computational effort to evaluate steady-state models is much less than that for transient models.

3.2.1 Steady-State Release Models for a Single Container

Both steady-state release models in the SUMO code are based on the assumption that each radionuclide is released from the waste form matrix congruently, at the rate of forward matrix dissolution multiplied by the fractional inventory of the nuclide in the matrix. If the release rate for a given radionuclide exceeds the rate of transport away from the waste package, then the radionuclide will reach its solubility limit at the surface of the

waste form, and the overall release rate will be governed by the transport rate. Inventory-limited release (e.g., spent-fuel gap inventory) is assumed to be solubility/transport-limited until the gap inventory is depleted.

The steady-state models include both diffusive and advective transport rates, with the release rate being set equal to the sum of these two rates for a given waste package, although it is recognized that diffusive and advective processes may not be independent of each other in a given physical setting. A coupled diffusive-advective model [e.g., that of Chambré et al. (1988)] could be implemented; however, the simpler approach of computing diffusive and advective terms separately has been followed for the SUMO code.

For the steady-state release model, release from the waste form through the failed container and backfill to the host rock is assumed to be instantaneous. Thus, there is no backfill inventory. (In fact, for the steady-state models, there is no backfill.)

3.2.1.1 Steady-State Advection Model

A general mass-balance equation for a radionuclide being released from the matrix of a waste form in contact with flowing groundwater (assuming negligible diffusive pathways) can be written as

$$V\, dC_i/dt = z_i(t) R_d A - R_{pi} - k_{ci} C_i + Q(t)\,(C_{io} - C_i) \qquad (3.1)$$

where V = control volume, m^3

C_i = concentration of radionuclide i at the surface of the waste form, g/m^3

t = time, yr

$z_i(t)$ = mass fraction of radionuclide i in waste form matrix

R_d = forward rate of matrix dissolution, $g/m^2 \cdot yr$

A = surface area of waste form in contact with water, m^2

R_{pi} = rate of precipitation of radionuclide i into alteration phases, g/yr

k_{ci} = first-order rate constant for the formation of colloids or other suspended matter containing radionuclide i, m^3/yr

$Q(t)$ = volumetric flow rate of water through control volume in contact with waste form, m^3/yr

C_{io} = concentration of radionuclide i in water approaching waste form, g/m^3.

In Equation (3.1), it is assumed that the release rate of each radionuclide from the matrix equals the forward rate of matrix dissolution multiplied by the mass fraction of the radionuclide in the matrix (i.e., congruent release is assumed). This assumption is implicit in this development of this release model.

The functional form of the forward rate of matrix dissolution, R_d, could vary, depending on the waste form and the mechanism of dissolution in the environment of interest. To date, spent-fuel dissolution experiments have not yielded results that support mechanistic model development, so a general form for the rate of dissolution of spent-fuel matrix of n constituents has been implemented in the source term model:

$$R_d = K_+ \left(1 - C_m/C_m^*\right) \prod_{i=1}^{n} \left[X_i\right]^{a_i} \qquad (3.2)$$

where k_+ = forward reaction rate constant, $g/m^2 \cdot yr\ (m^3/g)^{\sum_{i=1}^{n} a_i}$

$[x_i]$ = activity of constituent x in rate law, g/m^3

a_i = reaction order with respect to the n constituents

C_m = concentration of matrix constituent m that controls matrix dissolution rate (assumed to be UO_2 for spent fuel), g/m^3

C_m^* = arbitrary concentration of constituent m at which the forward rate of dissolution becomes zero, g/m^3.

The functional form of Equation (3.2) implies that the dissolution reaction is reversible and that the backward reaction rate is first order with respect to constituent m.

If the waste form is capable of equilibrating with the solution, then C_m^* in Equation (3.2) is set equal to C_{sm}, the saturation concentration of constituent m. In this case, the forward reaction will stop when $C_m = C_{sm}$, and the rate of precipitation of alteration phases for constituent m, R_{pm} [equivalent to R_{pi} in Equation (3.1)], will be zero because no alteration phases will form.

If the waste form is not capable of equilibrating with the solution, then the dissolution reaction will not be completely reversible. In this case, C_m^* in Equation (3.2) will be greater than C_{sm}, and the rate of matrix dissolution will remain nonzero even when the solution becomes saturated with respect to m (i.e., $C_m = C_{sm}$). (This situation is expected for both spent fuel and glass at Yucca Mountain because the primary matrix constituents, UO_2 and amorphous silica, are not thermodynamically stable in the unsaturated, oxidizing environment.) If the concentration of m has no effect on the forward dissolution rate, then C_m^* can be arbitrarily set to a very high value, forcing C_m/C_m^* to approach zero. In a closed system at steady state with no colloid formation, the rate of precipitation of m, R_{pm}, must be equal to the rate of dissolution, $z_m(t)R_dA$, to satisfy the mass balance. Before saturation, however, R_{pm} is assumed to be zero.

At steady state ($dC_i/dt = 0$), and assuming that C_{io} is equal to zero, Equation (3.1) becomes

$$0 = z_i(t)R_dA - R_{pi} - k_{ci}C_i - Q(t)C_i \qquad (3.3)$$

Equation (3.3) assumes that Q(t) and $z_i(t)$ are constants. Radioactive decay, however, will cause $z_i(t)$ to vary with time. Thus Equation (3.3) is only an approximation and is likely to give reasonable results only if $z_i(t)$ varies slowly with time. A steady-state mass balance on colloidal species yields

$$0 = k_{ci}C_i - Q(t)C_{ci} \qquad (3.4)$$

where C_{ci} is the concentration of radionuclide i in colloidal form, g/m^3. Using Equation (3.4), we can rewrite Equation (3.3) as follows:

$$0 = z_i(t)R_dA - R_{pi} - Q(t)(C_i + C_{ci}) \quad (3.5)$$

The release rate of radionuclide i is given by the last term in Equation (3.5).

3.2.1.2 Steady-State Diffusion Model

If the flow rate of groundwater, Q(t), is exceedingly low but the waste form remains in contact with a continuous diffusive pathway of water, diffusion could control the rate of radionuclide release from the waste package. To assess this possibility, an expression for steady-state diffusional release from a spherical waste form is used, in which it is assumed that at an infinite distance from the waste form the concentration of the diffusing constituent is zero (Chambré et al. 1985):

$$\text{Release Rate} = 4\pi D_i \epsilon r_o C_i \quad (3.6)$$

where D_i is the diffusion coefficient of radionuclide i, m^2/yr; ϵ is the porosity; and r_o is the effective radius of waste form, m. A spherical geometry is assumed because it results in higher, and therefore more conservative, release rates than do planar or cylindrical geometries.

Several observations can be made based on Equations (3.1), (3.5), and (3.6). When $C_i < C_{si}$ (the saturation concentration of i), it is apparent from Equation (3.5) that the release rate will be equal to $z_i(t)R_dA$ (that is, $R_{pi} = 0$). Alternatively, when $C_i = C_{si}$, the release rate will be equal to $Q(t)(C_{si} + C_{ci}^*)$, where C_{ci}^* is the concentration of nuclide i in colloidal form when $C_i = C_{si}$ (a hypothetically measurable quantity). This analysis suggests a simple test to determine whether the release rate for a given radionuclide is controlled by the forward matrix dissolution rate or the advective transport rate:

- If $z_i(t)R_dA < Q(t)(C_{si} + C_{ci}^*)$, then the matrix dissolution rate controls release, and the dominant release rate term is $z_i(t)R_dA$.

- If $z_i(t)R_dA > Q(t)(C_{si} + C_{ci}^*)$, then the advective transport rate controls release, and the dominant release rate term is $Q(t)(C_{si} + C_{ci}^*)$.

When colloidal species are present, Equation (3.6) must be modified to reflect the diffusion of colloidal species as well as dissolved species. Also, in unsaturated media, only a fraction of the waste form surface may actually be in contact with a diffusive water pathway. Equation (3.6) is therefore modified as follows:

$$\text{Release Rate} = 4\pi\epsilon r_o(A_d/A_t)(D_iC_i + D_{ci}C_{ci}) \qquad (3.7)$$

where A_d = area of waste form surface in contact with diffusive pathway, m^2

A_t = total surface area of surface of waste form, m^2

D_{ci} = effective diffusion coefficient for colloidal species containing radionuclide i, m^2/yr

C_{ci} = concentration of radionuclide i in colloidal form at waste form surface, g/m^3.

The right side of Equation (3.7) can be substituted for the term $Q(t)(C_i + C_{ci})$ in Equation (3.5) to evaluate whether radionuclide release under conditions of low flow rate is controlled by the matrix dissolution rate or the diffusive transport rate. A test analogous to the test for advective transport is devised:

- If $z_i(t)R_dA < 4\pi\epsilon r_o(A_d/A_t)(D_iC_{si} + D_{ci}C_{ci}^*)$, then the matrix dissolution rate controls release, and the release rate is $z_i(t)R_dA$.
- If $z_i(t)R_dA > 4\pi\epsilon r_o(A_d/A_t)(D_iC_{si} + D_{ci}C_{ci}^*)$, then the diffusive mass transport rate controls release, and the release rate is $4\pi\epsilon r_o(A_d/A_t)(D_iC_{si} + D_{ci}C_{ci}^*)$.

If either of these tests indicates that the matrix dissolution rate controls release, then matrix dissolution is the release-controlling process. If both tests indicate that the matrix dissolution rate does not control the release rate, then the release rate must be controlled by either advection or diffusion. To determine whether advection or diffusion dominates release, the following test can be applied:

- If $Q(t)(C_{si} + C_{ci}^*) >> 4\pi\epsilon r_o(A_d/A_t)(D_i C_{si} + D_{ci} C_{ci}^*)$, then advective mass transport controls release, and the release rate is $Q(t)(C_{si} + C_{ci}^*)$.
- If $Q(t)(C_{si} + C_{ci}^*) << 4\pi\epsilon r_o(A_d/A_t)(D_i C_{si} + D_{ci} C_{ci}^*)$, then diffusive mass transport controls release, and the release rate is $4\pi\epsilon r_o(A_d/A_t)(D_i C_{si} + D_{ci} C_{ci}^*)$.

This sequence of tests can be applied for each radionuclide to determine whether there is a dominant steady-state release rate expression. If neither model is dominant, the releases from both models are added together. The possible situations are summarized in Table 3.1.

3.2.2 Transient Mass-Transfer Models for a Single Container

Two principal transient mass-transfer models are used in the EBS release model; these are based on solubility-limited and inventory-limited releases. Subsection 3.2.2.1 describes the analytical solutions used for calculating time-dependent, solubility-limited fractional release rates from both the waste form and waste package. The emphasis of this model is its application to the release of radionuclides from the UO_2 matrix and, potentially, from the

TABLE 3.1. Summary of Logic for Release-Rate Expressions

Relative Rates[(a)]				
M	C	D	Mechanism for Control	Dominant Release Expression
1	2	3	Matrix Dissolution	$z_i(t)R_dA$
1	3	2	Matrix Dissolution	$z_i(t)R_dA$
2	1	3	Matrix Dissolution	$z_i(t)R_dA$
2	3	1	Matrix Dissolution	$z_i(t)R_dA$
3	1	2	Diffusion	$4\pi\epsilon r_o(A_d/A_t)(D_i C_{si} + D_{ci} C_{ci}^*)$
3	2	1	Advection	$Q(t)(C_{si} + C_{ci}^*)$

(a) M = matrix dissolution; C = advection; D = diffusion; 1 = slowest; 3 = fastest.

uniform corrosion of cladding. The justifications for applying a solubility-controlled mass-transfer model to UO_2 and cladding have been made by Liebetrau et al. (1987, Appendix D). Here we will discuss solubility control imposed by separate radionuclide-bearing solids (i.e., incongruent or apparently incongruent dissolution) and solubility control imposed by the congruent dissolution of the primary waste form (e.g., UO_2).

Section 3.2.2.2 presents a mass-transfer equation for calculating the time-dependent, fractional release rates for highly soluble radionuclides from the waste package. This model assumes rapid release of a fixed inventory of such nuclides into a void volume within a failed container and subsequent diffusional transport through the waste package and into the surrounding host rock. The inventory-limited model is applied to gap/grain boundary sources and cladding sources of radionuclides within the spent fuel.

3.2.2.1 Solubility-Limited Model for Matrix Release

The following equations have been derived by Chambré, Pigford, and their coworkers (Chambré et al. 1985) to describe the time-dependent, diffusive mass transport of a radionuclide from a waste package. The waste package geometry used in the SUMO code is based on a spherical waste form, equal in area to the planned actual cylindrical waste form container, that is surrounded by a spherical porous shell, typically a packing material. Both the waste form and packing (or analogous material) are embedded in a rock that extends infinitely in all directions. It is assumed that there are no radioactive-decay precursors (i.e., that the transport time from the waste package to the host rock is short enough to allow neglect of chain decay considerations during the transit time) and that each radionuclide is transported separately. Chain decay is modeled for the inventory remaining in the waste form. The governing equations used to describe the mass transfer of a radionuclide are

$$\frac{\partial C_1}{\partial t} = D_1 \nabla^2 C_1 \qquad R_\emptyset < r < R_1 \ , \ t > 0 \qquad (3.8)$$

$$\frac{\partial C_2}{\partial t} = D_2 \nabla^2 C_2 \qquad R_1 < r < \infty,\ t > 0 \qquad (3.9)$$

$$C_1(r,0) = 0 \qquad R_\emptyset \leq r \leq R_1 \qquad (3.10a)$$

$$C_2(r,0) = 0 \qquad R_1 \leq r < \infty \qquad (3.10b)$$

$$C_1(R_\emptyset,t) = C_s \qquad t \geq 0 \qquad (3.11)$$

$$C_1(R_1,t) = C_2(R_1,t) \qquad t \geq 0 \qquad (3.12)$$

$$\epsilon_1 \frac{\partial C_1}{\partial r} = \epsilon_2 \frac{\partial C_2}{\partial r} \qquad r = R_1,\ t \geq 0 \qquad (3.13)$$

$$C_2(\infty,t) = 0 \qquad t \geq 0 \qquad (3.14)$$

$$\dot{M}(r,t) = 4\pi r^2 \left(-\epsilon_1 D_f \frac{\partial C_1(r,t)}{\partial r} \right) \qquad R_\emptyset \leq r \leq R_1,\ t \geq 0 \qquad (3.15)$$

where C_1 = radionuclide concentration in the backfill region, g/cm^3

t = time after permanent closure of the repository, yr

D_f = diffusion coefficient in the water, cm^2/sec

$R_\emptyset$ = radius of the waste form, cm

r = radial distance from the center of the waste form, cm

R_1 = outer edge of packing radius, cm

C_2 = radionuclide concentration in the host rock region, g/cm^3

C_s = concentration at the surface of the waste form, g/cm^3

ϵ_1 = porosity of the packing, dimensionless

ϵ_2 = porosity of the host rock, dimensionless

$\dot{M}(r,t)$ = mass transfer rate, g/sec

$C(r,t)$ = time-dependent concentration of a radionuclide within the waste package, g/cm^3.

The first equation yields the mass-transfer rate

$$\dot{M}(r,t) = 4\pi(\epsilon_1 D_f R_\emptyset r C_s)\ 1/\{r[1 + \gamma(R_\emptyset/R_1)]\} \int_\circ^\infty [I_1 I_2 dn] \qquad (3.16)$$

where $\gamma = (\epsilon_1 - \epsilon_2)/\epsilon_2$

$D_1 = D_f/K_1$

K_1 = retardation coefficient in the packing, dimensionless

$D_2 = Df/K_2$

K_2 = retardation coefficient in the host rock, dimensionless.

n = variable of integration

λ = radioactive decay constant, 1/yr = ln 2/ half-life

$\beta = (K_1/K_2)^{1/2}$

$b = R_1 - R_\emptyset$ = packing thickness, cm

$a = (\epsilon_1 - \epsilon_2)/R_1$

for $R_\emptyset \leq r \leq R_1$, $t > 0$, where r is the radial distance from the center of the waste form and t is the time after permanent closure of the repository. The second equation yields the time-dependent concentration of a radionuclide within the waste package

$$C(r,t) = C_s(f(r) + \int_\emptyset^\infty [I_1 I(r,n)\ dn]) \qquad (3.17)$$

also for $R_\emptyset \leq r \leq R_1$, and $t > 0$. Other terms in Equations (3.16) and (3.17) are defined as

$$I_1 = \frac{1}{1 + \frac{D_1 n^2}{\lambda}} + \frac{\exp\ (-D_1 t n^2 - \lambda t)}{1 + \frac{\lambda}{D_1 n^2}} \qquad (3.18)$$

$$I_2 = \frac{2\epsilon_1 \epsilon_2 \beta_n}{\pi} \frac{n\{\cos(n[r - R_0\ ]) - \sin(n[r - R_0])/r\}}{H(n)} \qquad (3.19)$$

$$f(r) = \left(\frac{R_\emptyset}{r}\right)\left[\frac{1 + \gamma(r/R_1)}{1 + \gamma(R_0/R_1)}\right] \qquad (3.20)$$

$$I(r,n) = \left(\frac{-2R_\emptyset \epsilon_1 \epsilon_2 \beta}{\pi r}\right)\left[\frac{n\sin(n[r - R_\emptyset])}{H(n)}\right] \qquad (3.21)$$

$$H(n) = [\epsilon_1 n\cos(nb) + a\sin(nb)]^2 + \beta[\epsilon_2 n\sin(nb)]^2 \qquad (3.22)$$

Equations (3.16) and (3.17) can be solved at various locations within the waste package, such as the surface of the waste form ($r = R_\emptyset$) and the waste package boundary ($r = R_1$). Unfortunately, the integral in Equation (3.16) is highly oscillatory, resulting in singularities in the calculations. The present technique for handling the integral is to accumulate the area under the curve, using a small step size, as n goes from zero to infinity. If the nuclide of concern is stable (λ=0), then I_1 of the integrals in Equations (3.16) and (3.17) reduces to

$$I_1 = \exp(-D_1 t n^2) \qquad (3.23)$$

For the purposes of discussion, Equation (3.16) can be written in a more streamlined notation

$$\dot{M}(r,t) = 4\pi\epsilon_1 D_f R_\emptyset r C_s \psi(r,t) \qquad (3.24)$$

where $\psi(r,t)$ is the radionuclide-specific mass-transfer function

$$\psi(r,t) = \frac{1}{r\left[1 + \gamma\left(\frac{R_\emptyset}{R_1}\right)\right]} - \int_\emptyset^\infty [I_1 I_2 dn] \qquad R_\emptyset \le r \le R_1 \tag{3.25}$$

The mass-transfer rate, $\dot{M}(r,t)$, is related to the fractional release rate, $\dot{f}(r,t)$, as defined by 10 CFR 60, by the relationship

$$\dot{f}(r,t) = \frac{\dot{M}(r,t)}{I(1000)} \tag{3.26}$$

where I(1000) is the inventory of a given radionuclide 1000 years after permanent closure of the repository. A related parameter, the instantaneous fraction release rate, $\dot{F}(r,t)$, can also be defined

$$\dot{F}(r,t) = \frac{\dot{M}(r,t)}{I(t)} \tag{3.27}$$

$$t = t_r + t_f \tag{3.28}$$

where I(t) is the time-dependent inventory of a given radionuclide at time t, t_r is the time from containment failure to time t, and t_f is the time between repository closure and containment failure. If ingrowth resulting from chain decay is ignored, the time-dependent inventory can be related to the 1000-year inventory by

$$I(t) = I(1000)\ \exp[\lambda(1000-t)] \tag{3.29}$$

where λ is the decay constant of the radionuclide. If chain decay is being modeled in the waste form, the inventories can be obtained as a function of time by using the Bateman equations. This has been done by Kang (1990).

Incongruent Dissolution and Individual Solubility Limits. A general approach to calculating fractional release rates is to assume that the surface concentration term, C_s, of Equation (3.16) is equal to the solubility limit, C^*, imposed by a discrete radionuclide-bearing solid (Pigford and Chambré 1986; Zavoshy et al. 1985):

$$(C_s)_i = (C^*)_i \tag{3.30}$$

One complication is that the solubility, C^*, is expressed for an element that may have several isotopes that have different decay constants. Because of this "shared solubility," an effective isotopic solubility, C_e^*, must be defined:

$$(C_s)_i = (C_e^*)_i = X_i(C^*) = \frac{I_i(t)}{I_T(t)}(C^*) \tag{3.31}$$

where X_i is the time-dependent isotopic mass fraction of nuclide i $[I_i(t)]$ with respect to the total inventory of all nuclides $[I_T(t)]$ of the same element. The time-dependent X_i term is particularly important if two (or more) isotopes have extremely different half-lives, as in the case of ^{135}Cs and ^{137}Cs. In general, the C_s values for different radionuclides will be neither equal nor correlated. Because of this, the mass-transfer rates and fractional release rates of nuclides from the waste form surface will also not be equal to or correlated with each other. This difference in rates of fractional release from the waste form is augmented when fractional release rates from the waste form are evaluated. This increase occurs because for different radionuclides the properties (e.g., retardation coefficient, half-life) affecting transport through the porous region(s) between waste form and host rock differ. Because the time dependency of C_s induced by decay effects has been treated after the fact, there may be some inaccuracy in the congruent release rates relative to the rates that would have been calculated from the release equation with radionuclide decay. However, given that the more accurate solution has not yet been implemented, the inaccuracy of the current

approximation is not known. Also, the relative inventory relation in Equation (3.31) does not account for mass-transport losses because of the computational burden and because the accuracy associated with such an implementation is unknown.

Congruent Dissolution and Matrix Solubility Limit

Assume that a compositionally homogeneous waste form that is thermodynamically stable dissolves congruently under expected waste package conditions. In the presence of reducing conditions, which are assumed to be imposed by metal barriers or by iron-bearing packing and host rock materials, the UO_2 matrix of spent fuel might be such a waste form (Garisto and Garisto 1985; Johnson et al. 1985). By definition for congruent dissolution, the instantaneous fractional release rates of the uranium matrix and all nuclides included in it (i,j, ...,n) at the waste form surface are equal; thus

$$\dot{F}(R_\emptyset,t)_{UO_2} = \dot{F}(R_\emptyset,t)_i = \dot{F}(R_\emptyset,t)_j = \ldots = \dot{F}(R_\emptyset,t)_n \qquad (3.32)$$

The NRC-defined (10 CFR 60) fractional release rates do not conform to Equation (3.24) because their mass-transfer rates, $\dot{M}(r,t)$, are normalized to a fixed inventory evaluated at 1000 years after permanent closure rather than to an inventory corrected for radioactive decay. The fractional release rates are related for congruent (and incongruent) dissolution as follows:

$$\dot{f}(R_\emptyset,t)_i = \frac{\dot{F}(R_\emptyset,t)_i[I(t)_i]}{I(1000)_i} \qquad (3.33)$$

Combining Equations (3.32) and (3.33):

$$\dot{f}(R_\emptyset,t)_i = \dot{F}(R_\emptyset,t)_{UO_2}[I(t)_i/I(1000)_i][I(1000)_{UO_2}/I(t)_{UO_2}] \qquad (3.34)$$

For ^{238}U (half-life of 4.47E+9 years), which is the dominant uranium isotope in the matrix, the change in inventory between 1000 and 10,000 years after permanent closure is negligible, only 0.002%. Accordingly, over the time

frame of interest, the 1000-year and time-dependent uranium inventories are essentially equal. If i is also a long-lived nuclide, its time-dependent inventories and its inventory at 1000 years will also be approximately equal, so that Equation (3.34) reduces to

$$\dot{f}(R_\emptyset,t)_i \approx \dot{f}(R_\emptyset,t)_{UO_2} \tag{3.35}$$

Combining Equation (3.32) with Equations (3.24) and (3.27), the following additional equations apply at the surface of the waste form:

$$\dot{M}(R_\emptyset,t)_i = \dot{M}(R_\emptyset,t)_{UO_2}[I(t)_i/I(t)UO_2] \tag{3.36}$$

$$\dot{M}(R_\emptyset,t)_i = 4\pi\epsilon_1 D_f R_\emptyset^2 (C_s)_{U\emptyset_2} \psi(R_\emptyset,t)_{UO_2} [I(t)_i/I(t)_{UO_2}] \tag{3.37}$$

where ψ_{UO_2} is the specific time-dependent function for mass transfer for the UO_2 matrix, evaluated at the surface of the waste form [see Equation (3.17)]. Mass-transfer rates, and hence fractional release rates, for nuclides from a congruently dissolving waste form scale directly with $(C_s)_{UO_2}$ and the stoichiometric proportion of that radionuclide in the UO_2 matrix. This relationship applies to even that proportion of such highly soluble nuclides as ^{14}C, ^{129}I, and ^{135}Cs that may be uniformly distributed (though not necessarily chemically bound) within a congruently dissolving UO_2 matrix. This model assumes that the congruently dissolving waste form matrix, UO_2, is a stable solid phase with a fixed specific solubility (see Johnson et al. 1985).

Equations (3.32) to (3.37) assume that no nuclide-bearing solid forms after the congruent dissolution of the UO_2 matrix. That is, the equations are valid only if

$$(C_s)_i < (C^*)_i \tag{3.38}$$

where $(C_s)_i$ is the surface concentration of nuclide i controlled by congruent dissolution of the UO_2 matrix and $(C^*)_i$ is the solubility concentration of i imposed by the potential formation of a new solid phase at the UO_2 surface [Equation (3.30) or (3.31)]. If the condition in Equation (3.38) is not met, then nuclide i will be incongruently released with respect to uranium and the other nuclides included in the matrix. The remainder of this section will assume that the condition of Equation (3.38) is met.

The surface concentration of i, $(C_s)_i$, is no longer equal to a solubility limit imposed by its own nuclide-bearing solid as it was in the incongruent case. Combining Equations (3.24) and (3.35) gives the following expression for the time-dependent concentration of radionuclide i at the UO_2 surface:

$$(C_s)_i(t) = (C_s)_{UO_2}[I(t)_i/I(t)_{UO_2}][\psi(R_\emptyset,t)_{UO_2}/\psi(R_\emptyset,t)_i] \qquad (3.39)$$

Note that $(C_s)_i(t)$ is directly proportional to the solubility of UO_2, the time-dependent stoichiometric proportion of i in the UO_2 matrix, and the time-dependent ratio of mass-transfer functions. As steady-state release is approached, the ratio of the mass-transfer functions approaches a constant ratio, Y, leaving

$$(C_s)_i = Y(C_s)_{UO_2}[I(t)_i/I(t)_{UO_2}] \qquad (3.40)$$

for $t \rightarrow t_{ss}$, where t_{ss} is defined as the time at which quasi-steady state is approached (Zavoshy et al. 1985). Equations (3.32) to (3.37) are strictly valid only for time-independent values of $(C_s)_i$. For congruent dissolution, the same boundary condition [Equation (3.39)] evaluated at the waste form surface remains true. However, the simple relationships regarding mass-transfer rates [Equation (3.36)] and instantaneous fractional release rates [Equation (3.32)] do not apply at the waste package boundary ($r = R_1$). Instead, the following relationships based on Equations (3.24) and (3.26) apply:

$$\dot{M}(R_1,t)_i = 4\pi\epsilon_1 D_f R_\emptyset R_1 (C_s)_i \psi(R_1,t)_i \qquad (3.41)$$

$$\dot{M}(R_1,t)_{UO_2} = 4\pi\epsilon_1 D_f R_\emptyset R_1 (C_s)_{UO_2}\ \psi(R_1,t)_{UO_2} \qquad (3.42)$$

and

$$f(R_1,t)_i = \frac{\dot{M}(R_1,t)_i}{I(1000)_i} \qquad (3.43)$$

Combining Equations (3.41) and (3.24) and rearranging terms gives

$$\dot{M}(R_1,t)_i = (R_1/R_\emptyset)\ \dot{M}(R_\emptyset,t)_i\ [\psi(R_1,t)_i/\psi(R_\emptyset,t)_i] \qquad (3.44)$$

Substituting from Equation (3.36) gives

$$\dot{M}(R_1,t)_i = (R_1/R_\emptyset)\ \dot{M}(R_\emptyset,t)_{UO_2}[I(t)_i/I(t)_{UO_2}][\psi(R_1,t)_i/\psi(R_\emptyset,t)_i] \qquad (3.45)$$

At steady state, the ratio of the mass-transfer functions equals a constant value, Y, so that Equation (3.45) becomes

$$\dot{M}(R_1,t)_i = Y(R_1/R_\emptyset)\dot{M}(R_\emptyset,t)_{UO_2}[I(t)_i/I(t)_{UO_2}] \qquad t \rightarrow t_{ss} \qquad (3.46)$$

Equations (3.43), (3.45), and (3.46) demonstrate that, under congruent dissolution, the release rate of a radionuclide from the waste package will be directly related to the release rate of uranium at the waste form surface and the stoichiometric proportion of that nuclide within the UO_2 matrix.

3.2.2.2 Inventory-Limited Model for Gap and Cladding Release

A series of mass-transfer equations (Kim et al. 1986) describe the release of highly soluble inventory-limited radionuclides from a waste package. These equations are based on a planar geometry, assuming the presence of a waste form, a void volume over the waste form, a porous layer

(or equivalent), and the host rock. It is assumed that, over the time scale of interest, the void volume is filled by groundwater. A certain mass of radionuclide from the waste form is assumed to dissolve instantaneously into this void, providing an initial concentration of the nuclide. The parameters and dimensions of the barriers are transformed from the actual cylindrical geometry of a given waste package as described below. The governing equations for this setting are

$$\frac{\partial N_1}{\partial t} = D_1 \frac{\partial^2 N_1}{\partial x_2} - \lambda N_1 \qquad -R_\emptyset < x < R_1,\ t > 0 \qquad (3.47)$$

$$\frac{\partial N_2}{\partial t} = D_2 \frac{\partial^2 N_2}{\partial x_2} - \lambda N_2 \qquad x > R_1,\ t > 0 \qquad (3.48)$$

$$N_1(x,0) = 0 \qquad R_\emptyset < x < R_1 \qquad (3.49a)$$

$$N_2(x,0) = 0 \qquad x > R_1 \qquad (3.49b)$$

$$N_1(R_1,t) = N_2(0,t) \qquad t > 0 \qquad (3.50)$$

$$-\epsilon_1 D_f \frac{\partial N_1}{\partial x} = -\epsilon_2 D_f \frac{\partial N_2}{\partial x} \qquad x = R_1,\ t > 0 \qquad (3.51)$$

$$N_2(\infty,t) = 0 \qquad t > 0 \qquad (3.52)$$

$$-V_v \frac{\partial N_1(R_\emptyset,t)}{\partial t} = -D_f \epsilon_1 S \frac{\partial N_1(R_\emptyset,t)}{\partial x} + \lambda V_v N_1(R_\emptyset,t) \qquad t > 0 \qquad (3.53)$$

$$N_1(R_\emptyset,0) = N^\circ \qquad (3.54)$$

where $N_1(x,t)$ = radionuclide concentration in the backfill region, g/cm^3

$D_1 = D_f/k_1$

D_f = diffusion coefficient in the water, cm^2/sec

k_1 = retardation coefficient in the packing, dimensionless

$N_2(x,t)$ = radionuclide concentrations in the host rock region, g/cm^3

λ = radioactive decay constant, 1/yr = ln 2/half-life

$D_2 = D_f/k_2$

k_2 = retardation coefficient in the host rock, dimensionless

ϵ_1 = porosity of the packing, dimensionless

ϵ_2 = porosity of the host rock, dimensionless

V_v = volume of the void, cm^3.

An approximate equation for the mass-transfer rate into the host rock using these equations is

$$\dot{M}(R_1,t) = 2k_1\epsilon_1 N_o S_v \frac{\exp(-gt)}{\delta + 1} \sum_N \left(\frac{D_1}{\pi k}\right)^{1/2} \exp \left(\frac{-(2N +)^2 b^2}{4D,t}\right) - \gamma_o D_1 \exp[(2N + 1) b\gamma_o = D_1\gamma_\emptyset{}^2 t] \operatorname{erfc}\left[(2N + 1)\frac{b}{2(D_1T)^{1/2} + \gamma o(D,t)^{1/2}}\right]\left(\frac{\delta - 1}{\delta + 1}\right)^N \quad N = 0,1,... \tag{3.55}$$

and the functional rates are

$$\dot{f}(R_1,t) = \frac{\dot{M}(R_1,t)}{I(1000)} \tag{3.56}$$

$$\dot{F}(R_1,t) = \frac{\dot{M}(R_1,t)}{I(t)} \qquad (3.57)$$

$\dot{M}(R_1,t)$ = mass-transfer rate into the host rock, g/sec

N_o = initial concentration in void, g/cm^3

S_v = surface area of the void, cm^2

t = time, sec

$\delta = (K_1/K_2)^{1/2}\epsilon_1/\epsilon_2$

b = packing thickness, cm

$\gamma_o = k_1\epsilon_1 S_v/V_v$

erfc = complementary error function

$\dot{f}(R_1,t)$ = NRC fractional release rate, parts/year

$\dot{F}(R_1,t)$ = instantaneous fractional release rate, parts/year.

Equation (3.55) is an approximate solution. However, Kang (1990) has found that this solution agrees with a numerical implementation of the exact solution, for time $<10^5$ years, and disagrees only slightly for longer times. These results applied to the waste packing and host rock retardation coefficients being equal ($k_1 = k_2$) and at values of 1, 10, 100, and 1000.

The volume of the void, V_v, is equal to the difference between the volume of the cylindrical waste container and the total volume of enclosed spent fuel rods. The surface area, S_v, is the surface area of the cylindrical waste form container. The width of the void in this model is equal to the ratio V_v/S_v. The initial concentration in the void, $N_\emptyset$, is calculated by dividing the mass of a soluble nuclide by the volume of the void. The nuclide mass is derived from the fraction of the total inventory of that nuclide occurring in the readily soluble source. The complementary error function is estimated using the continued fraction algorithm (Stegun and Zucker 1970)

$$\text{erfc}(y) = \left[\exp(-y)^2\ F\right]/\pi^{1/2} \tag{3.58}$$

where F is a series fractional term given explicitly by Stegun and Zucker (1970). Thus the term [exp(x) erfc(y)] in Equation (3.55) is simplified to

$$[\exp(x - y)^2\ F]/\pi^{1/2} \tag{3.59}$$

The proportional mass of the instantaneously dissolved (gap) nuclide, m_i, can be expressed as a fraction of the total inventory of that nuclide, X_i, such that

$$N_o = \frac{m_i}{V_v} = \frac{X_i I(t)_i}{V_v} \tag{3.60}$$

From Equation (3.33), it can be shown that

$$\dot{f}(R_1,t)_i = \dot{F}(R_1,t)_i[I(t)_i/I(1000)_i] \tag{3.61}$$

A feature of the calculated release rate is that "instantaneous" release (Johnson et al. 1985) from the engineered barrier does not occur. It does not occur because materials released from the waste form are delayed by transport through the packing (or equivalent) barrier before release from the engineered barrier. This delayed mass transport is explicitly taken into account in the SUMO code. Such an approach is more realistic than equating instantaneous release from the waste form with instantaneous release from the EBS. Because of diffusion through the packing, release rates from the EBS remain finite, even though instantaneous dissolution into groundwater is assumed.

Another feature of the inventory-limited release model is a consideration of the effects of radioactive decay and mass transport on release rates from the source volume. Both processes lead to decreases in the concentration of nuclide i at the source, and hence to a decrease in the concentration gradient that drives release.

3.2.3 Radionuclide Sources from Spent Fuel

Studies of spent fuel (Barner 1984) and of the interaction of spent fuel with groundwater solutions (Gray and McVay 1984; Johnson et al. 1985; Werme and Forsyth 1985; Wilson and Oversby 1985) indicate that release of radionuclides from spent fuel can be divided into distinct sources: the matrix of UO_2 grains, the gap between the fuel and the cladding, the boundaries between the UO_2 grains, and the cladding. These sources can be distinguished on the basis of different physical forms, radionuclide inventories, and processes controlling release.

3.2.3.1 UO_2 Matrix

More than 99% of the radionuclides in spent UO_2 fuel are contained within the UO_2 matrix grains; therefore, attention has been directed toward the matrix dissolution rate and the mechanism under which dissolution occurs under a variety of repository conditions. Recent spent-fuel tests (Gray and McVay 1984; Johnson et al. 1985; Werme and Forsyth 1985; Wilson and Oversby 1985) suggest that actinide elements (Np, Pu, Am, and Cm) and some fission products dissolve at rates that are initially congruent with respect to calculated inventories and that they are released in fixed proportion to uranium dissolution rates. This concept is supported by chemical analysis of unreacted UO_2 grains of spent light-water reactor (LWR) fuel, which showed essentially no compositional zonation for a wide variety of elements (Ba, Ce, Cs, I, Pu, Ru, Tc, Te, and Zr) (Katayama et al. 1980). For this reason, the EBS release model includes an option to force a congruent dissolution assumption for releases from the waste form.

3.2.3.2 Gap and Grain Boundaries

The volatile and more mobile fission products, such as ^{79}Se, ^{93}Mo, ^{99}Tc, ^{129}I, ^{135}Cs, ^{137}Cs, and possibly ^{90}Sr, tend to migrate out of the UO_2 matrix and down thermal gradients in fuel pins. These radionuclides tend to accumulate both at grain boundaries as secondary phases precipitated in the fuel matrix and voids, and in the gap between fuel and cladding (including the gas plenum at the top of the fuel rod). Based on the limited amount of the total fission gases (typically <1.5%) released from LWR fuel (Bain et al. 1985; Barner

1984), the total of gap and grain-boundary sources should be less than 2% of the inventory of volatile fission products. The activation product ^{14}C may also be preferentially segregated from the fuel matrix phase. However, the ^{14}C distribution between the fuel, gap, and cladding is well characterized. After the initial rapid release of fission products from the gap, the preferential release rates of many of these elements are expected to gradually decrease and eventually approach the fuel matrix dissolution rate, as the limited inventory of these nuclides, which have been segregated from the fuel matrix, is exhausted. The inventory that is preferentially released during this period will also include the fission products located along grain boundaries. The individual release contributions of the gap and grain boundaries cannot be easily separated because the same mechanisms, such as grain growth, bubble formation, and diffusion, lead to the accumulation of both gap and grain boundary inventories. Furthermore, virtually no data are available on the chemical natures and proportions of grain boundary phases. Consequently, the SUMO code treats the gap and boundary inventories as a single source for modeling purposes. A key factor, therefore, in the calculated release from the gap and grain boundary sources is the inventory of nuclides contained in both. The combined inventory can represent 1 to 2% of fission product activity, depending on burnup and history. Particularly important is the irradiation temperature, which more than any other factor determines the degree of fuel restructuring, gas release, and phase segregation. Improved realism in gap and grain boundary releases requires more detailed characterization of the amounts and variability of readily soluble fission products located in these phases.

3.2.3.3 Cladding

The cladding of LWR fuel is typically a zirconium alloy and may include "crud" deposits that formed on the cladding during reactor operation. The cladding does contain a limited amount of nuclides produced by neutron activation. Of these nuclides, all but tritium exceed the cutoff point of 0.1% of the calculated total regulatory release-rate limit in performance evaluations (10 CFR 61). Consequently, cladding must be considered a waste form. In particular, the cladding contains an appreciable fraction of the total ^{14}C

inventory of spent fuel (Van Konynenburg et al. 1985). Because of the volatility of ^{14}C as CO_2 gas, both steam and saturated hydrologic phases are relevant to predictive modeling of cladding performance (as a waste form). There is evidence of rapid release of ^{14}C, probably as CO_2 gas, from the outside surface of intact cladding at 275°C in air (Van Konynenburg et al. 1985). In this situation, approximately 0.3% of the calculated ^{14}C inventory for the total spent-fuel assembly was released. However, ^{14}C releases from a ruptured fuel rod at the same high-temperature air conditions indicate that if all of the rods were to rupture, approximately 9% of the ^{14}C inventory would be released as a gas. This rapid release of ^{14}C-bearing CO_2 gas from the cladding under steam conditions can be modeled with the same inventory-limited mass-transfer model applied to gap release under aqueous conditions.

Modeling the interaction of cladding with groundwater is limited by the lack of detailed characterization and test data. At the two extremes, the release of ^{14}C could be controlled by slow uniform corrosion of the cladding, or the ^{14}C could be concentrated in the surface crud layer, from which it is rapidly released on contact with water. The few tests that have been performed on cladding/groundwater interaction show rapid release of an appreciable portion (approximately 0.05%) of the estimated cladding ^{14}C inventory (Wilson 1985, 1986). After this rapid release, the ^{14}C concentration in solution is observed to plateau, showing only slight increase or decrease. Thus, ^{14}C release from cladding probably includes contributions from both rapid dissolution of a surface crud layer and slower corrosion of the bulk cladding. The EBS model in the SUMO code models these two separate sources of nuclides from the cladding. An inventory-limited model is used to predict release rates from the outer crud or surface layer. A solubility-limited model is used to calculate release rates from the bulk cladding.

For spent fuel, a small percentage of certain radionuclides is not contained in the fuel matrix. These radionuclides accumulate in the gap or grain boundaries of the fuel during fuel irradiation (e.g., Cs and I) or as crud on the outer surface of fuel cladding (e.g., ^{14}C). In the SUMO code, the volatile radionuclides (e.g., ^{14}C) are assumed to be released instantly on

breaching of the containment. The nonvolatile radionuclides that are not contained in the matrix generally have high solubilities and are not expected to form colloids in oxidizing groundwaters. In the code, the nonmatrix release rate of these radionuclides is set equal to $Q(t)C_{si}$ or $4\pi\epsilon r_o(A_d/A_t)D_iC_{si}$, whichever is greater. The release rate remains at one of these two values until all of the nonmatrix inventory is depleted (hence the term "inventory-limited"), at which time the nonmatrix release rate is set equal to zero. Any further release must then come from the matrix.

3.3 WASTE-PACKAGE ENVIRONMENT

Site-specific information describing the physical and chemical environments of the waste package and the repository is required for realistic EBS calculations. In particular, the hydrological, geochemical, and thermal environments of the simulated waste packages must be considered.

3.3.1 Hydrologic Model

The source-term models require a water saturation value for the diffusion-based model and a water flux rate for the advection-based model. This information must be representative of the repository horizon because it is applied to every waste package. There are two alternatives for integrating this information into the source-term calculations.

The first alternative is to have the user explicitly enter a water flux rate and a saturation value to be used in the calculations. These values are assumed to apply for all times, spatial configurations, and thermal conditions.

The second alternative for obtaining the water flux rate and saturation values is to calculate them within the SUMO code. First the pressure equation (see Section 4.3) is solved for a steady-state flow field, given a recharge rate through the model geometry and specified boundary and initial conditions. This steady-state flow field solution neglects the effect of repository thermal loading on the regional flow regime. Once the steady-state flow field has been obtained, the water flux rate and saturation at a specified location are passed to the source-term model.

3.3.2 Geochemical Model

The composition of groundwater in a repository is determined by mass-transfer reactions between the groundwater and solids in the host rock, packing material, container, and waste form. These reactions are controlled by temperature, groundwater composition, the solubility of solid phases in contact with the groundwater, and the distribution of the aqueous mass among the various chemical species in solution. There is no provision in the SUMO code to explicitly model these complex phenomena. Instead, a detailed external geochemical model is used to build tables of groundwater composition that are then input into the SUMO code.

The current EBS release models do not quantify geochemical influences on releases. Even though Equation (3.7) includes a term for colloid formation and transport, no site-based information is available and the term is currently omitted. However, some of the current corrosion models do make explicit use of the groundwater composition, and the SUMO code can receive and store geochemical information as it relates to these corrosion models.

3.3.3 Thermal Model

There is currently no provision in the SUMO code to perform thermal loading calculations on the repository or waste-package scale. However, there are two methods for using waste package temperature profiles as a function of time in the SUMO code. The first method is to read a temperature-time profile generated by an external thermal analysis code and interpolate temperatures for desired times. The second method also reads information provided by an external thermal code but derives the temperature profiles differently, using reference cases.

3.3.3.1 Direct Input Approach for Thermal Modeling

To obtain waste package temperature profiles, the SUMO code can read a temperature-time profile generated by an external thermal analysis code. A recent study was performed to generate representative curves for Yucca Mountain (Altenhofen and Eslinger 1990). The analysis consisted of three steps: 1) the WASTES code (Ouderkirk 1988) was used to evaluate thermal characteristics of materials received by the repository, 2) the TEMPEST finite-difference

thermal code (Trent et al. 1983) was used to evaluate near-field temperatures of the host rock based on a three-dimensional repository geometry, and 3) the CANTEMP post-processor was used to estimate container surface temperatures from host rock temperatures and output temperature-time profiles for use in the SUMO code.

3.3.3.2 Reference Case Thermal Profiles

Temperatures of simulated waste packages can also be calculated by using a temperature-time profile of a reference case or design-basis waste package and adjusting the profile to reflect the differences between the waste package of interest and the reference package. The temperature of a simulated waste package is computed from a simulated initial temperature based on the assumption that the difference between the temperature of the simulated container and the ambient repository temperature is proportional to the difference between the temperature of the reference case waste package and the ambient repository temperature for all times.

The temperature history of the reference case waste package and the repository were obtained from waste package and repository-scale models using the ANSYS finite-element code (Swanson Analysis Systems 1986). This code is a widely used, general-purpose, finite-element code with both structural and thermal capabilities. Three-dimensional models were used to estimate short-term (less than 1000 years) waste-package-scale temperatures. One-dimensional models were then used to estimate the repository's average temperature. The average repository temperatures and the container temperatures were nearly equal after 1000 years, so repository average temperatures were used to estimate waste package temperatures at times greater than 1000 years (Altenhofen 1981). Temperature histories were then tabulated for input to the thermal module.

The initial waste package temperatures are obtained by sampling from a distribution of initial waste package temperatures that is derived, in turn, from a distribution of initial waste package heat-generation rates. The conversion of heat-generation rates to initial waste package temperatures depends on the thermal properties of the host medium. The distribution of heat-generation rates depends on assumed spent-fuel characteristics and repository

receipt scenarios. The derivation of values currently available in the SUMO code is described by detail in Liebetrau et al. (1987, Appendix B).

3.4 CONTAINER FAILURE TIME MODELS

The EBS model in the SUMO code considers distributed container failures; therefore the time of container failure must be modeled. Two options are available in the SUMO code: 1) the user may specify a time distribution for container failure, or 2) a corrosion model can be employed to estimate the time of container failure.

3.4.1 User-Specified Time Distribution for Container Failure

An analytic form for the container failure time distribution can be specified when running the SUMO code. The user chooses a single time or one of 12 standard statistical distributions, or chooses to specify a distribution through a table of values (Table 3.2).

3.4.2 Container Failure Times Based on a Corrosion Model

The SUMO code currently implements the corrosion model capabilities of the AREST code (Engel et al. 1989). Five types of corrosion or degradation can be modeled: uniform, stress corrosion cracking, pitting, fracture, and

TABLE 3.2. Statistical Distributions Implemented in the SUMO Code

Index	Distribution
0	Constant
1	Uniform
2	Loguniform (base 10)
3	Loguniform (base e)
4	Normal
5	Lognormal (base 10)
6	Lognormal (base e)
7	Exponential
8	Triangular
9	Gamma
10	Beta
11	Weibull
12	Logistic
13	Cauchy
14	User-supplied table of values

cladding failure. The first three types of corrosion are the most general. The other corrosion models, which were included in the AREST code, were not deleted when that code was incorporated into the SUMO code because no final determination of the appropriate corrosion model for Yucca Mountain has been made. However, detailed descriptions of the other models are not incorporated into this document.

All corrosion routines in the SUMO code are time dependent, and all return both corrosion rates and depth. These corrosion routines are 1) uniform corrosion for low-carbon steel in salt water, 2) uniform corrosion for low-carbon steel in basalt for both aqueous and steam environments, 3) uniform and pitting corrosion for low-carbon steel in basalt-bentonite for both aqueous and steam environments, 4) pitting of steel in an aqueous environment, 5) uniform corrosion of zircaloy in both aqueous and steam environments, 6) uniform corrosion of steel in an aqueous environment, and 7) uniform corrosion of iron-based materials in an aqueous salt environment. The corrosion rates output from these models are used to estimate container failure times, which are needed because mobilization of waste occurs at that time.

3.4.2.1 Container Corrosion Models

The integrity of engineered barriers will play an important role in determining the extent to which radionuclides are contained in or released from a waste repository. Currently, it is primarily engineered barriers made of metallic container materials that meet the NRC containment performance objectives at all U.S. repository projects. Because corrosion is the principal mechanism by which the metallic containers degrade, corrosion rate estimates are required for performance and safety assessments. This section describes models that estimate corrosion rates for metallic barriers in important repository environments.

The term "corrosion" describes a wide variety of complex phenomena involving both chemical and electrochemical interactions between a metal and its environment. These phenomena depend heavily on the material and its environment. As a result, both the mechanisms of corrosion and the morphology of the corrosion products are very diverse. Corrosion can be uniform or localized, can result from applied or residual stresses, or can occur because

of galvanic coupling with dissimilar materials. Even systems whose corrosion products have similar morphologies may corrode according to very different rate laws because the chemical species involved in corrosion and their reactivities differ. Because of this diversity, it is unlikely that any comprehensive corrosion rate equation can be developed. Development of a corrosion model for even a single-material repository system is not a trivial task, because the environments into which the metallic barriers will be placed have not yet been completely characterized, and it is not well established what they will be like after the hundreds and thousands of years of the repository's lifetime.

The current approach to corrosion modeling is based on empirical models fit to relatively short-term (less than 5 years) corrosion tests. Empirical models are, of course, appropriate only to the conditions and environments for which they were developed. Mechanistic models are also most accurate when applied to the conditions for which they were derived. However, because mechanistic models are based on a deeper understanding of the chemical origins of the corrosion process (deeper than that obtained on empirical grounds alone), they can, in principle, be extended to other conditions and environments where similar reaction mechanisms are known to occur. Unfortunately, there is an almost complete lack of data for requisite mechanistic model parameters in repository situations.

The modeling philosophy used in developing the SUMO code allows the inclusion of some of the uncertainty inherent in the models themselves, by providing stochastic information about the fitted parameters. The sensitivity of the models to the data deficiencies and the importance of these deficiencies can be determined from how the input uncertainties affect the results. Models for three specific types of corrosion are currently implemented in the SUMO code. They are uniform corrosion, pitting corrosion, and stress-corrosion cracking. These types of corrosion were chosen because they represent the most likely modes of degradation in a repository. Other modes may be added to the SUMO code if necessary. The materials considered are limited to low-carbon steels, stainless steels, and zircaloy. The inclusion of corrosion

models in the SUMO code serves two purposes. First, they are general empirical models, and a change in the empirical constants might possibly make them applicable. Second, they provide an important coding stub that incorporates thermal and geochemical information that can be used for later models.

3.4.2.2 Uniform Corrosion Model

Uniform corrosion occurs to some extent for most metals in most environments. Factors influencing the rate of corrosion include, but are not limited to, the composition of the material under consideration, the environment into which it is placed, the by-products of the corrosion process, and the temperature. The interrelationships between these factors and their effect on the actual chemical process responsible for corrosion are extremely complex. For this reason, it is unlikely that a purely mechanistic model of uniform corrosion could be developed that would be comprehensive enough to include all metals in all environments. In the absence of such a model, a family of empirical uniform corrosion models was developed that may be appropriate for any specific set of conditions and environments.

The most reliable uniform corrosion rate models currently available are empirical. A number of models have been developed for carbon steel in chloride-containing environments. Two such models have been included in the SUMO code. The two models will be used to develop a uniform corrosion model appropriate for a given set of repository conditions.

Posey and Palko (1979) at Oak Ridge National Laboratory have published a report on the corrosion of ferrous materials in synthetic geothermal brines. Using a specially designed flow-through autoclave system, they investigated the influence of pH (from neutral to moderately acidic) and temperature (up to 200°C) on the corrosion behavior of carbon steel in concentrated chloride solution (4 M NaCl). They derived the following empirical two-term expression for the corrosion rate:

$$j_{corr} = 1.90 \times 10^5 \exp(-3.98 \times 10^3/T) + 4.19 \times 10^6 (10^{-pH}) \exp(-2.10 \times 10^3/T) \quad (3.62)$$

where j_{corr} is the corrosion rate in mils per year (mpy), and T is the absolute temperature (Kelvins). In the region of near-neutral pH, from about pH 5 to 9 (at 25°C), the corrosion rate is relatively independent of pH, and Equation (3.63) reduces to the following:

$$j_{corr} = 1.90 \times 10^5 \exp(-3.98 \times 10^3/T) \quad (3.63)$$

However, Equation (3.63) gives corrosion rates higher than those found by other workers. For example, at 150°C (423 K), Equation (3.63) predicts a corrosion rate equal to 15.6 mpy. This value is significantly larger than the 0.575-mpy corrosion rate determined for carbon steel in similar brine environments by Westerman et al. (1986). [At 150°C (423 K), Westerman et al. (1986) found the corrosion rate of A216 steel in an anoxic simulated Permian Basin brine (PBB-2) equaled 0.575 mpy]. The reason for this disparity is probably that the corrosion rates were determined after different lengths of time after initiation of the experiments. In general, corrosion rate is a function of time, large shortly after the experiment is initiated and decreasing over a longer time. The data collected by Westerman et al. (1986) were taken after 4480 hours (0.511 year), but the time interval used by Posey and Palko (1979), although unspecified, seems to have been much shorter (less than 8 hours). Clearly, a more complete corrosion rate equation must include a functional dependence on time.

An empirical equation for calculating corrosion depth that contains an explicit time dependency was developed by Sastre et al. (1986) at Brookhaven National Laboratory (BNL), and variations of this equation are implemented in the SUMO code. This equation was developed from data for carbon steels over a range of temperatures, brine compositions, and times. Although it was far from complete, the data base was adequate for generating an approximate corrosion equation that was a function of temperature (between 25°C and 250°C),

chloride concentration (between 70 and 169,416 ppm), oxygen concentration (between 0.03 and 3.0 ppm), and time (between 0.083 and 16 years). This equation, which has been differentiated with respect to time to give an expression for corrosion rate, is

$$j_{corr} = 0.689\ t^{-0.531} \exp\ (-1402/T)\ (Cl)^{0.543}\ (O)^{0.2d} \qquad (3.64)$$

where t (time) is in years, (Cl) is the chloride concentration in ppm, (O) is the oxygen concentration in ppm, and d is an experimental parameter that can vary between 0.00147 and 676.

The wide range for d suggests that corrosion mechanisms vary widely over the experimental conditions studied. The equation should therefore be used with caution. It is useful, however, to consider what value of d is required to fit the equation to data collected recently by Westerman et al. (1986). Using the corrosion rate found by Westerman et al. for A216 steel in PBB-2, and taking T = 432 K, (Cl) = 191,000 ppm, (O) = 0.1 ppm for "anoxic" brine, and t = 0.511 year, d is calculated to be 0.0368. This value is within the range specified by the BNL model. Using this value for d, Equation (3.64) reduces to the following:

$$j_{corr} = 0.0254\ t^{-0.531} \exp(-1402/T)\ (Cl)^{0.543}\ (O)^{0.2} \qquad (3.65)$$

Under the conditions used by Westerman et al. (1986), at 423 K, Equation (3.65) reduces further to the following:

$$j_{corr} = 0.429\ t^{-0.531} \qquad (3.66)$$

Appendix A of Liebetrau et al. (1987) contains an extended discussion of the appropriateness of these models to match other empirical data. Because this model is not strictly applicable to the Yucca Mountain Project, it will not be discussed further even though it is included in the SUMO code.

3.4.2.3 Pitting Corrosion Models

Pitting corrosion is a local phenomenon that can cause rapid penetration of a metallic specimen. Pitting corrosion is initiated by local variations in either the material or the solution in contact with the material. Differences in the microstructure of the material, such as grain boundaries or inclusions of second-phase particles, are likely spots for the initiation of pitting corrosion. Welds or discontinuous joints in the material may cause the solution to stagnate and may promote crevice corrosion, which is similar to pitting corrosion. Once a pit is initiated, the conditions necessary for pit propagation are sustained, and the process becomes autocatalytic. The time and location of pit initiation as well as pit growth are essentially random. During formation of a pit, a local environment is produced and sustained that may be very different from that of the bulk solution. The concentrations of reactants and products that contribute to pitting produce a situation different from that of uniform corrosion. The pit is primarily a site for anodic dissolution of the metal, while large portions of the canister may act as a cathode. The very large ratio of cathodic to anodic areas results in rapid metal dissolution. The model chosen to describe this process is one by Stahl and Miller (1985). This model is a simple treatment of the very complex environment within the pit itself. Pitting is treated as a one-dimensional transport process. The corrosion rate is assumed to be limited by diffusion of the metal cation through a dilute binary electrolyte. The diffusion is driven by gradients of both concentration and potential. Reactions and reaction rates within the pit are neglected, as is transport of material between the pit and the environment. The resulting equation is

$$\frac{dh}{dt} = \frac{W}{\rho}\left[\frac{|z_+|}{z_-} + 1\right] D \frac{C_+(0)}{h}\left[\exp\left(\frac{z_- F}{RT}\,\Delta\phi\right)\right]^{-1} \qquad (3.67)$$

where $\frac{dh}{dt}$ = the rate of pit depth increase, cm/sec

W = the molecular weight of the metal, g/mole

ρ = the density of the metal, g/cm^3

z_+, z_- = the proton charge on the constituents of the binary electrolyte, equivalents

D = the diffusivity of the metal cation in the pit, cm^2/sec

$C_+(0)$ = the concentration of the cation at the pit opening, $mole/cm^3$

h = the pit depth, cm

F = the Faraday constant, 96,500 coulombs/equivalent

R = the ideal gas constant, 8.314 joules/mole-K

T = the temperature, K

ϕ = the drop in potential along the pit depth, volts.

In Equation (3.67), all of the parameters are defined physical quantities except $\Delta\phi$ and $C_+(0)$. Because the pit solution is markedly different from the bulk solution, a direct connection between $\Delta\phi$ and the environment is difficult to make. In this model, it is assumed to be a constant that may take on a range of values. A suitable value for this quantity is suggested by voltage drop measurements done by Postlethwaite and Onofrei (1979), in which a potential drop of about 20 mV was measured during the pitting of both zircaloy and stainless steel. This drop is on the same order of magnitude as the 9-mV drop calculated by a semitheoretical approach by Vetter and Strehblow (1974). The quantity $C_+(0)$ is likely to depend on the bulk solution. Specifically, it will depend in part on the rate at which it is transported away from the pit mouth or is consumed by secondary reactions. Specifically, the assumed form for the quantity $C_+(0)$ will be

$$C_+(0) = a(1 + Eh) + b[Cl^-] \tag{3.68}$$

where Eh is the redox potential and $[Cl^-]$ is the concentration of chloride ions in $moles/cm^3$. The form for the term that is dependent on Eh is chosen to ensure that $C_+(0)$ remains positive. Other specific ions could be added to Equation (3.67) and their inclusion may be necessary as more data become available. The form of Equation (3.67) indicates that the pit depth increases as the square root of time for a given set of conditions. Such a dependence is

indicative of a diffusion-controlled process and is similar to the t•49 dependence reported by Marsh (1983). Table 3.3 lists the numerical values used by the model. Ranges for the parameters are estimates based on the fact that pitting rates may vary by an order of magnitude or more. The numbers presented apply to a generic steel and do not make a distinction between a low-carbon steel and a stainless steel, even though stainless steel is less susceptible to pitting. The values calculated for the required parameters are based on a very limited data base. Ranges were estimated for some parameters to partially account for the wide variations in pitting corrosion data. Pitting data were not available for zircaloy, and so no values can be given for this case.

3.4.2.4 Stress Corrosion Cracking

The stress corrosion cracking (SCC) process occurs under the combined influence of a corrosive environment with a tensile stress. Tensile stresses are likely to occur in a repository because of lithostatic or hydrostatic

TABLE 3.3. Values Used in Pitting Corrosion Model for Ferrous Materials

Variable	Value	Unit
W	55.8	g/mole[(a)]
ρ	7.86	g/cm^3
D	5.0×10^{-6}	cm^2/sec[(b)]
z_+	2[(c)]	
z_-	-1[(d)]	
ϕ	0.02	volts[(e)]
a	2.47×10^{-5}	
b	0.630	

(a) Fe.
(b) Fe^{2+} in 1N H_2SO_4.
(c) Fe^{2+}.
(d) Cl^-.
(e) Estimated range: -0.01 to 0.04 volts.

loads, residual stress developed during fabrication, or stresses imposed on the material by accident. The process of SCC is modeled as a series of steps whereby a tensile stress causes the fracture of a relatively brittle, passive film on the material, which is followed by rapid dissolution of the metal. As the dissolution of the metal proceeds, a new passive layer builds up at the crack tip. Stress again fractures the layer, and the process repeats itself. Thus, SCC can be considered to be a repetitive series of passive layer fracturing and healing. The rate at which SCC occurs depends on the stress level to which the material is subjected and also the passivation rate of the material in the given environment. A general form for the SCC rate equation is

$$v = L_f/t_f = pQ_f/t_f \tag{3.69}$$

where v = the crack tip velocity, m/sec

L_f = the depth of metal lost between oxide rupture events, m

t_f = the time between oxide rupture events, sec

p = a Faradaic constant, m^3/coulomb

Q_f = the amount of electric charge associated with L_f, coulombs/m^2.

Different interpretations of these parameters result in various theories for predicting the rate of SCC. In the SUMO code, a development in terms of stress intensities is used (Newman 1981). An alternate approach in terms of strain rates was used by Ford (1982), although strain rates are more difficult to calculate than stress levels. Newman's (1981) work indicates that Q_f is relatively insensitive to the environment but depends on the level of stress. An indirect dependency on stress intensity (Si^{-1}) can be predicted on the basis of a simple linear elastic analysis of the crack tip. The quantity t_f is environmentally dependent, because it is a function of the passivation rate of the material. Crack tip velocity is predicted by the following process. The amount of charge accumulation between oxide rupture events at a given stress intensity is determined experimentally. For a specific set of environmental conditions, the time required for that amount of charge to accumulate is also determined. Then, by insertion into Equation (3.69), these two

quantities give the crack tip velocity. The functional dependence of the crack tip velocity on the stress intensity predicted by this model has some general characteristics. First, a rapid increase in crack tip velocity is seen for small increases in stress intensity until a plateau is reached. Then, at higher stress intensities, the crack tip velocity again increases rapidly as the strength limits of the material are reached. The model indirectly predicts a threshold stress intensity below which crack propagation does not occur. This threshold is defined as the stress at which the crack tip velocity is equal to the rate of uniform corrosion for the given conditions. If the crack tip velocity is below the rate of uniform corrosion, the passive film will be physically healed faster than it can be fractured and the crack tip will not advance. Specific values for the parameters in this model for a variety of materials are given by Liebetrau et al. (1987).

3.5 DISTRIBUTED RELEASES FROM THE ENGINEERED BARRIER SYSTEM

Release from the EBS is dependent on the failure time of individual containers. The source-term model calculates the times at which individual containers fail and the amount of release from each container. The release from the EBS is then the sum of releases from individual containers that fail at random times. The source-term model provides a radionuclide flux (Ci/yr) to the transport model for each nuclide as a function of time. A capability is included to subdivide the repository into four separate regions or panels. Each panel can have a different waste form and different thermal characteristics. This capability will allow future analysis of both glass-based and spent-fuel waste forms in the same set of computer runs. Also, a combined analysis with different rate form characteristics results in more accurate concentration gradients.

Release from the EBS is computed until the inventory of all nuclides being modeled has been depleted or until a user-specified time limit has been reached. The current implementation in the SUMO code allows the radionuclides contained in the gap/grain boundary to start releasing when the container fails. However, releases from the waste form matrix are not allowed until the container's surface temperature has dropped to a user-specified value, even if

the waste container has failed. This limitation reflects the argument that liquid water cannot contact the waste form until it has cooled below the boiling point. Because air-based transport is not yet included in the SUMO code (even though plans for it are in progress), the radionuclide releases that are in fact in the air phase (e.g., ^{14}C as CO_2) are included in the water-phase release values.

4.0 FAR-FIELD TRANSPORT MODEL

The underlying theory and the implementation of the transport model in the SUMO code are described in this section. The transport model and the supporting documentation are an adaption of the model implemented in the PORFLO-3D code and its documentation (Runchal and Sagar 1989). This section gives an overview of the transport model, introduces the conceptual model for transport, describes the mathematical equations, and concludes with a derivation of the numerical discretization scheme.

4.1 OVERVIEW

Several features are available in the transport model. By choosing appropriate combinations of features, it is possible to solve a wide range of problems.

4.1.1 Spatial Dimensionality

The code is designed to solve three-dimensional problems. However, it can be adapted to solve one- and two-dimensional problems by specifying a grid size of three in the directions that are to be omitted. In effect, this specification results in the solution of a pseudo-three-dimensional problem.

4.1.2 Problem Geometry

A problem can be defined in terms of either Cartesian or cylindrical coordinates. In both coordinate systems, z is the direction of the vertical coordinate. The horizontal plane is represented by x-y in the Cartesian system, and by r-θ in the cylindrical system. For a one-dimensional problem, any of the three axes (x, y, or z) can be selected as the direction of interest. Two-dimensional problems can be solved in the x-y, x-z, or y-z plane. The computational elements can vary in size across the coordinate system, but their geometry is restricted to that of a rectangular parallelepiped.

4.1.3 Time Dependence

The transport model can handle either transient or steady-state problems. All problem parameters except the spatial grid can change with time. The

values of some parameters, such as the source terms for fluid, heat, and mass, can be assumed to change continuously with time. Such quantities can be specified in the form of tables.

4.1.4 Space Dependence

Most of the problem parameters are allowed to vary over the spatial grid. The model domain can be divided into zones, each zone having some distinct feature, such as a material property or source strength. The material properties can also be anisotropic.

4.1.5 Coupling of Equations

The SUMO code assumes that fluid flow is isothermal. There are thus two main equations, one for fluid flow and one for mass transport. The state variables in these equations are the hydraulic head (P) and the radionuclide concentration (C). These equations can be solved either independently or in coupled mode.

4.1.6 Boundary Conditions

Various types of boundary conditions can be specified in the SUMO code. Dirichlet (specified values of the dependent variables hydraulic head, temperature, or concentration), Neumann (specified fluxes of fluid or mass), or mixed (combination of specified values and fluxes) boundary conditions can be stipulated. Different types of boundary conditions can be designated over different portions of the boundary. This feature can be combined with the time-dependence features to solve a large variety of problems with space- and time-dependent boundary conditions.

Occasionally, the domain in which the mass-transport equations are required to be solved is large. If, in such cases, the rates of mass transport are slow, the option of solving these equations in grids that are smaller than the total domain may be used. With this option, a user can specify a location between the source and external boundary of the domain to be a temporary subdomain. This temporary subdomain can be expanded or eliminated when a specified condition is satisfied. This option can save computational time for problems that are characterized by large domain sizes with mass sources concentrated in a small portion of the overall domain.

4.1.7 Methods for Solving Governing Equations

The governing equations are solved by first discretizing them over the spatial grid and time steps, and then solving the resulting system of linear algebraic equations. The fluid flow equation is discretized based on quadratic approximating functions; these functions are equivalent to a central difference scheme. The second-order partial derivative terms in the mass-transport equations are also discretized through quadratic approximating functions. However, the first-order partial derivative terms in these equations can be discretized by either a hybrid or an exponential scheme. The nature of these schemes is described in Section 4.4. The discretization method used is based on integrating the approximating functions for each grid element. This method results in solutions that automatically conserve fluid, heat, and mass locally within every grid element, as well as for the entire model domain.

Alternate solution methods for the linear systems of algebraic equations are provided. These include the explicit method of point successive over-relaxation and the implicit methods of alternating direction implicit, Cholesky decomposition, and Gauss elimination.

4.1.8 Variable Saturation

Problems in which the geologic media are either fully or partially saturated, or in which some parts are fully saturated while others are partially saturated, can be solved with the SUMO code. In the partially saturated environment, liquid (water) and gas (air) phases are assumed to exist. However, the movement of only the liquid phase is addressed. Consideration of mass transfer is also restricted to the liquid phase (i.e., vapor transport is not considered). Consequently, the SUMO code is a "single-phase" computer code.

As part of the solution, the degree of liquid or water saturation is determined at each grid node of the domain. The boundary between the areas of positive and negative pressures is the water table. The water table can be moved up and down only from grid node to grid node; no adjustment for water table position can be made that does not coincide exactly with node locations.

4.1.9 Pore Structure

The user can define up to three types of porosities in the SUMO code. The smallest of these is the effective or flow porosity, which consists of the connected pores through which fluid flow occurs. The second is the diffusive porosity. Diffusive porosity is greater than, or equal to, the effective porosity. It includes the dead-end pores that are assumed not to contribute to fluid flow but are assumed to facilitate the diffusion of mass. The third porosity is the total porosity. Total porosity is greater than, or equal to, the diffusive porosity. In addition to the pores that compose the effective and diffusive porosities, total porosity includes the isolated pores that are assumed to be inert to fluid flow and diffusion.

4.1.10 Sources/Sinks

Several options are provided for describing sources and/or sinks of fluid and mass. Spatially variable sources and/or sinks can be specified by identifying their zones of occurrence. The strength of the source and/or sink can either be constant or vary with time. For mass, the sources can be limited by their inventory, their solubility, or both.

4.2 CONCEPTUAL FRAMEWORK

A mathematical model can provide only a simplified representation of the complex hydrogeologic system. A variably saturated groundwater system can be viewed at different scales--from the very small (molecular) to the very large (regional)--and its description will vary according to the scale of choice. Even when a scale has been selected, a number of conceptual assumptions have to be made regarding 1) the processes to be treated in the model, 2) the constitutive equations for these processes, 3) the level of coupling between the processes, 4) geometric representation of the physical system, and 5) the spatial and temporal variations of the parameters and boundary conditions. Decisions on all these factors produce what may be called a "conceptual model." A conceptual model for a given physical system is not unique but depends on the objective of the model and our level of understanding of the site at the moment in time when the model is formulated. For a numerical model to represent a given problem reasonably well, the mathematical model

embodied in it should be compatible with the user's conceptual model of the particular problem. For this reason, this section addresses the conceptual framework of the SUMO code and hence the conceptual models that this code can simulate.

4.2.1 Scale of Representation

Geologic media as well as the fluid and the constituents it transports (e.g., heat energy and chemical or radionuclide mass) can be visualized at many scales. The scale may be as small as a molecule or as large as a whole geologic region. Obviously, as the scale increases, some of the finer details important to the smaller scale are lost. Thus the mathematical representation depends on the scale of visualization. In the SUMO code, the characteristic scale may be called "macroscopic," which is much bigger than a molecule but much smaller then the regional scale. At this scale, both the medium and the fluid are considered to be continuous. In the context of transport through geologic media, this means that each pore is not distinguished individually and that the fluid and the medium effectively occupy the same space simultaneously (Bear 1972). Thus, pressure and concentration can be defined at any point in space, whether that point is occupied by the solid or the fluid. Obviously, such an assumption does not hold at the molecular and microscopic scales.

Another scale of interest is the scale at which the properties of the medium and the fluid vary. In the most general case, these properties can vary continuously in space. In practice, especially when recourse is taken to numerical solutions, as is the case in the SUMO code, it is more common to assume that the properties are piecewise-continuous (e.g., varying from computational cell to cell but constant across a cell). The model has a large amount of flexibility in this regard, and the user may choose any scale of variation, limited only by the system's available memory. Thus, the porous medium can be assumed to consist of layers, each layer having distinct properties, or the medium can be assumed to have arbitrary piecewise variation of properties. Similarly, fluid properties, such as density, can vary in a

piecewise fashion. However, once the computational domain is discretized, variation of all parameters is limited to the scale defined by that discretization.

In addition to being heterogeneous, the material properties can also be directionally dependent, i.e., anisotropic. However, consideration of anisotropy in the SUMO code is limited to the special case where the coordinate axes coincide with the principal directions of anisotropy. The case of arbitrarily oriented anisotropy has been omitted from the model.

4.2.2 Porosity

Three types of porosity are used for the rock and soil matrix in the SUMO code. The total porosity includes all of the pore space in the rock or soil matrix. This porosity is important for heat transfer by conduction. The effective or flow porosity reflects only interconnected nonstagnant pores. The effective porosity is used in calculating fluid velocity and convective transport of heat and mass. The diffusional porosity is equal to the effective porosity plus stagnant but interconnected pores. Diffusional porosity is of primary importance in heat and mass transfer by molecular diffusion. The total porosity is greater than or equal to the diffusional porosity, which is greater than or equal to the effective porosity.

The pores represented by the difference between the total porosity and the diffusional porosity are assumed to be filled with immobile liquid, even in partially saturated media. Although an alternative would be to assume that these pores are filled with air, this alternative is not included in the SUMO code. Thus, in the unsaturated flow problems, these pores contain residual moisture that is not drained even under extreme soil-moisture tensions. During mass transport, this residual porosity would further retard a contaminant pulse.

4.2.3 Sources and Sinks

In the majority of waste management problems, sources and sinks of fluid, heat energy, and chemical species are present within the domain of interest. Usually considerable effort is required to frame these sources and sinks into a form suited to the mathematical model. In the SUMO code, the sources and

sinks may be both spatially and temporally distributed. Special discretization in space and time may be required to accurately accommodate sources and sinks in such cases.

The simplest types of sources (and sinks) are constant in time and are specified at just a few discrete locations. Somewhat more complex are those that vary in time according to a regular function. For example, radioactively decaying sources vary exponentially in time. To account for time-varying or dynamic sources and sinks, the SUMO code allows a time-varying function to be approximated and entered in the form of a table.

The most complex type of source for chemical species available in the SUMO code is one that is specified in terms of its inventory (or initial mass) and solubility. The inclusion of this type of source requires that the concentration in the source region be maintained at a level that is consistent with the solubility of the inventory item(s) while the mass depletes continuously with time. Thus, with a sufficiently high initial mass, the concentration in the source region will be equal to its solubility, remaining constant at this level until the mass is depleted to a point low enough that this concentration cannot be maintained. At that point, the concentration in the source zone becomes a decreasing function of time.

4.2.4 Medium and Fluid Compressibility

In geologic media, the transfer of mechanical stresses between the fluid and the rock matrix occurs slowly. Mechanical equilibrium under applied stresses is maintained by a sharing of the load between the fluid and the rock. If the rock is significantly compressible, causing significant strains, then deformation of rock elements may have to be explicitly considered in modeling fluid flow and mass transport. In the SUMO code, the medium is considered to be only slightly compressible, so the deformation is assumed to be small enough that the position of rock elements can be considered to remain static. However, the compressibility of rock is not neglected entirely. Its effect is included in the "specific storage" term, which represents the amount of fluid expelled by a unit volume of the saturated medium when the stress on it is increased by a unit amount.

4.2.5 Darcy Flow

The flow of fluids in all elements of the geologic medium is described by Darcy's equation. In the detailed mathematical treatment given later, Darcy's equation is substituted for more complex momentum transfer equations. This simplifies the mathematical description of flow considerably.

Only the flow of liquids is considered explicitly in the current version of the SUMO code. In unsaturated media, the gas phase is considered to be at ambient pressure at all times and locations. This assumption is reasonable in most cases, but it may not hold in situations where the escape route of the gas is blocked, or where the gas is moving rapidly.

In the case of partially saturated flow, the volumetric moisture content and the hydraulic conductivity are assumed to be functions of the soil moisture tension. In many soils and rocks, these relations vary depending on whether liquid is imbibing into or draining from the soil/rock; in fact, they depend on its wetting/drying history. This hysteresis effect is not included in the formulation of the SUMO code.

4.2.6 Thermo-Mechanical Stresses

Mechanical stresses created by thermal loading are small and are neglected. Rock deformation resulting from thermal loading is assumed to have no effect on fluid flow.

4.2.7 Rock Sorption

A linear relationship for partitioning the species mass between the fluid and the rock matrix is included in the SUMO code. The partitioning is assumed to occur instantaneously (i.e., all kinetics are neglected). In addition, a perfect balance between adsorption and desorption is assumed (i.e., hysteresis is not considered). This is a highly simplified representation of the actual chemical phenomena.

4.2.8 Chain Decay

Radionuclides can be treated as single isotopes or can be embedded in decay chains. The current version of the SUMO code handles chains of any

length. If a decay chain is longer than four members, a temporary "scratch" file is used for intermediate storage; otherwise the length of the decay chain would be severely limited by computer memory.

4.2.9 Radionuclide Source Term

The radionuclide source term in the SUMO code is specified as a piecewise-varying function in time. The parent code PORFLO-3 offers two other options: a solubility-limited source term and an inventory-limited source term. These options have not been removed; however, they are not currently accessible to the SUMO user.

The chemical phenomenon of waste dissolution from the source term in fluid is considered to be instantaneous (i.e., as soon as the waste comes into contact with the fluid, it dissolves to the solubility limit).

4.3 THE GOVERNING EQUATIONS

Two governing equations form the mathematical basis of the SUMO code. The two dependent variables are fluid pressure (or hydraulic head) and solute concentration. The classic principles of mass, momentum, and energy conservation form the basis for the governing equations. A number of auxiliary equations, including the equation of state and the constitutive equations, supplement the governing equations. These auxiliary equations can be solved in three-dimensional Cartesian or radial coordinate systems. The theoretical basis for these equations is discussed in a number of textbooks (e.g., Bear 1972).

4.3.1 Equation for Fluid Flow

4.3.1.1 The Equation of Continuity

Consider an arbitrary control volume, V, that is bounded by a control surface S, as shown in Figure 4.1. The control volume is filled with geologic material of uniform properties. The solid geologic material has three types of pores:

1. those that are interconnected and through which fluid flow occurs--these pores constitute the effective (or flow) porosity, n_E

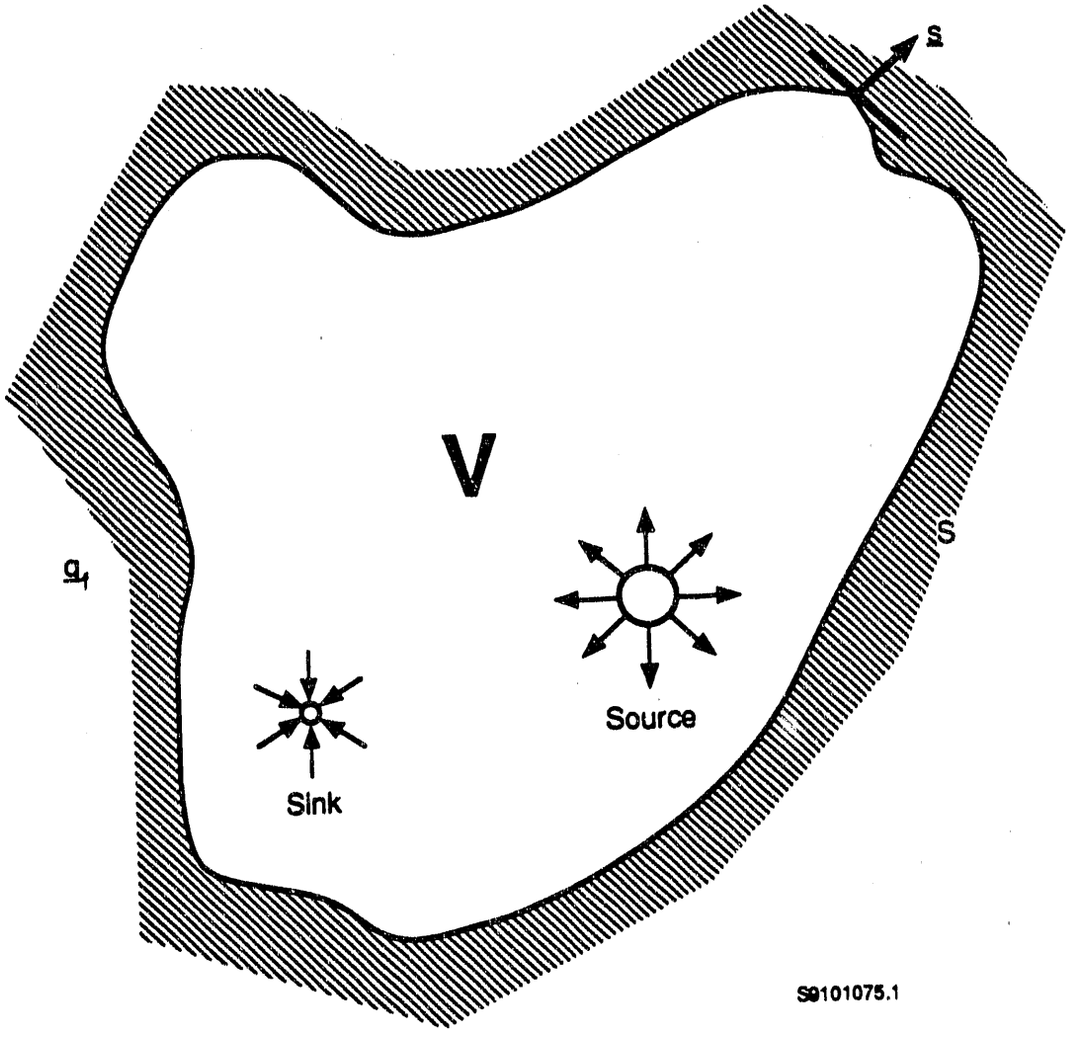

FIGURE 4.1. Illustration of the Control Volume Concept

2. those that do not participate in fluid flow but are filled with liquid and participate in heat and mass diffusion--the sum of the effective porosity and the porosity provided by these pores will be called the diffusive porosity, n_D

3. those that are isolated from other pores and participate in neither fluid flow nor heat and mass diffusion, but which conduct heat--the sum of the diffusive porosity and these isolated pores will be called the total porosity, n_T.

The effective porosity, n_E, in the control volume is assumed to be partitioned between liquid water and air. In the limiting condition, when n_E is determined entirely by liquid water, the medium becomes fully saturated. It is assumed that the solid, liquid, and air (when present) exist in continuous phases in the control volume.

The mass of the liquid, M, at time t in volume V is given by the integral

$$M = \int_V n_E \sigma \rho \, dV \tag{4.1}$$

where σ is the liquid saturation (volume of liquid water/diffusive porosity), and ρ is the liquid density. The mass may vary with time either because liquid crosses the surface, or because some fluid is directly injected into, or withdrawn from, the interior of V.

The incoming fluid flux, q_f, at the bounding surface, S, can be written as

$$q_f = - \int_S \rho \vec{V} \cdot \vec{s} \, dS \tag{4.2}$$

where $\vec{V}$ is the apparent velocity vector of fluid and $\vec{s}$ is an outward unit normal to the surface S. Note that the velocity in Equation (4.2) is not the pore-level fluid velocity, because it is assumed that flow occurs over the entire surface S, regardless of whether a particular point on it is occupied by a solid particle or a pore. This velocity is identified as the Darcy velocity and discussed further in the next section. By an application of the Gauss divergence theorem, Equation (4.2) becomes

$$q_f = - \int_V \vec{\nabla} \cdot (\rho \vec{V}) \, dV \tag{4.3}$$

Assuming an internal mass-injection rate of m per unit volume, the principle of mass conversion requires that

$$\partial_t \int_V \theta\, \rho\, dV + \int_V \vec{\nabla} \cdot (\rho \vec{V})\, dV = \int_V m\, dV \qquad (4.4)$$

where $\theta = n_D \cdot \sigma$ is the volumetric moisture content and ∂, is an abbreviation for $\partial/\partial x$. With the assumptions that the product $(\theta\rho)$ is at least once differentiable in time and deformation of V is small [see Abriola (1984) for a derivation with large deformations],

$$\int_V \left[\partial_t(\theta\, \rho) + \vec{\nabla} \cdot (\rho \vec{V}) - m\right] dV = 0 \qquad (4.5)$$

Because the volume V is assumed to be arbitrary, for Equation (4.5) to hold

$$\partial_t(\theta\, \rho) + \vec{\nabla} \cdot (\rho \vec{V}) - m = 0 \qquad (4.6)$$

Equation (4.6) is the continuity equation for liquid water. A similar continuity equation can be written for the gas phase. However, in the present version of the SUMO code, the gas phase is assumed to be at atmospheric pressure and passive. Therefore, its motion is not considered.

4.3.1.2 Darcy's Law for Flow Dynamics

The velocity vector, $\vec{V}$, m/sec, in Equation (4.6) must be obtained based on dynamic considerations. The principle of conservation of momentum would dictate use of the Navier Stokes equations (Bear 1972). However, for laminar, porous media flow with low velocities, the much simpler Darcy's equation is employed. Darcy's equation, which was originally derived from experimental observations, has since been derived from basic principles and the assumption that the inertial forces are negligible (Hassanizadeh 1986a,b). The equation is

$$\vec{V} = -\left(\underset{\approx}{k_s}\, k_r/\mu\right)\left[\vec{\nabla} p + \rho g\, \vec{\nabla} z\right] \qquad (4.7)$$

where $\underset{\sim}{k}_s$ = saturated intrinsic permeability tensor, m^2

k_r = (scalar) relative permeability, dimensionless

μ = fluid dynamic viscosity, kg/m•sec

p = thermodynamic pressure, $kg \cdot m/sec^2 \cdot m^2$

ρ = fluid density, kg/m^3

g = acceleration due to gravity, m/sec^2

z = coordinate in the vertical direction, m.

The x and y coordinates are assumed to lie in the horizontal plane.

In Equation (4.7), $\underset{\sim}{k}_s$ is a property of the porous medium. For anisotropic media, $\underset{\sim}{k}_s$ is a tensor of the second order. For the equations in the SUMO code, it is assumed that the coordinate directions and the principal directions of k_s coincide, so that all of the off-diagonal components of the $\underset{\sim}{k}_s$ tensor are zero. On the other hand, k_r is a scalar and equals unity for fully saturated media. For partially saturated media, $k_r < 1$. It has been assumed that gravitational acceleration acts in a direction opposite the positive direction of the z coordinate.

The limits of applicability of the Darcy flow equation for saturated flows have been explored by a number of investigators (Bear 1972; Cheng 1978). It is generally believed that the Darcy equation [Equation (4.7)] is applicable without appreciable error for flows with a Reynolds number of less than 10, where the Reynolds number is based on a representative "grain" size for the equivalent porous medium.

4.3.1.3 Governing Equation for Hydraulic Head

To maintain clarity, for initial development of the governing equation for hydraulic head we assume anisothermal conditions. The isothermal condition in the SUMO code is then represented by removing the appropriate terms from the final governing equation. Substitution of Equation (4.7) into Equation (4.6) gives the following equation for fluid pressure:

$$\partial_t(\theta\,\rho) - \vec{\nabla} \cdot \left[\left(\underset{\approx}{k_s}\, k_r\, \rho/\mu\right)\left(\vec{\nabla}p + \rho\, g\, \vec{\nabla}z\right)\right] - m = 0 \tag{4.8}$$

To simplify Equation (4.8), a new variable, P, is defined as

$$P = p/(\rho^* g) + z - z^* \tag{4.9a}$$

or

$$P = -\psi + z - z^* \tag{4.9b}$$

where ρ is the reference fluid density and pressure (kg/m^3), z^* is an arbitrarily defined datum from which z is measured (m), and ψ is the soil-moisture tension (m). The datum may be arbitrarily selected, but it is commonly the water table, ground surface, or mean sea level. Although z^* may be assigned any numerical value, it is often convenient to give it a zero value by locating the origin of the coordinate axes at the datum.

The new variable, P (in units of length), is a normalized pressure that is equivalent to a hydraulic head defined with respect to the reference density ρ^*. However, P is not a true potential function because it is not defined with respect to the local fluid density. The thermodynamic pressure, p, is negative (i.e., it is less than atmospheric pressure, which is taken to be zero) in partially saturated media and is positive in fully saturated media. For partially saturated systems, soil-moisture tension, ψ, is defined as in Equation (4.9b). The soil-moisture tension ψ is defined only when $0 < \sigma < 1$.

To obtain a more convenient form of Equation (4.8), the time derivative is expanded to

$$\partial_t(\theta\,\rho) = \theta\,\partial_t(\rho) + \rho\,\partial_t(\theta) \tag{4.10}$$

The fluid density, ρ, is in general a function of pressure (p) and temperature (T), i.e.,

$$\rho = \rho(p,T) \tag{4.11a}$$

and therefore

$$\partial_t(\rho) = \partial_p(\rho)|_T \partial_t(p) + \partial_T(\rho)|_p \partial_t(T) \tag{4.11b}$$

Defining fluid compressibility as

$$\beta_p = (1/\rho)\ \partial_p(\rho)|_T \tag{4.12a}$$

and the fluid thermal expansion coefficient as

$$\beta_T = -(1/\rho)\ \partial_T(\rho)|_p \tag{4.12b}$$

Equation (4.11b) becomes

$$\partial_t(\rho) = \left[\beta_p\ \partial_t(p) - \beta_T\ \partial_t(T)\right] \rho \tag{4.13a}$$

or in terms of P

$$\partial_t(\rho) = \left[\beta_p\ \rho^*\ g\ \partial_t(P) - \beta_T\ \partial_t(T)\right] \rho \tag{4.13b}$$

The volumetric moisture content, θ, in Equation (4.10) is a product of diffusive porosity (n_D) and saturation (σ). For saturated media, $\sigma = 1$ (constant), and n_D is a much stronger function of p than of T. For unsaturated media, n_D remains constant and σ varies. Thus, for saturated

media ($\sigma = 1$), and neglecting temperature effects on n_D, the variation of θ may be written as

$$\partial_t(\theta) = \partial_t(n_D) = \partial_p(n_D)\ \partial_t(p) \tag{4.14a}$$

For unsaturated media it can be written as

$$\partial_t(\theta) = n_D\ \partial_p(\sigma)\ \partial_t(p) \tag{4.14b}$$

Defining porous medium compressibility as

$$\alpha_p = \partial_p(n_D) \tag{4.15}$$

Equation (4.14a) becomes, in terms of P,

$$\partial_t(\theta) = \alpha_p\ \rho^*\ g\ \partial_t(P) \tag{4.16a}$$

while Equation (4.14b), in terms of P, takes the form

$$\partial_t(\theta) = n_D\ \partial_p(\sigma)\ \partial_t(P) \tag{4.16b}$$

Substituting Equations (4.13b) and (4.16a) in Equation (4.10), for $\sigma = 1$

$$\partial_t\ (\theta\ \rho) = (\alpha_p + n_D\ \beta_p)\ \rho\ g\ \rho^*\ \partial_t(P) - n_D\ \rho\ \beta_T\ \partial_t(T) \tag{4.17a}$$

Similarly, for $\sigma < 1$ and using Equation (4.16b),

$$\partial_t(\theta, \rho) = n_D\ \partial_p(\sigma)\ \rho\ \partial_t(P) - \theta\ \rho\ \beta_T\ \partial_t(T) \tag{4.17b}$$

On the right-hand side of Equation (4.17), the first term is a "storage" term; the second term depends on the time-variation of temperature. For fully saturated media ($\sigma = 1$), the coefficient of specific storage is defined as

$$S_s = (\alpha_p + n_D \beta_p) \rho \rho^* g \tag{4.18a}$$

The units of S_s are (1/L) where L denotes unit of length (e.g., feet or meters). For partially saturated media ($\sigma < 1$), the coefficient of specific storage is

$$S_s = n_D \partial_p(\sigma) \tag{4.18b}$$

Commonly, S_s for unsaturated media ($\sigma < 1$) is written in terms of ψ, i.e.,

$$S_s = - \partial_\psi(\theta) \tag{4.18c}$$

For unsaturated media, the $\theta \cdot \psi$ relationship is known as the soil (or rock) characteristic curve and is determined experimentally. In saturated media, the specific storage can be either directly specified or estimated from the liquid and media compressibilities. In the SUMO code, S_s is specified. The reason for specifying S_s (rather than compressibilities) for saturated media is that S_s is usually estimated directly from the analysis of pumping test data. Thus, in terms of S_s, the time derivative of Equation (4.8) becomes

$$\partial_t(\theta \rho) = \rho S_s \partial_t(P) - \theta \rho \beta_T \partial_t(T) \tag{4.19}$$

Now substituting Equation (4.9a) into the remaining term of Equation (4.8),

$$\rho S_s \partial_t(P) = \vec{\nabla} \cdot \left[\left(\underset{\approx}{k}_s k_r \rho \rho^* g/\mu \right) \left(\vec{\nabla} P + (R-1) \vec{\nabla} z \right) \right] + \theta \beta_T \partial_t(T) + m \tag{4.20}$$

where

$$R = \rho/\rho^* \tag{4.21a}$$

is the ratio of fluid densities. Setting hydraulic conductivity at reference fluid density as

$$\underset{\approx}{K} = \underset{\approx}{k}_s \, \rho^* \, g/\mu^* \tag{4.21b}$$

the buoyancy gradient as

$$B = R - 1 \tag{4.21c}$$

the viscosity ratio with reference viscosity μ^* as

$$\xi = \mu^*/\mu \tag{4.21d}$$

and the volumetric source term as

$$m_v = m/\rho^* \tag{4.21e}$$

Equation (4.20) becomes

$$R \, S_s \, \partial_t(P) = \vec{\nabla} \cdot \left\{ \left(R \, \xi \, \underset{\approx}{K} \, k_r \right) \left(\vec{\nabla} P + B \vec{\nabla} z \right) \right\} + \theta \, R \, \beta_T \, \partial_t(T) + m_v \tag{4.22}$$

Because conditions are isothermal, and $\partial_t(T)$ are both zero, Equation (4.22) becomes

$$S_s \, \partial_t(P) = \vec{\nabla} \cdot \left\{ \underset{\approx}{K} \, k_r \, \vec{\nabla} P \right\} + m_v \tag{4.23}$$

Equation (4.23) governs pressure for single-phase fluid flow under isothermal conditions. The coefficient of specific storage, S_s, and the hydraulic conductivity tensor, K, in Equation (4.22) are at the reference values of fluid density (ρ^*) and viscosity (μ^*) and are therefore constant. In its general form, considering both Cartesian and cylindrical coordinate systems, this equation is

$$S_s\, \partial_t P = (1/r)\, \partial_x\left(rK_x \delta_x P\right) + \partial_y\left(K_y \partial_y P\right) + \partial_z\left(K_z \partial_z P\right) + m_v \qquad (4.24)$$

In Cartesian coordinates, $r \to \infty$; in cylindrical coordinates, r is the radial distance and its direction coincides with the x coordinate.

4.3.1.4 Equations for Velocity Components

The equations for the Darcy velocity are now written as

$$U = - K_x\, \partial_x P \qquad (4.25a)$$

$$V = - K_y\, \partial_y P \qquad (4.25b)$$

$$W = - K_z\, \partial_z P \qquad (4.25c)$$

where K_x, K_y, and K_z are the principal components of the hydraulic conductivity tensor, $\underset{\sim}{K}$, along the x, y and z directions, respectively.

The average fluid velocity in the pores, known as the pore velocity, is obtained by dividing the Darcy velocity by the effective porosity, n_E. These pore velocity components are given by

$$u = U/n_e \qquad (4.26a)$$

$$v = V/n_e \qquad (4.26b)$$

$$w = W/n_e \tag{4.26c}$$

4.3.2 Equation for Mass Transfer

4.3.2.1 Conservation of Chemical Species

The derivation of an equation for conservation of chemical species parallels that for the conservation of heat. From the principle of mass conservation, it follows that the rate of change of the mass of a chemical species in a control volume V must be equal to the sum of the rate at which the species is added through the boundary S of the control volume plus the rate of species generation inside the control volume (Figure 4.1) minus the rate at which the species are consumed through chemical reaction or radioactive decay.

The rate of change of mass (M_c) of a species in control volume V is

$$M_c = \partial_t \left[\int_V C_e \, dV\right] \tag{4.27}$$

where C_e is the mass density (or concentration) of the chemical species in the fluid-solid matrix per unit volume.

The rate at which the species enters the control volume, $\vec{J}_c$, is given by

$$\vec{J} = -\int_S (\vec{V}\, C + \vec{J}_c + \vec{J}_D) \cdot \vec{s}\, dS \tag{4.28}$$

where C is the mass of the species in the fluid per unit volume of fluid, $\vec{J}_c$ is the species flux resulting from diffusion, and $\vec{J}_D$ is the flux resulting from dispersion (Bear 1972, p. 643). Other forms of species exchange, such as those caused by the Soret effect (thermal-related) are assumed to be negligible.

With S_c as the rate of mass-species generation resulting from direct injection and chemical reaction per unit volume of the system, the rate of increase of the species (E_c) in the control volume is

$$E_c = \int_V S_c \, dV \tag{4.29}$$

With R_c as the rate of reaction or decay, the rate of disappearance of the chemical species (e_c) caused by either radioactive decay or an Arrhenius-type chemical reaction in the fluid-solid matrix is given by

$$e_c = -\int_V R_c \, C_e \, dV \tag{4.30}$$

Combining Equations (4.27) through (4.30) with the Gauss divergence theorem and the fact that the V is arbitrary leads to the governing equation for the conservation of chemical species

$$\partial_t C_e + \vec{\nabla} \cdot \left(\vec{V} \, C \right) = -\vec{\nabla} \cdot \left(\vec{J}_c + \vec{J}_D \right) + S_c - R_c \, C_e \tag{4.31}$$

4.3.2.2 Governing Equation for Species Concentration

The quantity C_e in Equation (4.31) depends on how the chemical species is partitioned between the solid matrix and the fluid. Denoting the fluid and solid concentrations by C and C_s, respectively, C_e becomes

$$C_e = \theta \, C + (1 - n_T) \, C_s \tag{4.32}$$

where it is assumed that no chemical species are contained in the isolated pores (n_T - n_D) (i.e., the processes of advection, diffusion, and dispersion do not exchange mass in these pores).

In the SUMO code, adsorption-desorption processes are responsible for the partitioning of the radionuclide mass between the fluid and the solid phases. In general, descriptions of the sorption process may be classified as 1) local equilibrium models and 2) disequilibrium models. In either kind of model, sorption occurs at the interface between the liquid film and solid surface.

The disequilibrium models assume a time-dependent mass exchange between the immobile and mobile liquids, and between the liquids and the solid (Goltz and Roberts 1988). The disequilibrium models are more complex and assume a certain geometry for the immobile region and diffuse mass from the immobile to the mobile region (Sudicky and Frind 1982). The disequilibrium models result in two concentration equations, one each for the mobile and the immobile regions, and require extra parameters to characterize the processes.

The local equilibrium models assume that the solid and liquid phases are in continuous reversible equilibrium (i.e., any change in the concentration in the liquid is accompanied by an instantaneous corresponding change in the concentration in the solid phase). Also, the concentration in the mobile and immobile fluid regions is assumed to be the same. In the simplest of these models, which is included in the SUMO code, the solid surface available for sorption is assumed to be inversely proportional to the density of the solids. This same model assumes that the sorption process is described by a linear Freundlich isotherm (Freeze and Cherry 1979, p. 403), such as that for saturated media

$$C_s = \rho_s \, k_d \, C \qquad (4.33a)$$

where k_d is variously called the distribution, sorption, or partition coefficient. Equation (4.33a) implies that the adsorption reaction is fully reversible, that is, that as the concentration C in the solution increases, the mass adsorbed by the solids is released back into the solution.

One additional assumption regarding the extent of wetted surface under variable saturation is required before Equation (4.33a) can be used for unsaturated media. One possible assumption is that the wetting fluid will wet all of the available solid surface, regardless of liquid saturation. With this assumption, which appears to be appropriate for higher saturations, no modification to Equation (4.33a) is required. On the other hand, especially at lower saturations, one could assume that some of the pores are dry and that therefore the solid surface available for sorption is proportional to saturation. With the latter assumption, Equation (4.33a) is modified to

$$C_s = \sigma \rho_s k_d C \qquad (4.33b)$$

Substitution of Equation (4.33a) into (4.32) gives

$$C_e = \theta C + (1 - n_T) \rho_s k_d C \qquad (4.34)$$

which can be written

$$C_e = \theta C \left[1 + \frac{(1-n_T)\rho_s k_d}{\theta}\right] \qquad (4.35a)$$

Substitution of Equation (4.33b) in (4.32) gives

$$C_e = \theta C \left[1 + \frac{(1-n_T)\rho_s k_d}{n_D}\right] \qquad (4.35b)$$

The quantity within the brackets in Equation (4.35) is called the retardation coefficient, R_D. In terms of R_D, Equation (4.35) takes the form

$$C_e = \theta R_D C \qquad (4.36)$$

In moving fluid, R_D represents the ratio between the migration velocities of the fluid and the radionuclide. In general, it is analogous to specific storage in the flow equation. It represents the capacity of the medium to store the chemical species. In the present version of the SUMO code, the more general definition of R_D provided by Equation (4.35b) is used. This is because at higher saturations, $\theta \rightarrow n_D$ and the equation is identical to Equation (4.35a); otherwise, at lower saturations, Equation (4.35b) is more appropriate.

From Fick's Law, the diffusion flux term is written as

$$\vec{J}_C = - \theta D_M \vec{\nabla} C \tag{4.37}$$

where D_M is the molecular diffusivity of species in the fluid, m^2/sec. In saturated media, $\theta = n_D$, and the entire diffusive porosity participates in mass exchange through molecular diffusion.

The mechanical dispersion term is written as (Bear 1972, p. 646)

$$\vec{J}_D = - \eta_D \underset{\approx}{D} \vec{\nabla} C \tag{4.38}$$

where $\underset{\approx}{D}$ is a second-order tensor of principal diagonals of fluid dispersion, m^2/sec.

Substitution of Equations (4.32) through (4.36) into Equation (4.31) gives the species concentration equation

$$\partial_t \left(\theta R_d C\right) + \vec{\nabla} \cdot \left[\vec{V} C\right] = \vec{\nabla} \cdot \left[\left(\theta D_M + \eta_D \underset{\approx}{D}\right) \vec{\nabla} \cdot C\right] + S_c - \theta R_d R_c C \tag{4.39}$$

In terms of the generalized Cartesian or cylindrical three-dimensional coordinates of the SUMO code, this equation is

$$\begin{aligned} &\partial_t(\theta R_d C) + (1/r)\, \partial_x(r U C) + \partial_y(V C) + \partial_z(W C) = \\ &(1/r)\partial_x\left[r(\theta D_M + \eta_D D_x)\, \partial_x C\right] + \partial_y[(\theta D_M + \eta_D D_y)\partial_y C] + \\ &\partial_z[(\theta D_M + \eta_D D_z)\partial_z C] + S_c - \theta R_d R_c C \end{aligned} \tag{4.40}$$

4.3.3 Coupling Terms

There is a one-way coupling between the concentration equation and the pressure equation; that is, while the pressure field has an impact on the concentrations through the velocity field, the reverse is not true.

The concentration equation is coupled to the pressure equation through the convective velocities. The strength of this coupling depends on the magnitudes of the velocities. The ratio of the convective to the dispersive transport of species is known as the Peclet number. How the concentration equation is solved depends largely on the value of the Peclet number. In the absence of convective transport, the equation is fully parabolic. When the transport by dispersion and diffusion is negligible compared to that from convection, the equation becomes hyperbolic. The Peclet number plays a crucial role in proper discretization of these equations.

4.3.4 General Form of the Governing Equations

Both governing equations [Equations (4.23) and (4.40)] have similar mathematical structures. They are second-order, coupled, parabolic equations and may be represented by the general transport equation

$$a\,\partial_t \Gamma + (1/r)\partial_x(r\,b\,U\,F - r\,c_x\,\partial_x F) + \partial_y(b\,V\,F - c_y\,\partial_y F) + \partial_z(b\,W\,F - c_z\,\partial_z F) = S_F - s_F\,F \tag{4.41}$$

where F is the dependent variable (P or C) and the various other coefficients and source terms are as summarized in Table 4.1. In later discussions of the solution of the governing equations, reference will be made to Equation (4.41) and its generic dependent variable, F.

4.3.5 Auxiliary Equations

In addition to the governing equations just described, several auxiliary equations are needed for complete descriptions of the flow and transport processes. These auxiliary equations include descriptions of the initial and boundary conditions and equations of state that describe the dependence of the fluid and solid properties on pressure, saturation, and mass concentration.

TABLE 4.1. Coefficients and Source Terms of the General Transport Equation for the Two Dependent Variables of the SUMO Code

F	a	b	c_x	c_y	c_z	S_F	s_F
P	S_s	0	K_x	K_y	K_z	m_v	0
C	θR_d	1	$\theta D_M + \eta_D D_x$	$\theta D_M + \eta_D D_y$	$\theta D_M + \eta_D D_z$	S_C	$\theta \rho R_d R_C$

4.3.5.1 Fluid Properties

For most applications of the SUMO code, the primary fluid is liquid water. For water at 100°C, compressibility ($m \cdot sec^2/kg$) is on the order of 10^{-6}; therefore changes in water density resulting from pressure variations are neglected in the SUMO code. However, if the fluid of interest is a gas, the pressure dependence of density may have to be accounted for.

4.3.5.2 Hydraulic Properties of Saturated Media

The two main parameters in the saturated flow equation [Equation (4.23)] are the coefficient of specific storage and the hydraulic conductivity tensor. Therefore the reference values of S_s and K must be specified for application of this equation to saturated flow.

4.3.5.3 Hydraulic Properties of Partially Saturated Media

Though a single governing equation [Equation (4.23)] was written for both saturated and unsaturated flow, there are two major differences between these two types of flow. In saturated flows, $k_r = 1$ and is therefore eliminated from Equation (4.23). It cannot be eliminated for unsaturated flows, where k_r depends on saturation, σ, and is less than 1. Also, while S_s is directly specified for saturated flow, this is not possible for unsaturated flow. The value of S_s is the (negative) slope of the soil-moisture tension curve and therefore also depends on saturation. As will be discussed below, saturation depends on pressure head, so in the unsaturated flow case the flow equation is nonlinear.

Because of the simultaneous presence of both liquid (i.e., water) and gas (i.e., air) in unsaturated media, liquid-gas interfaces are formed throughout. These concave interfaces extend from grain to grain across each pore channel.

The radius of curvature on each interface reflects the surface tension on that interface. Liquid in the unsaturated zone is held under these surface tension forces. The greater this force, the smaller the amount of moisture held. The relation between the tension forces and moisture content is dependent on soil (or rock) particle sizes and their arrangements in the aggregate. This relation is often measured in the laboratory and can be measured directly in the field. It is then specified as a basic hydraulic property of the medium. The relation $\theta \cdot \psi$ is hysteretic, i.e., it has different shapes for wetting and drying episodes. However, hysteretic effects are neglected in the SUMO code.

Soil-moisture retention ($\theta \cdot \psi$) curves can be specified either as an analytic function or as a table. Two options for analytic functions are provided in SUMO. These are

1. The van Genuchten (1978) relation

$$\theta^* = [1 + (\psi/\alpha)^n]^{-m}, \; h < 0 \tag{4.42a}$$

$$\theta^* = 1, \; h \geq 0 \tag{4.42b}$$

where α, m, and n are empirical constants and θ^* is the normalized water content (or saturation), which is defined as

$$\theta^* = \frac{\theta - \theta_r}{n_D - \theta_r} \tag{4.43}$$

in which θ_r is the residual (or immobile) moisture content. In the SUMO code, because of the way the diffusive and effective porosities have been defined,

$$\theta_r = n_D - n_E \tag{4.44a}$$

The coefficients m and n are related through the equation

$$m = (1 - 1/n) \tag{4.44b}$$

2. The Brooks and Corey (1966) relation

$$\theta^* = (\psi/\psi^*)^{-\beta}, \; h < -\psi^* \tag{4.45a}$$

$$\theta^* = 1, \; h \geq -\psi^* \tag{4.45b}$$

where ψ^* is the air entry head and β is an empirical constant.

From Equation (4.45a), it is apparent that when $\psi = \psi^*$, $\theta^* = 1$ (i.e., full saturation is approached as $\psi \rightarrow \psi^*$). Thus, for $\psi \leq \psi^*$, the soil is saturated. No such cutoff point is stipulated in the van Genuchten relation.

In addition to the analytical functions embedded in the SUMO code, any arbitrary soil-moisture curve can be specified as a table of $\theta \cdot \psi$ values. For any ψ that is not included in the table, the corresponding value of θ is obtained through linear interpolation.

Measurement of unsaturated hydraulic conductivity in situ is difficult. Therefore, unsaturated hydraulic conductivities [or relative hydraulic conductivities, k_r in Equation (4.7)] are usually estimated based on certain physical attributes of the porous medium (e.g., pore radii, porosity, and tortuosity factor). The simplest formula for k_r is based on generalization of Kozney's approach (Brutsaert 1967)

$$k_r = (\theta^*)^{\gamma} \tag{4.46}$$

where γ is an empirical coefficient. A value of $\gamma = 3.5$ has been found to agree well with experimental observations (Averjanov 1950).

Other more complex formulae for k_r have been derived using basic theory of flow in capillaries. Burdine (1953) derived the relation

$$k_r = (\theta^*)^2 \int_0^{\theta^*} \frac{1}{\psi^2}\, d\theta \Big/ \int_0^1 \frac{1}{\psi^2}\, d\theta \tag{4.47}$$

Substituting the van Genuchten relation, Equation (4.42), into (4.47),

$$k_r(\theta^*) = (\theta^*)^2\left[1 - (1 - \theta^{*1/m})^m\right] \tag{4.48a}$$

If the Brooks and Corey moisture retention curve, Equation (4.45), is used instead of the van Genuchten relation, then

$$k_r(\theta^*) = \theta^{*(3+2/\beta)} \tag{4.48b}$$

By setting $\beta=[2/(\gamma-3)]$, Equation (4.48b) reduces to the simple formula given in Equation (4.46).

The formulae for k_r can also be written in terms of ψ. The formula corresponding to the van Genuchten moisture retention curve is

$$k_r(\psi) = \frac{1-(\psi/\alpha)^{n-2}\,[1+(\psi/\alpha)]^{-m}}{[1+(\psi/\alpha)^n]^{2m}} \tag{4.49a}$$

while for the Brooks and Corey moisture retention curve, it is

$$k_r(\psi) = (\psi/\psi^*)^{-2-3\beta} \tag{4.49b}$$

Mualem (1976) used a pore-size distribution in a modified form of the Childs and Collis-George (1950) relation to obtain

$$k_r = (\theta^{*1/2}) \int_0^{\theta} \frac{1}{\psi}\, d\theta \Big/ \int_0^1 \frac{1}{\psi}\, d\theta. \tag{4.50}$$

Using Equation (4.50), the formula for k_r in terms of θ is, for the van Genuchten relation,

$$k_r(\theta) = \theta^{*1/2}\left[1 - (1 - \theta^{*1/m})^m\right]^2 \qquad (4.51a)$$

and for the Brooks and Corey relation,

$$k_r(\theta^*) = \theta^{*(5/2 + 2/\beta)} \qquad (4.51b)$$

The corresponding relations in terms of ψ become

$$k_r(\psi) = \frac{\left\{1-(\psi/\alpha)^{n-1}\,[1+(\psi/\alpha)^n]^{-m}\right\}^2}{[1+(\psi/\alpha)^n]^{m/2}} \qquad (4.52)$$

and

$$k_r(\psi) = (\psi/\psi^*)^{-2-5\beta/2} \qquad (4.53)$$

Although other formulae for relative permeability are available from the literature, only these are used in the SUMO code. In addition, an option is available to specify either the $k_r \cdot \theta$ or the $k_r \cdot \psi$ curve in tabular form. If a table is provided, linear interpolation is used to obtain the value of k_r for any value of ψ or θ.

4.3.5.4 Mechanical Dispersion

Transport by mechanical dispersion is caused by the nature of flow in the interconnected pores of the medium (Bear 1972, p. 579). This phenomenon occurs only in moving fluid and is the result of the velocity variations at smaller scales that are not resolved by the model.

In general, the coefficient of mechanical dispersion, D, is a second-order symmetric tensor (Bear 1972, p. 605), and a function of both the medium and the fluid. To simplify this term, a set of material parameters called

dispersivities are defined. Based on experimental evidence, longitudinal and transverse dispersivities are defined to represent the process of mechanical dispersion in the direction of the average fluid velocity and the directions orthogonal to it, respectively. The x, y, and z coordinates in the SUMO code are assumed to coincide with the principal directions of the hydraulic conductivity. In contrast, the average fluid velocity does not generally coincide with the x, y, or z axis. To obtain the components of the dispersion coefficient in the directions of the axes, the following equations suggested by Scheidegger (1961) are used:

$$D_x = \alpha_L U' + \alpha_T (V'+W') \tag{4.54a}$$

$$D_y = \alpha_L V' + \alpha_T (W'+U') \tag{4.54b}$$

$$D_z = \alpha_L W' + \alpha_T (U'+V') \tag{4.54c}$$

where α_L and α_T are the longitudinal and transverse dispersivities, respectively, and

$$U' = U^2/\xi \tag{4.55a}$$

$$V' = V^2/\xi \tag{4.55b}$$

$$W' = W^2/\xi \tag{4.55c}$$

where

$$\xi = (U^2 + V^2 + W^2)^{1/2} \tag{4.55d}$$

4.3.5.5 Boundary and Initial Conditions

The boundary conditions for the three governing equations can be represented in general as

$$- a\partial F/\partial N = b(F - F_o) + c \qquad (4.56)$$

where F represents P or C, depending on which governing equation is under consideration; N is a direction normal to the boundary; and a, b, c, and F_o are constants. By selecting appropriate values of a, b, c, and F_o, three types of boundary conditions can be represented by Equation (4.56). These boundary conditions are

1. Dirichlet boundary condition: Obtained by specifying that a = c = 0, and b = 1. In other words, this condition is represented by

$$F = F_o \qquad (4.57a)$$

   where F_o is the specified value of F at the boundary. This boundary condition is also known as a fixed head or concentration boundary condition for the P and C equations, respectively.

2. Neumann boundary condition: Obtained by specifying that b = 0. In this case, a is equal to either the hydraulic conductivity or the dispersion coefficient for the fluid flow and mass transport equations, respectively. Thus, this boundary condition is

$$- a\partial F/\partial N = c \qquad (4.57b)$$

   where c is the specified flux of fluid or chemical species per unit surface area of the boundary.

3. Mixed (or radiation) boundary condition: Obtained by substituting c = 0 in Equation (4.56), resulting in

$$- a\partial F/\partial N = b(F - F_o) \qquad (4.57c)$$

   In this case, a has the same meaning as for Neumann boundary condition; b is the fluid or mass-transfer coefficient; and F_o is the equilibrium value of F. Using the fluid flow equation as an example, F_o may be specified as the steady-state pressure.

The initial condition can be any reasonable value of the variable under consideration. For ease of specification, linearly varying initial and boundary conditions are allowed, i.e.,

$$F = a + bx + cy + dz \qquad (4.58)$$

where a, b, c, and d are constants, and x, y, and z are the coordinates of a point either in the interior of the domain or on its boundary.

4.4 SOLUTION OF GOVERNING EQUATIONS

The numerical solution to the governing and auxiliary equations described in Section 4.3 is obtained in two steps: 1) using the nodal point integration method, the governing equations are discretized into a set of algebraic equations; and 2) the matrix of algebraic equations is solved. Alternate choices for "integration profiles" in step 1 and different "matrix solution" methods in step 2 provide adaptability to problems of increasing difficulty. This section is devoted to a discussion of these two steps. The generic transport equation given in Equation (4.41) provides a convenient basis for these discussions and will be referred to throughout this section.

4.4.1 Discretization Method

To transform the differential equations into their algebraic analogues, the method of Nodal Point Integration (NPI) is employed (Gosman et al. 1969; Patankar 1980; Runchal 1969). The NPI method is also referred to in the literature as the "finite-volume" or the "integrated finite-difference" method (Edwards 1969; Narasimhan and Witherspoon 1976). The method does not involve direct replacement of the governing equation derivatives with numerical ones, as would conventional finite-difference schemes. Rather, the basic principle of the NPI method is to analytically integrate assumed polynomial profiles for the dependent variable [F in Equation (4.41)] over a time step and a finite volume that is located within the overall calculation domain. This integration approach bears some resemblance to the finite-element method. However, it also differs from the finite-element method, in that it intrinsically maintains (approximately) the mass and material balances at the local scale of an element, leading to a potentially more accurate numerical formulation than that of the finite-element method.

The NPI method implemented in the SUMO code uses hybrid profile functions (Runchal 1972). These functions are constructed after the spatial domain is discretized into a set of finite volumes by imposing a grid.

4.4.1.1 The Spatial Grid

The spatial grid used in the SUMO code is constructed with three mutually perpendicular surfaces. In the Cartesian coordinate system, these surfaces are planes that correspond to the right-handed orthogonal (x,y,z) coordinates. In both coordinate systems, the z axis is taken to be vertical and positive in the upward direction. Except as noted otherwise, the (x,y,z) notation will be used. The discussion can also relate, however, to the (r,θ,z) system by substituting r for x and θ for y. The grids are shown in Figures 4.2 and 4.3 for Cartesian and cylindrical coordinates, respectively. The dashed lines represent the grid surfaces. Horizontal cross sections through these grids are shown in Figures 4.4 and 4.5.

In the following discussion, the grid surfaces (or grid lines, in two dimensions) are identified by the indices I, J, and K the x, y, and z directions, respectively. Over the domain, these grid surfaces are numbered from 1 to IMAX, 1 to JMAX, and 1 to KMAX in the x, y, and z directions, respectively. Grid nodes are points where the three mutually perpendicular surfaces intersect. The total number of nodes (internal plus boundary) in the domain is thus IMAX•JMAX•KMAX.

The actual integration and solution of the governing equations of the SUMO code proceeds by reference not to the grid surfaces or nodes but to the elements. These elements are also referred to as the control volumes or cells. Each internal grid node has an associated element or control volume, and the boundary grid nodes are on the edges of elements. The control volume for each node is obtained by drawing surfaces that are located exactly midway between the grid surfaces. The cell surfaces are drawn as solid lines in Figures 4.2 through 4.5. Because the grid surfaces may be unevenly spaced, the control volume sizes associated with nodes may vary from one node to another. The actual physical domain of a problem is thus completely covered by a discrete number of contiguous elements. The boundary nodes surrounding the physical domain are employed to impose boundary conditions on the problem.

A typical cell, or element, is shown for the Cartesian grid system in Figure 4.6 and for the cylindrical grid in Figure 4.7. A horizontal cross section through the Cartesian element of Figure 4.6 is shown in Figure 4.8.

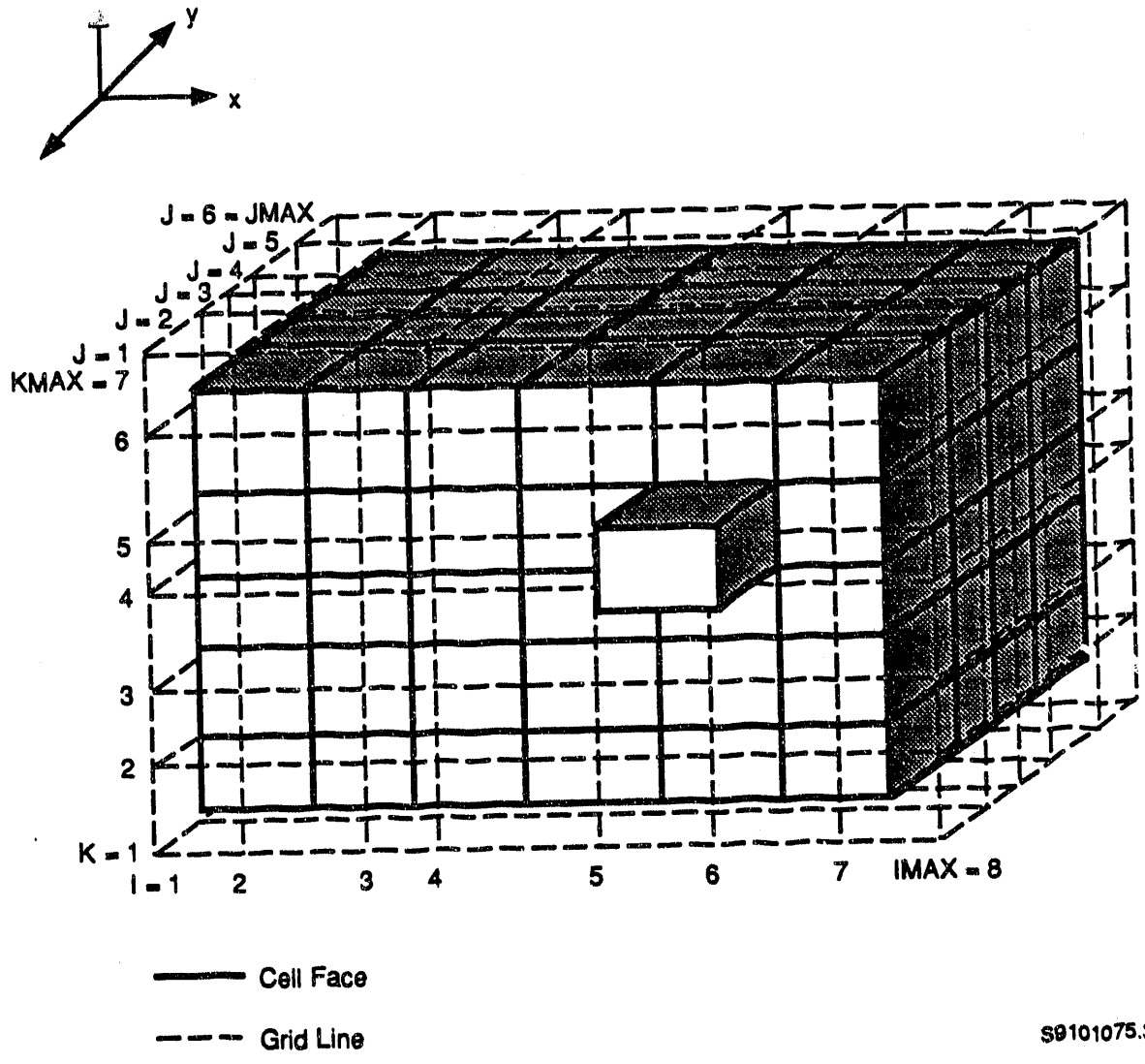

FIGURE 4.2. Illustration of the Cartesian Grid Arrangement

The node, P, enclosed in the cell has the grid indices (I,J,K). The value of the dependent variable F at node P (and all internal nodes) is assumed to be influenced by the six nodes that are the node's immediate neighbors; these are denoted by E (east), W (west), N (north), S (south), U (up), and D (down). The respective indices for these nodes are (I+1,J,K), (I-1,J,K), (I,J+1,K), (I,J-1,K), (I,J,K+1), and (I,J,K-1). The corresponding cell faces are denoted

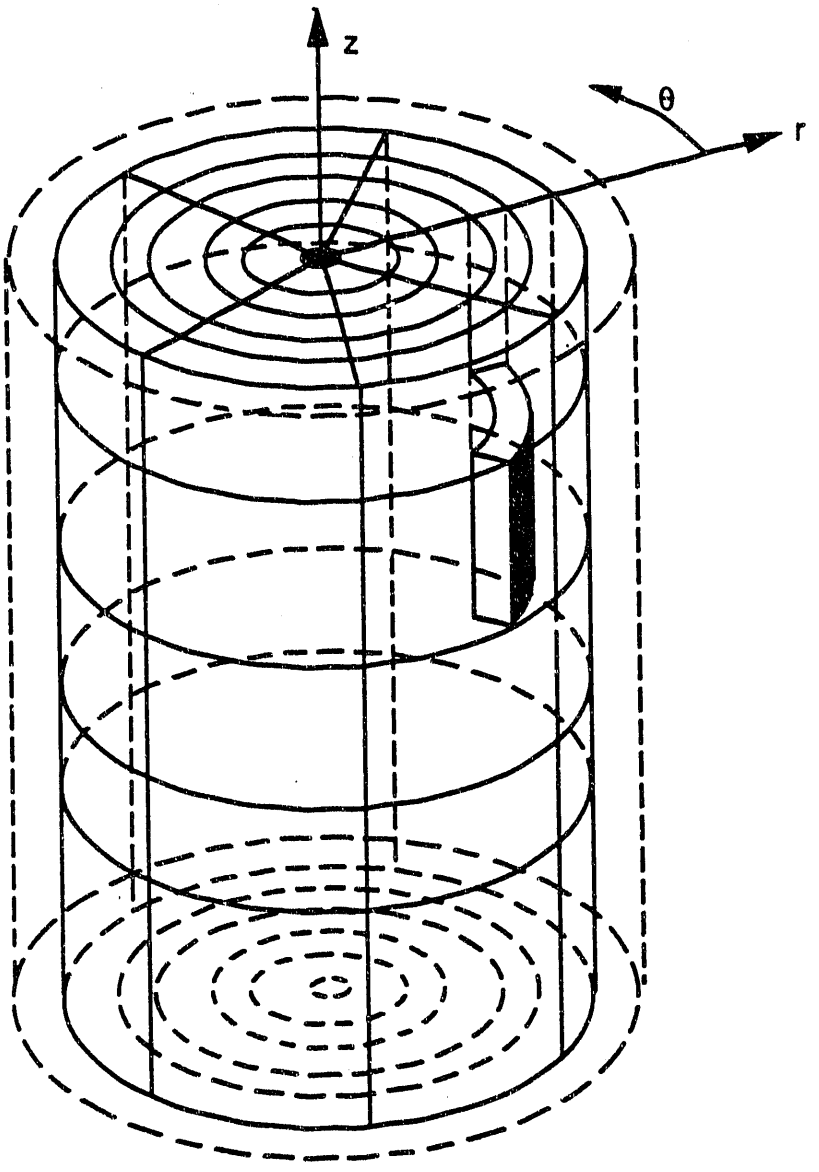

S9101075.2

FIGURE 4.3. Illustration of the Cylindrical System

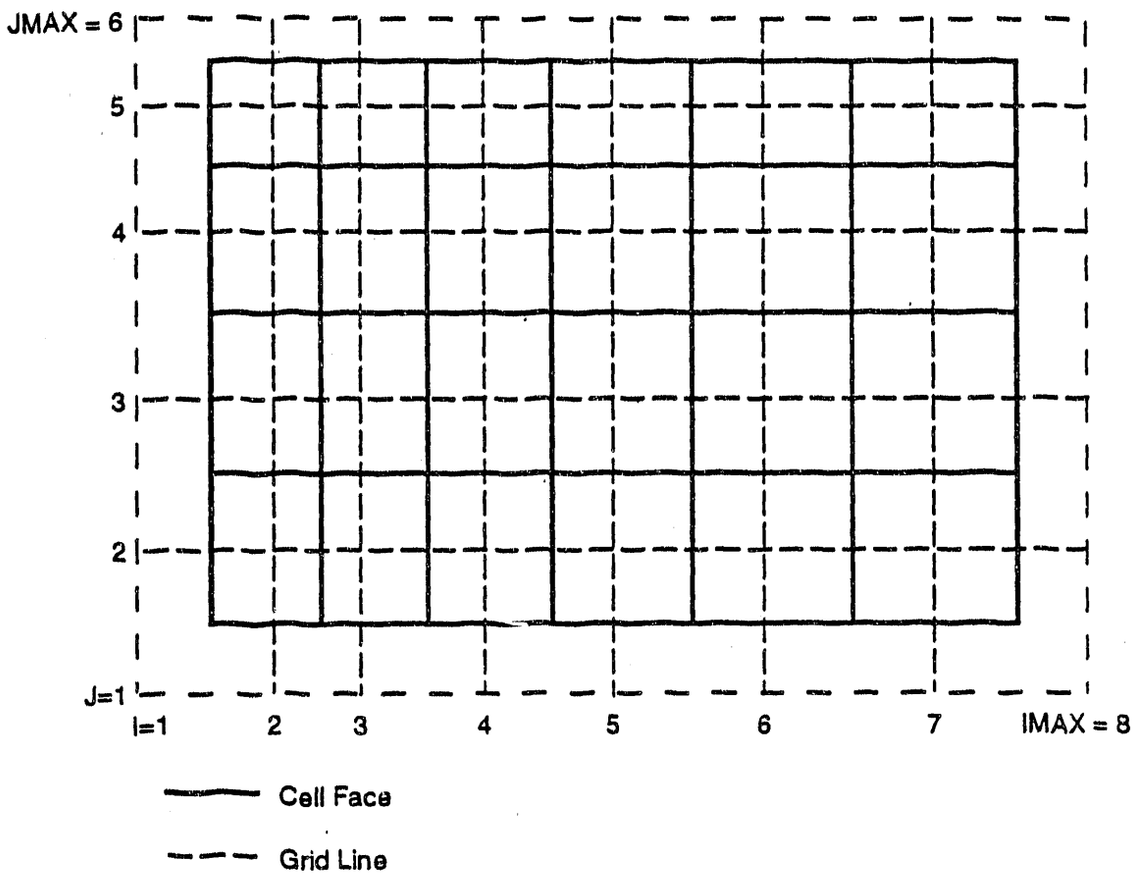

FIGURE 4.4. Horizontal Cross Section Through a Z Plane for the Cartesian Grid System

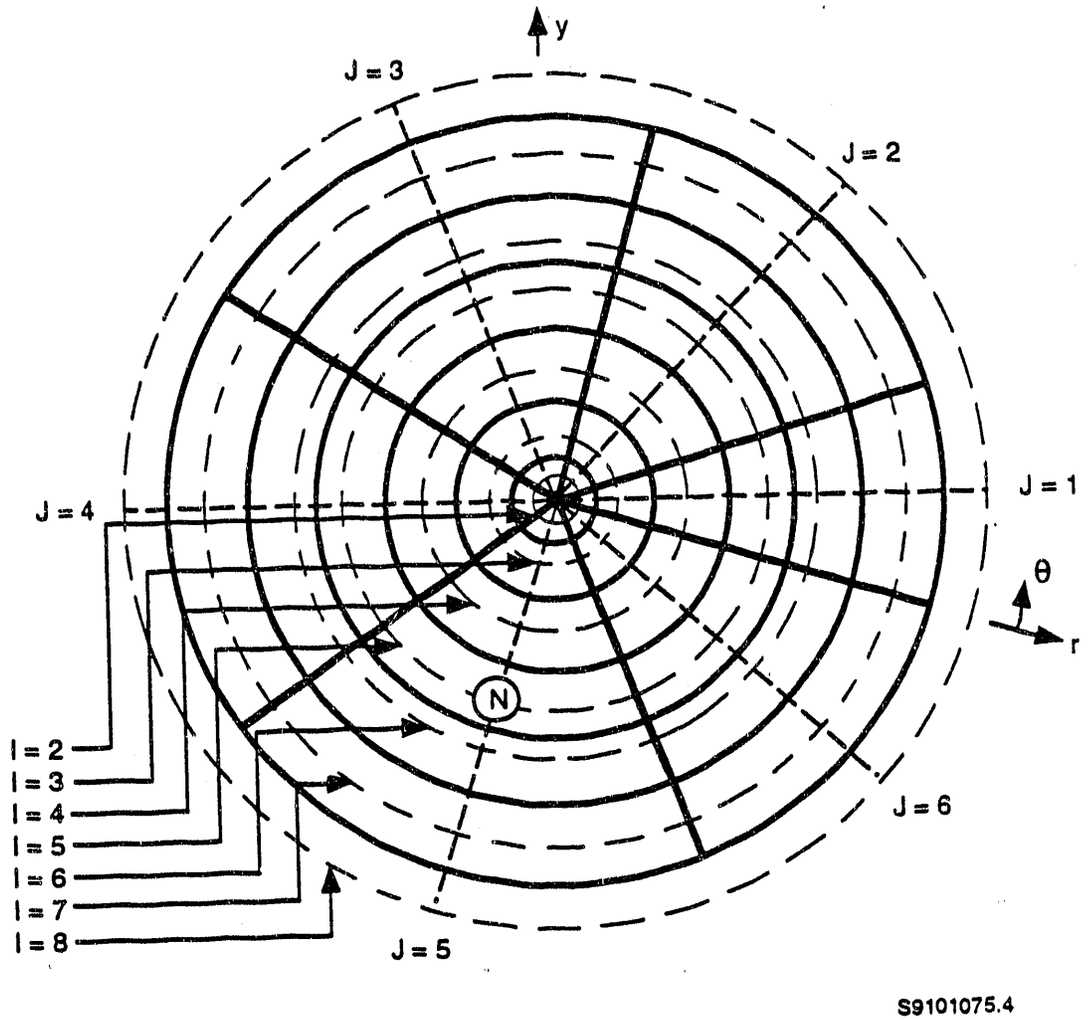

FIGURE 4.5. Horizontal Cross Section Through a Z Plane for the Cylindrical Grid System

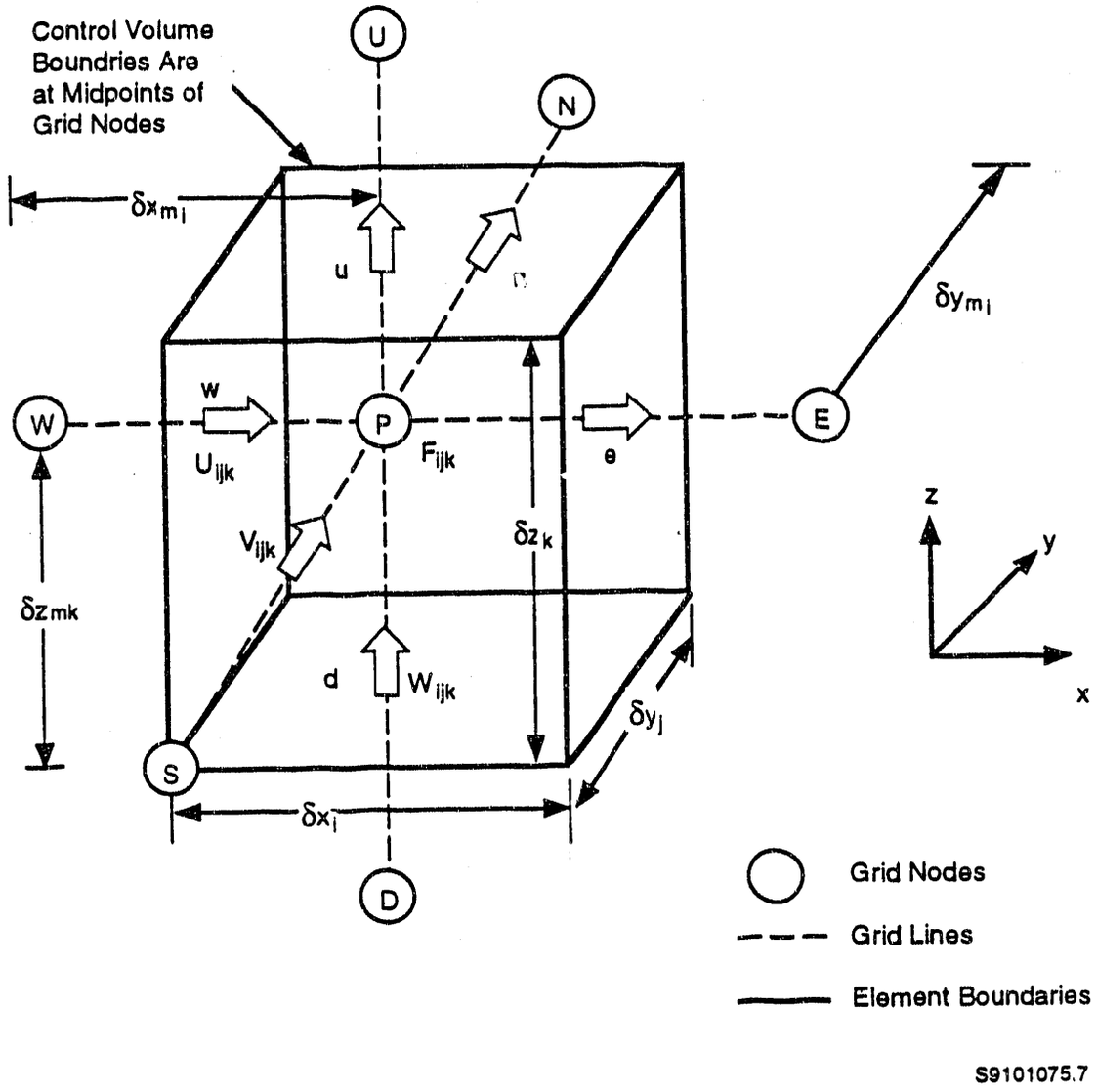

FIGURE 4.6. Typical Grid Cell in Cartesian Coordinates

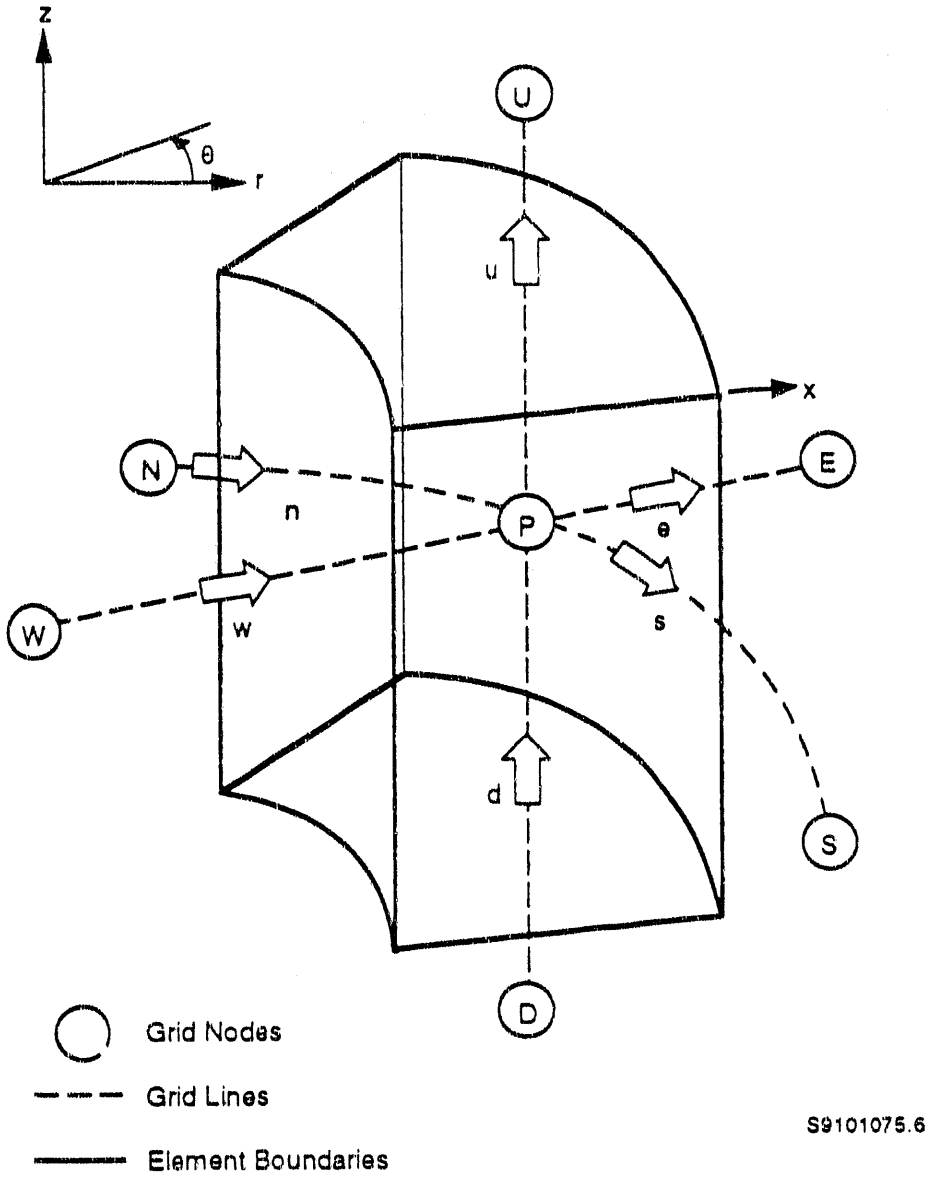

FIGURE 4.7. Typical Grid Cell in Cylindrical Coordinates

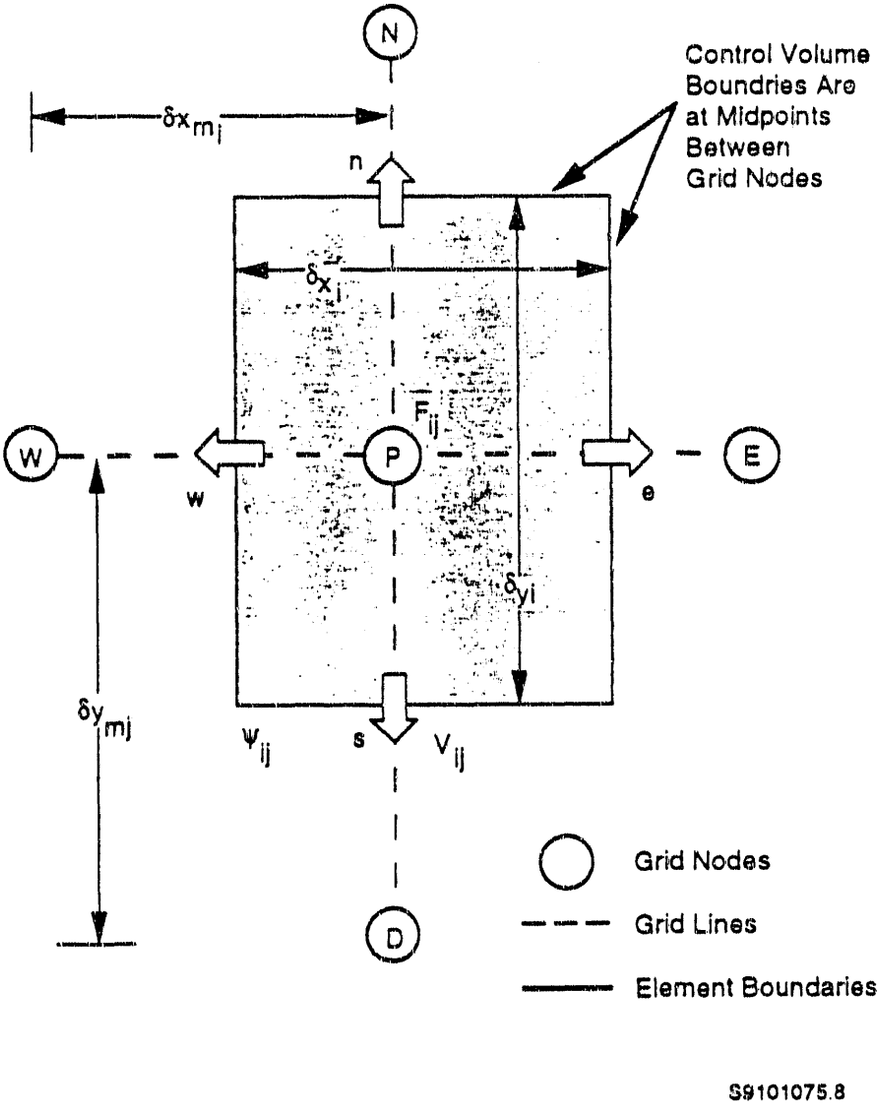

FIGURE 4.8. A Horizontal Cross Section Through a Typical Grid Cell in Cartesian Coordinates

by e, w, n, s, u, and d. Each of the cell faces lies exactly midway between the element node P and the nearest neighbor in the given direction. The number of internal nodes and, equivalently, the total number of cells is (IMAX-2)•(JMAX-2)•(KMAX-2).

During numerical manipulations, the values of pressure head and concentration are defined at the grid nodes. The flux variables (i.e., velocity and mass fluxes) are defined at the cell faces. The U velocity locations fall midway between the grid nodes in the x direction, the V velocity locations fall midway between the grid nodes in the y direction, and the W velocity locations fall midway between the grid nodes in the z direction. The use of this "staggered" grid approach allows a more natural description of the physical system where fluxes are defined at element boundaries and intrinsic properties at element interiors. The index notation employed is such that the velocity components at the w (west), s (south), and d (down) faces of the control volume are denoted by the same i, j, and k index values as the F values at the associated grid node (i.e., F_{ijk} and U_{ijk} indices are the same).

4.4.1.2 Integration over a Cell

Conceptually, discretization of the governing equations derives from integration over each individual cell and over each time step. Given the general Equation (4.41), for a node P as shown in Figure 4.8, the integral is

$$\int_t^{t+\delta t} \int_{V_p} \left[\partial_t(a\ F) + L_x + L_y + L_z - S_F + s_F\ F\right] dV\ dt = 0 \qquad (4.59)$$

where L_x, L_y, and L_z are partial derivative operators, i.e.,

$$L_x = \partial_x\left[(b\ U\ F) - (c_x\ \partial_x F)\right] \qquad (4.60a)$$

$$L_y = \partial_y\left[(b\ V\ F) - (c_y\ \partial_y F)\right] \qquad (4.60b)$$

$$L_z = \partial_z[(bWF) - c_z\partial_z F)] \qquad (4.60c)$$

If a polynomial profile for F (and other terms, such as S_F) is assumed during the time interval [t, t+δt] and over the volume V, then Equation (4.59) can be integrated analytically to obtain an algebraic equation applicable to node P. This procedure is followed to obtain an algebraic equation for each internal node.

4.4.1.3 Temporal Integration

Assuming a linear time variation of F at node P(I,J,K), the time integral of the term containing the time derivative and decay terms of Equation (4.59) is

$$\int_t^{t+\delta t} \int_V \left[\partial_t(a\,F) + s_F\,F\right] dV\,dt = \int_V \left[a(F^{n+1} - F^n) + s_F\,\delta_t\,F^{n+1}\right] dV \qquad (4.61a)$$

In Equation (4.61a), F^{n+1} and F^n are the values of F at points in volume V at time steps n+1 and n, respectively [i.e., $F^{n+1} = F(t_{n+1})$ and $F^n = F(t_n)$ where $t_{n+1} = t_n+\delta t$]. For the remaining terms in Equation (4.59), the time integral is written as

$$\int_t^{t+\delta t} \int_V (L_x + L_y + L_z - S_F)\,dV\,dt = \delta t\left[\int_V \left(L_x^k + L_y^m + L_z^i - S_F^j\right) dV\right] \qquad (4.61b)$$

The superscripts k, m, i, and j in Equation (4.61b) each correspond to some time in [t,t+δt]. In terms of time steps, $n \le k,m,i,j \le n+1$. Particular choices of values for k, m, i, and j give rise to different numerical schemes and solution methods. The schemes used in the SUMO code are

1. k=m=i=j=n. That is, all values in Equation (4.61b) are evaluated at the previous time step and hence are known. This is a fully explicit formulation. In this formulation, only one unknown, F(t+δt), remains in the equation for a node. The point successive over-relaxation (PSOR) method in the SUMO code uses this type of formulation.

2. k=m=i=j=n+1. That is, all values in Equation (4.61b) are those at the new time step. In this case, values of F(t+δt) for not only

node P, but also all of its neighboring nodes, appear in the equation for node P. This is the fully implicit formulation. The Gaussian elimination routine uses this formulation.

3. Three substeps are taken to complete the solution for a time step. In the first substep, k = n+1; in the second, m = n+1; and in the third, i = n+1, while all other superscripts are held equal to n. This formulation is used in conjunction with the alternating direction implicit (ADI) method of solution in the SUMO code.

These various solution methods have their own accuracies and stability characteristics and differ greatly in requirements of computer memory.

4.4.1.4 Spatial Integration

Alternative methods are provided in the SUMO code for spatial integration of the terms appearing in Equation (4.61). From an inspection of this equation, it is apparent that the spatial terms fall into four categories: 1) the diffusion terms with characteristic second-order space derivatives, 2) the convection terms with first-order space derivatives, 3) the source and sink terms, and 4) the accumulation terms with first-order time derivative.

In the NPI formulation, integration proceeds by the assumption of a suitable inter-nodal profile for the piecewise variation of the state variables [F of Equation (4.41)] from one grid node to another. In the approach taken, the diffusive and convective terms are considered separately, each with its own characteristic profile. This approach is illustrated below for the Cartesian coordinate system. The development of the equations proceeds identically for the cylindrical coordinate system.

The integral of the x-directional component (I_1) of the diffusion term in Equation (4.61) is written

$$I_1 = \int_t^{t+\delta t} \int_{V_p} \partial_x (c_x \, \partial_x F) \, dV \, dt \qquad (4.62)$$

By application of the divergence theorem, this equation is

$$I_1 = \int_t^{t+\delta t} \int_{S_{ijk}} (c_x \, \partial_x F) \, i \cdot dS \, dt \qquad (4.63)$$

where i is the vector component in the x direction and S_{ijk} is the bounding surface of the element for point P at (I,J,K). In the Cartesian coordinate system, the surface is made up of six rectangular surfaces. Equation (4.63) becomes

$$I_1 = \int_t^{t+\delta t} \left[\int_e (c_x \, \partial_x F) \, dy \, dz - \int_w (c_x \, \partial_x F) \, dy \, dz \right] dt \tag{4.64}$$

where e and w denote the values of the quantity at the e and w faces of the element, as shown in Figure 4.8.

Further integration now proceeds by assuming that in the interval $x_{i-1} \le x \le x_{i+1}$, $y_{j-1} \le y \le y_{j+1}$, and $z_{k-1} \le z \le z_{k+1}$, the state variable F is represented by the piecewise quadratic polynomial

$$F = a_\emptyset + a_1 x + a_2 x^2 + a_3 y + a_4 y^2 + a_5 z + a_6 z^2 \tag{4.65}$$

where the a's are arbitrary constants. This yields

$$\partial_x F|_w = a_1 + 2a_2 x_{i-1/2} \tag{4.66a}$$

$$\partial_x F|_e = a_1 + 2a_2 x_{i+1/2} \tag{4.66b}$$

Also, Equation (4.65) implies that for nodes W, P, and E of Figure 4.8,

$$F_W = a_\emptyset + a_1 x_{i-1} + a_2 x_{i-1}^2 + a_3 y_j + a_4 y_j^2 + a_5 z_k = a_6 z_k^2 \tag{4.67a}$$

$$F_P = a_\emptyset + a_1 x_i + a_2 x_i^2 + a_3 y_j + a_4 y_j^2 + a_5 z_k + a_6 z_k^2 \tag{4.67b}$$

$$F_E = a_0 + a_1 x_{i+1} + a_2 x_{i+1}^2 + a_3 y_j + a_4 y_j^2 + a_5 z_k + a_6 z_k^2 \qquad (4.67c)$$

Because

$$x_{i-1/2} = (x_i + x_{i-1}) / 2 \qquad (4.68a)$$

and

$$x_{i+1/2} = (x_i + x_{i+1}) / 2 \qquad (4.68b)$$

Equation (4.67) yields

$$(F_P - F_W) / (x_i - x_{i-1}) = a_1 + 2a_2 x_{i-1/2} \qquad (4.69a)$$

and

$$(F_E - F_P) / (x_{i+1} - x_i) = a_1 + 2a_2 x_{i+1/2} \qquad (4.69b)$$

Comparison of Equation (4.69) with (4.66) gives

$$\partial_x F|_w = (F_P - F_W) / (x_i - x_{i-1}) \qquad (4.70a)$$

and

$$\partial_x F|_e = (F_E - F_P) / (x_{i+1} - x_i) \qquad (4.70b)$$

In the notation of Figure 4.8, these may be written more compactly as

$$\partial_x F|_w = (F_P - F_W) / \delta x_w \qquad (4.71a)$$

and

$$\partial_x F|_e = (F_E - F_P) / \delta x_e \qquad (4.71b)$$

where δx_w is $x_i - x_{i-1}$ and δx_e is $x_{i+1} - x_i$.

On the assumption that c_x stays constant across a cell face, Equation (4.64) becomes

$$I_1 = \int_t^{t+\delta t} \left\{ \left[c_{xe} \, (F_E - F_P) / \, \delta x_e \right] A_e - \left[c_{xw} \, (F_P - F_w) / \, \delta x_w \right] A_w \right\} dt \qquad (4.72)$$

where the cell face areas A_e and A_w are given by

$$A_w = (y_{j+1/2} - y_{j-1/2}) \, (z_{k+1/2} - z_{k-1/2}) = A_e \qquad (4.73)$$

and C_{xe} and C_{xn} are respectively the average values for C_x in the east and west directions from point P.

To complete the transformation of this integral, assume that a representative (average) value of F^m between $F(t)$ and $F(t+\delta t)$ exists. In general, this may be written as

$$F^m = \alpha \, F(t) + (1-\alpha) \, F(t+\delta t) \qquad (4.74)$$

Three choices for α are provided in the SUMO code. These are the fully explicit scheme with $\alpha = 1$, the implicit scheme with $\alpha = 0$, and the ADI scheme with intermediate values of α.

The final form of the integral I_1 is now

$$I_1 = B_w \left(F_w^m - F_P^m \right) + B_E \left(F_E^m - F_P^m \right) \qquad (4.75)$$

where

$$B_w = c_{xw} \, A_w \, \delta t \, / \, \delta x_w \qquad (4.76a)$$

$$B_E = c_{xe} A_e \delta t / \delta x_e \tag{4.76b}$$

Similarly, the integrals for the y and z directional diffusion terms of Equation 4.61b may be written as

$$I_2 = B_S\left(F_S^m - F_P^m\right) + B_N\left(F_N^m - F_P^m\right) \tag{4.77}$$

$$I_3 = B_D\left(F_D^m - F_P^m\right) + B_U\left(F_U^m - F_P^m\right) \tag{4.78}$$

where

$$B_S = c_{ys} A_s \delta t / \delta y_s \tag{4.79a}$$

$$B_N = c_{yn} A_n \delta t / \delta y_n \tag{4.79b}$$

$$B_D = c_{zd} A_d \delta t / \delta y_d \tag{4.79c}$$

$$B_U = c_{zu} A_u \delta t / \delta y_u \tag{4.79d}$$

such that

$$\delta y_s = y_j - y_{j-1} \tag{4.80a}$$

$$\delta y_n = y_{j+1} - y_j \tag{4.80b}$$

$$\delta z_d = z_k - z_{k-1} \tag{4.80c}$$

$$\delta z_u = z_{k+1} - z_k \tag{4.80d}$$

$$A_s = (z_{k+1/2} - z_{k-1/2})\ (x_{i+1/2} - x_{i-1/2}) = A_n \tag{4.80e}$$

$$A_d = (x_{i+1/2} - x_{i-1/2})\ (y_{j+1/2} - y_{j-1/2}) = A_u \qquad (4.80f)$$

The values of the diffusion coefficients at the interfaces, C in Equations (4.76) and (4.79), are taken to be functions of the values at their nearest neighbor nodes. Four choices for these functions are available in the SUMO code: 1) harmonic mean, 2) geometric mean, 3) arithmetic mean, and 4) upwind value. For c_{xw}, these four functional forms are, respectively,

$$c_{xw} = 2\ c_{xW}\ c_{xP} \ /\ (c_{xW} + c_{xP}) \qquad (4.81a)$$

$$c_{xw}\ (c_{xW}\ c_{xP})^{1/2} \qquad (4.81b)$$

$$c_{xw} = (c_{xW} + c_{xP}) \ /\ 2 \qquad (4.81c)$$

$$c_{xw} = c_{xW},\ \text{if } U > 0;\ c_{xw} = c_{xP},\ \text{if } U < 0 \qquad (4.81d)$$

where c_{xW} and c_{xP} are the values of the diffusion coefficient c_x at the nodes W and P (Figure 4.8). In fully saturated flow problems, the harmonic mean option appears to give the best results; for the unsaturated flow problems, the geometric mean option seems to work best.

The integral of the x-directional component of the convection term in Equation (4.41) is written as

$$I_4 = -\int_t^{t+\delta t} \int_{V_p} \partial_x(b\ U\ F)\ dV\ dt \qquad (4.82)$$

Proceeding as we did for the diffusion term, this integral can be written as

$$I_4 = -\left(b_e U_e^m\ F_e^m\ A_e - b_w U_w^m\ F_w^m\ A_w\right)\ \delta t \qquad (4.83)$$

where

$$b_e = (b_E + b_p) / 2 \tag{4.84a}$$

$$b_w = (b_W + b_p) / 2 \tag{4.84b}$$

$$F_e^m = f_e F_E^m + (1 - f_e) F_p^m \tag{4.84c}$$

$$F_w^m = f_w F_W^m + (1 - f_w) F_p^m \tag{4.84d}$$

Because the second-order polynomial [Equation (4.64)] is used,

$$f_e = f_w = 1/2 \tag{4.85}$$

However, the use of this polynomial for the convective terms may lead to numerical instability if the grid Peclet number exceeds a critical value of 2 (Patankar 1980, p. 82). In the present context, the grid Peclet number for the x-direction flux at location e of the control volume would be

$$P_e = b_e |U_e| \delta x_e / c_{xe} \tag{4.86}$$

where x_e is the local grid size and U_e is the velocity component in the x direction. To combat this instability, the SUMO code employs the hybrid approach (Runchal 1972; Spalding 1972) to select suitable values for f in Equation (4.84). In this approach, the second-order polynomial of Equation (4.64) is employed if the local grid Peclet number is less than 2. Otherwise, an upwind (or donor) scheme is employed. The general expressions for f in Equation (4.84) are then given by

$$f_e = 0.5 - 0.25 \left(P_e/|P_e|\right) \left[1 + \left(|\,|P_e| - 2|\right) / \left(|P_e| - 2\right)\right] \tag{4.87a}$$

$$f_w = 0.5 + 0.25\,(P_w/|P_w|)\left[1 + (|\,|P_w| - 2|) / (|P_w| - 2)\right] \tag{4.87b}$$

The convective integral of Equation (4.83) can alternatively be written as

$$I_4 = C_E\left(F_E^m - F_P^m\right) + C_W\left(F_W^m - F_P^m\right) + \left(C_W^{'} - C_E^{'}\right) F_P^m \tag{4.88}$$

where

$$C_W^{'} = b_w\, U_w^m\, A_w\, \delta t \tag{4.89a}$$

$$C_E^{'} = b_e\, U_e^m\, A_e\, \delta t \tag{4.89b}$$

$$C_W = f_w\, |C_W^{'}| \tag{4.89c}$$

$$C_E = f_e |C_E^{'}| \tag{4.89d}$$

By analogy, the convective integrals in the y and z direction are written as

$$I_5 = C_N\left(F_N^m - F_P^m\right) + C_S\left(F_S^m - F_P^m\right) + \left(C_S^{'} - C_N^{'}\right) F_P^m \tag{4.90}$$

$$I_6 = C_U\left(F_U^m - F_P^m\right) + C_D\left(F_D^m - F_P^m\right) + \left(C_D^{'} - C_U^{'}\right)F_P^m \tag{4.91}$$

where

$$C_S^{'} = b_s\, U_s^m\, A_s\, \delta t \tag{4.92a}$$

$$C_N' = b_n U_n^m A_n \delta t \tag{4.92b}$$

$$C_D' = b_d U_d^m A_d \delta t \tag{4.92c}$$

$$C_U' = b_u U_u^m A_u \delta t \tag{4.92d}$$

$$C_S = f_s |C_S'| \tag{4.92e}$$

$$C_N = f_n |C_N'| \tag{4.92f}$$

$$C_D = f_d |C_D'| \tag{4.92g}$$

$$C_U = f_u |C_U'| \tag{4.92h}$$

where the b's and f's are defined analogously to Equations (4.84) and (4.87).

The source term, S_ϕ of Equation (4.41) is discretized as

$$I_7 = \int_t^{t+\delta t} \int_{V_p} S_\phi \, dV \, dt \tag{4.93a}$$

$$= S_p^m V_p \delta t \tag{4.93b}$$

where

$$V_p = \left[(x_{i+1} - x_{i-1}) (y_{j+1} - y_{j-1}) (z_{k+1} - z_{k-1})\right]/8 \tag{4.94}$$

As indicated in Equation (4.61a), the decay rate term, $s_F F$, of Equation (4.41) is always discretized at the time level $t+\delta t$, so

$$I_8 = \int_t^{t+\delta t} \int_{V_p} s_F F \, dV \, dt \tag{4.95a}$$

$$= s_p^{n+1} F_p^{n+1} V_p \delta t \tag{4.95b}$$

For the accumulation term, I_g, the F is assumed to remain constant over the cell so that

$$I_g = \int_t^{t+\delta t} \int_{V_p} a \, \partial_t F \, dV \, dt \tag{4.96a}$$

$$= a_p\left(F_p^{n+1} - F_p^n\right) V_p \tag{4.96b}$$

4.4.1.5 Algebraic Analogue of the General Transport Equation

The algebraic analogue of the general transport equation [Equation (4.41)] can now be obtained by combining Equations (4.75) through (4.96). The new equation is written as

$$\begin{aligned} a_p\left(F_p^{n+1} - F_p^n\right) V_p = {} & A_E\left(F_E^m - F_p^m\right) + A_W\left(F_W^m - F_p^m\right) + A_N\left(F_N^m - F_p^m\right) + \\ & A_S\left(F_S^m - F_p^m\right) + A_U\left(F_U^m - F_p^m\right) + A_D\left(F_D^m + F_p^m\right) + \\ & S_p^m V_p \delta t - s_p^{n+1} F_p^{n+1} V_p \delta t - \\ & \left(C_W' - C_E' + C_S' - C_N' + C_D' - C_U'\right) F_p^m \end{aligned} \tag{4.97}$$

where

$$A_W = B_W + C_W \tag{4.98a}$$

$$A_E = B_E + C_E \tag{4.98b}$$

$$A_S = B_S + C_S \tag{4.98c}$$

$$A_N = B_N + C_N \tag{4.98d}$$

$$A_D = B_D + C_D \tag{4.98e}$$

$$A_U = B_U + C_U \tag{4.98f}$$

and the superscript m indicates the time at which various values are taken ($t_m=t_n$ or $t_m=t_{n+1}$).

From the continuity equation, the last term on the right-hand side of Equation (4.97) is identically zero for incompressible fluids and negligible for fluids with small compressibility. Equation (4.97) can be written in a more compactly as

$$A_P F_P^{n+1} = a_P V_P F_P^n + \sum_M \left[A_M \left(F_M^m - F_P^m \right) + \sum_M (-1) k C_M' F_P^m \right] + S_P^m V_P \delta t \tag{4.99}$$

where M takes values of E, W, N, S, U, and D, respectively; k is +1 for M = W, S, or D, and is -1 otherwise; and

$$A_P = a_P V_P + s_P^{n+1} V_P \delta t \tag{4.100}$$

Both the explicit and implicit versions of Equation (4.100) can be solved with the SUMO code.

4.4.2 Inclusion of Boundary Conditions in Algebraic Analogue

The general form of the boundary condition, as discussed in Section 4.3, is

$$- a\ \partial F/\partial N = b(F - F_o) + c \qquad (4.101)$$

where N represents a direction normal to a boundary. Suitable choices for a, b, c, and F_o allow representation of Dirichlet, Neumann, and mixed boundary conditions. The algebraic equations for nodes located next to boundaries are modified to account for Equation (4.101). As an example, consider that the node W, to the west of node P in Figure 4.8, is a boundary node. To incorporate Equation (4.101) into the algebraic analogue for node P, it is written as

$$- a\ (F_P - F_W) \ / \ \delta x_w = b(F_w - F_o) + c \qquad (4.102)$$

where the value of F_P is taken at the advanced time $t+\delta t$ (or at time step n+1). Equation (4.102) is now solved for F_W to yield

$$F_W = a\ F_P + \left[\delta x_w(c - bF_o)\right] / \left(a - b\delta x_w\right) \qquad (4.103)$$

Finally, Equation (4.103) is substituted into the algebraic equation [Equation (4.99)] for node P, which eliminates F_W from that equation.

Thus, when the coefficient matrix is formed, the boundary conditions are included in it implicitly. Once the equations are solved (i.e., the value of F_P is obtained), Equation (4.103) is used again to obtain the value of F (in the case of Neumann and mixed boundary conditions) at the boundary.

4.4.3 Solution of Algebraic Equations

4.4.3.1 Explicit Solution Method

For explicit solution of Equation (4.99), the superscript m is replaced by n; that is, all of the F^m values appearing on the right-hand side of

Equation (4.99) are assumed to be those at time t [see Equation (4.74)]. Equation (4.99) can then be rearranged to read

$$F_P = (1/A_P)\ a_P\ V_P\ F_P^n + \sum_M A_M\left(F_N^m - F_P^m\right) + \sum_M (-1)^k\ C_N'\ F_P^m + S_P^m\ V_P\ \delta t \qquad (4.104)$$

Because all quantities on the right-hand side of Equation (4.104) are known from initial conditions at time t, F_P^{n+1} is easily evaluated by a simple substitution. The substitution is performed in a point-by-point manner. Three alternatives are available for the order of this substitution. In the first, the substitution starts along the x direction (I = 1 to IMAX), then along the y direction (J = 1 to JMAX), and finally along the z direction (K = 1 to KMAX). This is called a "sweep in the x direction." For the second alternative, the substitution is performed in the order y, z, and x, and in the third, it is performed in the order z, x, and y. These last two alternatives are called sweeps in the y and z directions, respectively.

4.4.3.2 Implicit Solution Method

For the implicit solution of Equation (4.99), the superscript m is replaced by n+1; Equation (4.99) then becomes

$$\left\{A_P + \sum_M \left[A_M + (-1)^{k+1}\ C_M\right]\right\} F_P^{n+1} = \sum_M A_M\ F_M^{n+1} + S_P^n \qquad (4.105a)$$

where

$$S_P^n = a_P\ V_P\ F_P^n + S_P^n\ V_P\ \delta t \qquad (4.105b)$$

There are at most seven unknowns (at node P and its six nearest neighbors) in Equation (4.105a). For those nodes that have no boundary node as their neighbor, the number of unknowns is exactly seven. Values of F for boundary nodes are eliminated for equations of nodes located next to domain boundaries. Thus, for these nodes, the number of unknowns is less than seven. Writing the set of equations for all the nodes creates a hepta-diagonal

matrix. This coefficient matrix is of banded form and very sparse. The actual band width depends on the way the nodes are numbered. In the SUMO code, nodes are numbered in the order of first increasing the I index, then the J, and then the K index. With this numbering system, the band width is 2*(IMAX-2)*(JMAX-2). To get an idea of the sparsity of the coefficient matrix, consider a grid whose dimensions are 10 by 12 by 15. The total number of nodes in this grid is 1800. The number of internal nodes is 1040. Thus, the coefficient matrix has 1040*1040 = 1,081,600 elements, of which less than 1040*7 = 7,280 are nonzero.

Only iterative methods for solving the matrix of equations are included in the SUMO code. Although direct solution methods are accurate, elements within the band width become nonzero during elimination procedures; thus these methods require a large amount of storage and can be used only for relatively small grids. Iterative methods can be implemented with a limited amount of storage space and are therefore preferable for large grids.

The alternating direction implicit (ADI) method completes the solution for each time step in three substeps. In the first substep, Equation (4.102) is replaced with

$$\left(A_P + \sum_M A_M + (-1)^k C_M'\right) F_P^{**} = A_E F_E^{*} + A_W F_W^{*} S_P^n S^n \qquad (4.106a)$$

where

$$S^n = A_S F_S^n + A_N F_N^n + A_D F_D^n + A_U F_U^n \qquad (4.106b)$$

Equation (4.106) generates a tri-diagonal (no more than three unknowns per node) matrix that is easily solved using the Thomas algorithm to yield values of F^*. For the next substep, another approximation, F^{**}, is obtained from

$$\left(A_P + \sum_M A_M + (-1)^k C_M'\right) F_P^{**} = A_S F_S^{**} + A_N F_N^{**} + S^* + S_P^n \qquad (4.107a)$$

where

$$S^{*} = A_W F^{*} + A_E F^{*} + A_D F^{*} + A_U F^{*} \qquad (4.107b)$$

Finally, the solution for δt is completed by a third approximation, F_P^{***}, which is obtained from

$$\left[A_P + \sum_M A_M + (-1)^k C_M'\right] F_P^{***} = A_D F_D^{***} + A_U F_U^{***} + S^{**} + S_P^n \qquad (4.108a)$$

where

$$S^{**} = A_W F_W^{**} + A_E F_E^{**} + A_S F_S^{**} + A_N F_N^{**} \qquad (4.108b)$$

In many instances, F_P^{***} provides an acceptable approximation to F_P^{n+1}. However, the SUMO code provides for the iterative solution of Equations (4.106) through (4.108) for a user-specified number of cycles at each time step.

The procedure above describes the solution process that proceeds first in the x direction [Equation (4.106)], then in the y direction [Equation (4.107)], and finally in the z direction [Equation (4.108)]. In a manner similar to the explicit solution method, the SUMO code also provides for sweeps to be conducted in the y-z-x and z-x-y directions.

4.4.4 Treatment of Nonlinearities

The governing equation for fluid pressure, Equation (4.24), may have mild nonlinearities as a result of expressions such as storativity (S_s) and relative permeability (K_r) being functions of pressure. If time steps are suitable, these minor nonlinearities present no great difficulty in solution.

In general, it is assumed that the values of these pressure-dependent expressions are taken from the solutions at the previous time step. That is, these quantities lag the solution by one time step.

The governing equation for pressure, Equation (4.23), under conditions of partial saturation can be highly nonlinear. This is apparent from the soil-moisture relations discussed in Section 4.3. For most soils and rocks, the degree of nonlinearity increases as the saturation decreases. To deal with these nonlinearities, an iterative method is followed in the SUMO code.

Three iterative methods for nonlinear equations are discussed by Huyakorn and Pinder (1983, p. 156): 1) Picard, 2) Newton-Raphson, and 3) Chord Slope. Of these, the Picard method is the simplest, requires no additional storage, and is currently implemented in the SUMO code.

In the Picard (or successive substitution) method, solution begins with an initial guess, usually the user-specified initial conditions. Values of parameters that are functions of the dependent variable are calculated using this guess and then substituted into Equation (4.99). Solution of Equation (4.99) provides a new estimate of the solution, and the process is repeated until a user-specified convergence criterion is satisfied.

Two options for determining convergence are provided in the SUMO code:

$$\max_{i=1,N} \left| (1 - F_i(k+1)/F_i(k) \right| \leq \epsilon \tag{4.110}$$

and

$$(1/N)\left[\sum_{i=1}^{N} \left(1 - [F_i(k+1)/F_i(k)]\right)^2\right]^{1/2} \leq \epsilon \tag{4.111}$$

where N is the total number of internal nodes, k is the iteration number, and e is the specified convergence limit.

4.4.5 Choice of Spatial Grid and Time Steps

The design of the spatial grid and the choice of time steps for a given problem depend on several competing objectives. A need for detailed and accurate solutions suggests the use of a fine-mesh spatial grid and small time steps, but limitations on computer resources (specifically memory and execution time) restrict their use. In practice, considerations of computational cost, the accuracy and stability of the numerical solution, output needs with respect to locations and times, and accommodation of special physical features (boundaries, heterogeneities, and sources) all influence the design of the spatial grid and the choice of time steps. Some of the factors that should be considered in choosing grid spacing and time steps are discussed below.

4.4.5.1 Design of Spatial Grid

The spatial variation in hydraulic, thermal, and mass transport properties should be adequately represented by the grid. The material properties are specified at grid nodes and are assumed to remain constant within a cell. If these properties change in a discontinuous manner, as is common in layered media, spatial grids should be designed such that a cell face coincides with the boundary between two layers that have differing characteristics. For problems with continuously varying properties, the cell size should be smaller in regions where the variation in properties is relatively rapid, and larger where the variation is more gradual. In general, a uniformly accurate solution may be expected if the properties of interest vary uniformly across the cells of interest.

To design the grid, it is helpful to sketch the domain and all of the zones in which the properties have different values. Because the material properties between a cell's node and its face (in a given direction from the node) are constant, cell faces should be located wherever properties are expected to change abruptly. As a practical minimum, three cells are necessary to adequately define a distinct geologic layer. A layer as thin as 1 m should be represented by three cells; more cells will be required for representing thicker formations.

For a variety of reasons, solutions may be needed on a finer scale in some parts of the domain than in others. For example, interest may be focused on areas where temperatures or chemical concentrations are high. In such areas, smaller cells should be used.

Geologic and artificial features, such as fractures and igneous dikes or boreholes, wells, and tunnels, are distinguishable from the geologic continuum by their physical properties and scales. To accurately represent these features, cell sizes that are comparable to the sizes of these features (i.e., to the sizes of their openings, thicknesses, and diameters) should be used.

Hydraulic head and chemical concentrations are expected to change relatively rapidly close to sources and sinks of fluid and mass. If large cells are used in such areas, unacceptable errors may occur in the solution. As a general principle, finer-mesh grids should be used in areas where the values of the state variables are expected to change rapidly.

Some boundaries are natural geologic features. For instance, a river may form a boundary at which it is appropriate to specify hydraulic heads. Cell sizes should be comparatively small in proximity to these boundaries. In contrast, arbitrary boundaries that do not represent natural geologic features are usually located at large distances (in theory, at infinite distance) from the area of interest. Near these boundaries, coarse-mesh grids can be used. However, in problems with boundaries at infinity, it is advisable to discern whether the boundaries are indeed located sufficiently far away that they do not affect the solution.

The amount of computer memory required for solving a problem is proportional to the number of computational cells. Consequently, an upper limit to the number of computational cells is imposed by the capacity of the available computer memory. An estimation of appropriate cell size, based on considerations discussed above, may require adjustment to remain within this limit.

The time required to solve a problem is a nonlinear function of the number of grid cells. The time of computation increases in a ratio that

varies from the square to the cube of the number of cells. In some cases, the maximum allowable computation time may restrict the maximum number of computational cells.

4.4.5.2 Choice of Time Steps

The size of time steps is determined by the time scales that are characteristic of the propagation of pressure, diffusion, and convective transients. These time scales depend on the cell sizes and on the material properties.

The choice of time steps is also influenced by numerical stability. In general, a stable numerical scheme controls the growth of numerical error as the solution advances with time. The two types of instabilities that may be encountered are weak instability, in which the solution oscillates about a mean value, and strong instability, in which divergence from the true solution increases monotonically. Both types of instabilities can be removed by shortening the time steps. However, for overcoming strong instability, alternate solution methods may be more economical.

Let δL represent the length of one edge of a computational cell. Depending on the coordinate direction under consideration, δL equals δx, δy, or δz. Let K_L represent the hydraulic conductivity in the L direction of the cell under consideration (L could be in the x, y, or z direction). The characteristic time scale (δt_{pL}) for the propagation of transient pressure (or hydraulic head) effects in the L direction for that cell is given by

$$\delta t_{pL} = S_s \, \delta L^2 / K_L \qquad (4.112)$$

A similar equation can be written for each cell. The smallest of these characteristic time-scale values for all cells in the grid represents the time scale for pressure transients (δt_p). The term δt_p is an approximation of the time required to propagate a pressure change across a cell. If the computational time step, δt, is much larger than δt_p, then it is possible that the variation of pressure with time will be missed across some of the cells in the grid. Therefore, for problems in which prediction of time-dependent pressures

is important, δt_p can be used as a guide in selecting appropriate time steps. For the ADI method of solution, there is no theoretical limit on δt for stability, but for physically accurate solutions, δt should be kept less than 10 times δt_p.

Pressure transients may be thought of as waves of different frequencies. As the high-frequency components pass across the computational grid, the severity of pressure transients decreases. Therefore, it is possible to gradually increase the size of the time step as the solution advances with time.

A time scale for diffusion is defined in a manner similar to the time scale for pressure transients:

$$\delta t_D = \delta L^2/(2D_L) \tag{4.113}$$

where D_L is the hydrodynamic dispersion coefficient in the L direction (which can be x, y, or z). It is the sum of the molecular diffusion coefficient and the coefficient of mechanical dispersion. As with δt_D, the smallest value of δt_D in the grid is selected. If diffusion and dispersion are major considerations, the choice of size of the time step should be guided by the value of δt_D. For the PSOR method to be stable, the computational time step size, δt, should be less than δt_D. For other methods, δt should be less than 10 times δt_D.

Time Scale of Convection. The time scale of convection is based on the flow velocity of fluid and is defined as

$$\delta t_C = \delta L/U_L \tag{4.114}$$

where U_L is the fluid velocity in the L direction (which can be x, y, or z). The constraint on size of the computational time step, δt, based on Equation (4.114), is often stated in terms of the Courant number, or Co, which is defined as

$$Co = \delta t/\delta t_c = (U_L\ \delta t)/\delta L \qquad (4.115)$$

For the PSOR method to remain stable, Co must not exceed unity. For other methods, Co must not exceed 10 times δt_c.

Other Time Scales. The time scales defined above are the most common ones. However, in certain problems, other time scales may apply. These other time scales apply whenever time-dependent phenomena are included in the problem. For example, time-varying sources and sinks and time-dependent boundary conditions would inherently have associated time scales. The general rule in such cases is that the size of the computational time step, δt, must be kept less than any of the other time scales of a problem. Thus the effect of the variation of time on any phenomenon with a time scale less than δt will not manifest itself in the solution.

5.0 POPULATION DOSE AND HEALTH EFFECTS MODEL

A generic illustration of exposure pathways to humans from an arbitrary contaminant source is given in Figure 5.1. This section describes the particular exposure pathways and associated dose models that are implemented in the SUMO code. The discussion is divided as follows:

- Calculation of the effective dose equivalent
- Pathway dose calculations: models to determine total population doses from important pathways
- Incorporation of sources: specification and use of source terms
- Airborne release: models for estimating average air concentrations downwind of an airborne release and definition of the population-exposure factor
- Waterborne release: definition of the population exposed to a waterborne release
- Environmental concentrations: models to estimate important air and water pathway concentrations
- Special models for ^{3}H and ^{14}C: models that impute health effects to only the portions of these species that are released from a repository
- General considerations.

The first-generation SUMO code uses only the waterborne dose model. However, because the capability to model airborne releases has been retained in the code in anticipation of future analyses of gas-phase ^{14}C releases, the exposure models for both airborne and waterborne releases are described. The dose models and supporting documentation are extracted from the GENII system (Napier et al. 1988). However, all of the coded routines have been substantially modified to fit into the SUMO framework.

The analyses performed by the dose models are structured in time to correspond to a series of consecutive 70-year periods. Within each 70-year period, average parameter values (appropriate to the period) are used to perform the analyses.

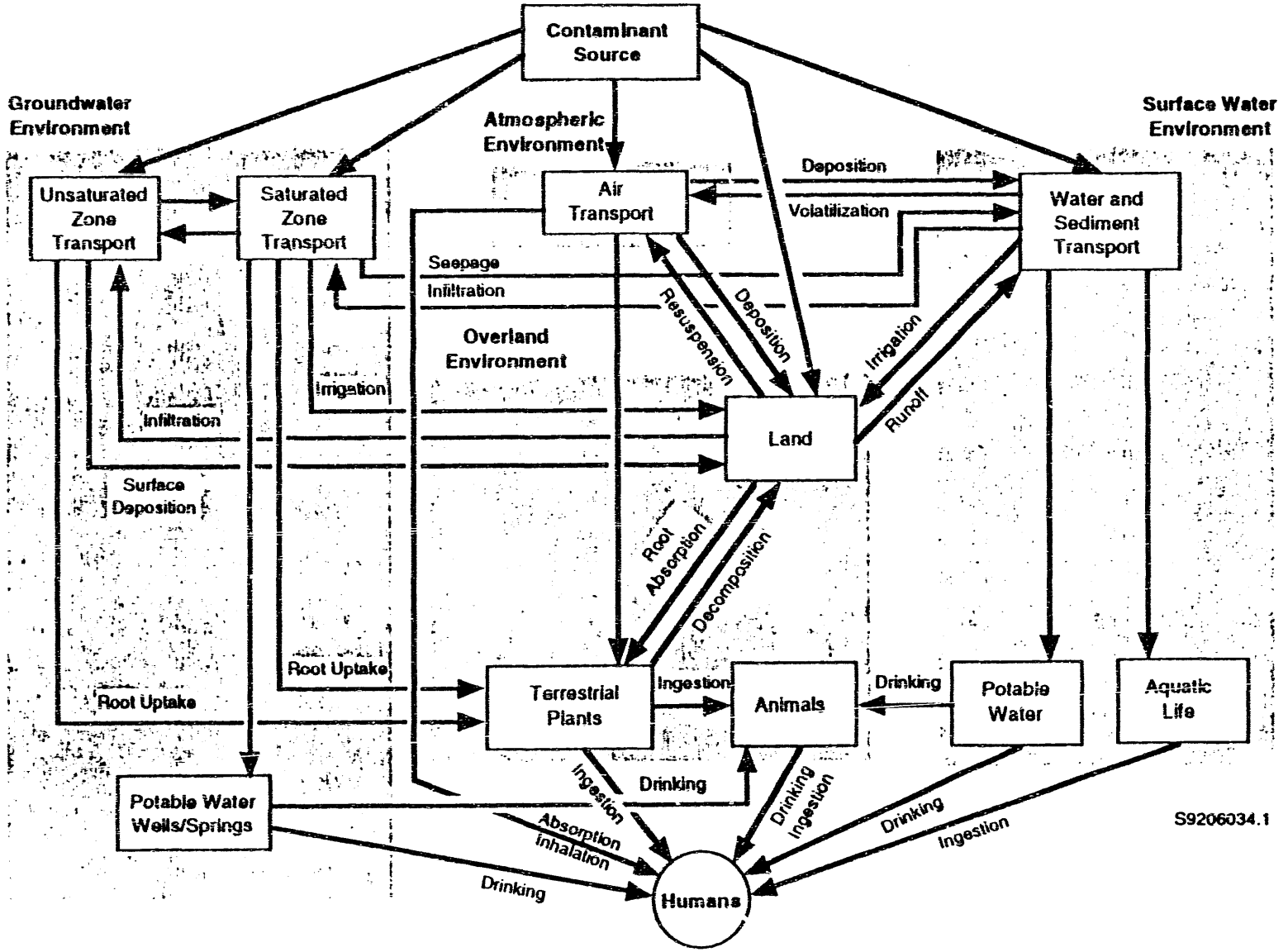

FIGURE 5.1. Generic Pathways to Humans from an Arbitrary Contaminant (Droppo et al. 1989)

5.1 CALCULATION OF THE EFFECTIVE DOSE EQUIVALENT

The total dose or lifetime effective dose equivalent, D_L, is calculated by summing the external dose, DEXT, and the weighted sum of the internal dose, $DINT_o$, to each organ. The lifetime effective dose equivalent for a 70-year period is

$$D_L = \sum_o DINT_o \, W_o + DEXT \tag{5.1}$$

External doses and cumulative doses to each internal organ are calculated for each 70-year period. The external dose, DEXT, is the sum, over all radionuclides, of the external exposures to water, the external exposure to shoreline soil, and submersion in air. It is given by

$$DEXT = \sum_i D_{iew} + \sum_i D_{ies} + \sum_i D_{iea} \tag{5.2}$$

where D_{iem} is the dose from external exposure to radionuclide i from medium m (water, soil, or air), in person•rem.

The internal dose for organ o, $DINT_o$, is the sum, over all radionuclides, of the inhalation, terrestrial pathways, and aquatic pathways doses for that organ and is given by

$$DINT_o = \sum_i D_{ohi} + \sum_i D_{oti} + \sum_i D_{oai} \tag{5.3}$$

where D_{omi} equals internal dose for organ o from radionuclide i and pathway m (inhalation, terrestrial, or aquatic).

The internal doses for the six designated body organs and the doses for the five remaining organs with the highest doses are each multiplied by an organ-weighting factor, W_o, and summed to give an effective dose equivalent. The weighting factors for the body organs are given in Table 5.1. The weighting factor for each of the five remaining organs is 0.06.

TABLE 5.1. Organ Weighting Factors (W_o)

Organ	Weight
Testes/Ovaries	0.25
Muscle	0.15
Blood Marrow	0.12
Lung & Lymph	0.12
Thyroid	0.03
Bone Surface	0.03

5.2 PATHWAY DOSE CALCULATIONS

The exposure pathways are described in the following subsections. Except where noted, the symbols used to represent terms are those given in Table 5.2.

5.2.1 Air Submersion

Contributions for external exposure from air submersion are included for 1) submersion in the release plume, 2) submersion in resuspended activity resulting from an initial airborne release, and 3) submersion in suspended activity resulting from an initial irrigation water deposition. The dose is calculated as

$$D_{oei} = D_{ei}\ 5.29 \times 10^{10}\ \lambda_{ri} \left\{ A_c(i,t) + 1.49 \times 10^{-6} \left[S_{ca}(i,t) + S_{cw}(i,t) \right] \right\} \quad (5.4)$$

where D_{oei} = dose from air submersion exposure for organ o and radionuclide i, person•rem

D_{ei} = external exposure dose conversion factor for air submersion, rem per Ci•sec/m^3

5.29×10^{10} = conversion factor, (rem per Ci)/(Sv per 70 Bq)

λ_{ri} = radiological decay constant for radionuclide i, yr^{-1}

$A_c(i,t)$ = population-weighted airborne release for radionuclide i over 70-yr period t, person•Ci•yr^2/m^3

TABLE 5.2. Symbols Used to Represent Concentrations

Symbol	Pathway Concentration
A_c	Air concentration
A_{ca}	Animal product concentration, air medium
A_{cw}	Animal product concentration, water medium
A_{dw}	Drinking water concentration, water medium
A_{fw}	Aquatic food concentration, water medium
L_{ca}	Leaf concentration, air medium
L_{cw}	Leaf concentration, water medium
P^{cw}	Plant concentration, air medium
P^{ca}	Plant concentration, water medium
S^{cw}	Soil concentration, air medium
S_{ca}	Soil concentration, water medium
S_{cw}	Sediment concentration, air medium
S_{da}	Sediment concentration, water medium
S_{dw}	Water concentration
W_c^{dw}	

1.49×10^{-8} = resuspension factor constant, kg/m^3; $(1 \times 10^{-9}\ m^{-1})$ (224 kg $soil/m^2$) (1/15).

$S_{ca}(i,t)$ = soil concentration of radionuclide i, from airborne releases for period t, person•Ci•yr^2/kg

$S_{cw}(i,t)$ = soil concentration of radionuclide i for period t for irrigation deposition, person•Ci•yr^2/kg.

The contribution from deposited material is calculated based on the concentration at the end of the current period. This concentration is assumed to occur throughout the period, which is a conservative assumption but by no more than a factor of two. The calculated resuspension is based on a constant resuspension factor of $10^{-9}\ m^{-1}$, representing resuspension of aged deposited material (Anspaugh et al. 1975). The resuspended activity is assumed to expose individuals in the vicinity of the soil from which it was suspended. Downwind transport of resuspended activity is not considered. The decay constant, λ_{ri}, is included to convert the units of radionuclide concentration from mass to activity. The calculations are performed in units proportional to mass to meet requirements of the chain decay processor.

5.2.2 Inhalation

Inhalation exposure includes contributions from the released airborne activity plus activity that has been resuspended after airborne and irrigation water deposition. The dose is calculated as

$$D_{ohi} = D_{hio}\ 5.29 \times 10^{10}\ B_r\ 3.156 \times 10^{7}\ \lambda_{ri} \left\{A_c(i,t) + 1.49 \times 10^{-8} \left[S_{ca}(i,t) + S_{cw}(i,t)\right]\right\} \quad (5.5)$$

where D_{ohi} = dose from inhalation exposure for organ o and radionuclide i, person•rem

D_{hio} = inhalation dose conversion factor for radionuclide i and organ o, Sv per 70 Bq

B_r = breathing rate, m^3/sec

3.156×10^7 = conversion factor, sec/yr.

5.2.3 Terrestrial Ingestion Pathways

Terrestrial pathways include ingestion of crops and animal products. The seven terrestrial ingestion pathways included in the SUMO code are vegetables, grains, eggs, milk, beef, pork, and poultry. The dose for each pathway is calculated from the time-integrated food-product concentration. For plants, the dose is calculated as

$$D_{oti} = D_{gio}\ 5.29 \times 10^{10}\ \lambda_{ri}\ U_p \left[P_{ca}(i,p,t) + P_{cw}(i,p,t)\right] \quad (5.6)$$

and for animal products, the dose is calculated as

$$D_{oti} = D_{gio}\ 5.29 \times 10^{10}\ \lambda_{ri}\ U_p \left[A_{ca}(i,p,t) + A_{cw}(i,p,t)\right] \quad (5.7)$$

where D_{oti} = dose from terrestrial ingestion pathways for organ o and radionuclide i in person-rem

D_{gio} = ingestion dose conversion factor for radionuclide i and organ o in Sv per 70 Bq

U_p = usage rate by humans of food product p in kg/yr (L/yr for milk)

$P_{ca}(i,p,t)$ = time integral of plant concentration for radionuclide i and pathway p, from air-deposited contaminants on plants and root uptake over the period t, person•Ci•yr^2/kg

$P_{cw}(i,p,t)$ = plant concentration of radionuclide i and plant type p for period t, from irrigation deposition onto plant and root uptake through soil, person•Ci•yr^2/kg

$A_{ca}(i,p,t)$ = time integral of animal product concentration for radionuclide i, animal product p, and period t, person•Ci•yr^2•kg (person•Ci/yr^2/L for milk)

$A_{cw}(i,p,t)$ = time integral of concentration in animal product p, for period t, for radionuclide i and animal product p for period t from waterborne pathways, person•Ci•yr^2/kg (person•Ci•yr^2/L for milk).

The total dose from terrestrial ingestion pathways is calculated by summing contributions from all plant and animal-product food types.

5.2.4 Aquatic Ingestion Pathways

Ingestion pathways resulting from release of radionuclides to surface or groundwater include ingestion of drinking water and aquatic foods. The five pathways available are fish, crustacea, molluscs, water plants, and drinking water. The dose for each pathway is calculated from the time-integrated aquatic media concentration, as follows for aquatic foods:

$$D_{oai} = D_{gio}\ 5.29 \times 10^{10}\ \lambda_{ri}\ U_a\ A_{fw}(i,p,t) \qquad (5.8)$$

and for drinking water

$$D_{oai} = D_{gio}\ 5.29 \times 10^{10}\ \lambda_{ri}\ U_a\ A_{dw}(i,t) \qquad (5.9)$$

where D_{oai} = dose from ingestion of aquatic food or water for organ o and radionuclide i, person•rem

U_a = the usage rate by humans of aquatic-food pathway a, kg/yr (L/yr for drinking water)

$A_{fw}(i,p,t)$ = time integral of aquatic food p, concentration for radionuclide i in period t, person•Ci•yr^2/kg

$A_{dw}(i,t)$ = time integral of drinking water concentration for radionuclide i in period t, person•Ci•yr^2/L.

5.2.5 External Exposures

External exposures result from proximity to contaminated ground, shoreline, and water. Swimming and shoreline doses are calculated from the time-integrated sediment concentration and water concentration as

$$D_{iew} = \lambda_{ri} \left[S_{dw}(i,t)\ D_{is}\ U_{sh}\ W + W_c(i,t)\ D_{iw}\ U_{sw} \right] \qquad (5.10)$$

where D_{iew} = dose from external exposure to shoreline and water for radionuclide i, person•rem

$S_{dw}(i,t)$ = sediment concentration parameter for radionuclide i for period t, person•Ci•yr/m^2

D_{is} = external dose factor for radionuclide i for exposure to contaminated soil on shoreline, rem/h per Ci/m^2

U_{sh} = time of exposure to contaminated shoreline, h/yr

W = shore-width factor for shoreline exposure, dimensionless

$W_c(i,t)$ = population-weighted water concentration for radionuclide i and period t, person•Ci•yr^2/L

D_{iw} = external dose factor for radionuclide i for submersion in contaminated water, rem/h per Ci/L

U_{sw} = time of exposure to contaminated water, h/yr.

The shore-width factor is an approximate correction to the infinite-plane geometry of the external exposure factors. To correct for the actual geometry

of a river bank or beach, a shore-width factor is applied that corresponds to the particular exposure situation. Suggested shore-width factors are given in Table 5.3.

Soil can be contaminated by deposition of airborne material or irrigation with contaminated water. The dose from external exposure to contaminated soil is calculated as

$$D_{ies} = \lambda_{ri} E_t D_{is} 224 \left[S_{ca}(i,t) + S_{cw}(i,t)\right] \quad (5.11)$$

where D_{ies} = dose from external exposure to soil for radionuclide i in person-rem

E_t = time of exposure to contaminated ground in h/yr

224 = soil areal density in kg/m^2.

The external exposure is based on the integrated soil concentration for the current 70-year period.

5.3 INCORPORATION OF SOURCES

The environmental source terms represent the rate at which radionuclides enter the environment through airborne or waterborne routes. The SUMO code allows the source-term data to be either read from external files or provided by the transport section of the code. In either case, radionuclide release-rate data are provided as time/rate data pairs. Each data pair gives a time (years after some reference time) and a release rate in curies per year for a

TABLE 5.3. Suggested Values for Shore-Width Factor

Shoreline Type	Shore-Width Factor
River shoreline	0.2
Lake shore	0.3
Nominal ocean site	0.5
Tidal basin	1.0

given radionuclide. The data for each radionuclide are also provided in a set of time-release data pairs. Using this procedure, a different set of time points can be used for each radionuclide. Because there are distinct transport properties for each of the radionuclides of interest in radioactive waste, it is important to be able to specify releases over a range of times.

To accomplish the 70-year-increment calculational scheme, the release rate data are interpolated and integrated to give the total activity released in each 70-year increment.

5.4 AIRBORNE RELEASES

Atmospheric processes transport radionuclides throughout the region surrounding the release point. The resulting distribution of material is important in determining the radiation exposure received by members of the regional population through potential exposure pathways. This section describes the methods available for specifying and estimating atmospheric dispersion.

Population exposure is calculated based on a spatial grid such as that shown in Figure 5.2. Sixteen directions and up to ten distance intervals are used. The population data set is specified as the number of people living within each area element of the grid at a given time. The atmospheric dispersion calculation is based on joint frequency of occurrence data for wind speed, wind direction, and atmospheric stability for the site. One set of joint frequency data is used, irrespective of the population data. The downwind normalized air concentration for each area element is provided by the transport portion of the code or is supplied by the user. The dispersion factors are used with the population distribution data to provide a population-weighted dispersion factor. This factor is a population-weighted estimate of the average normalized air concentration for the region. The factor is calculated as

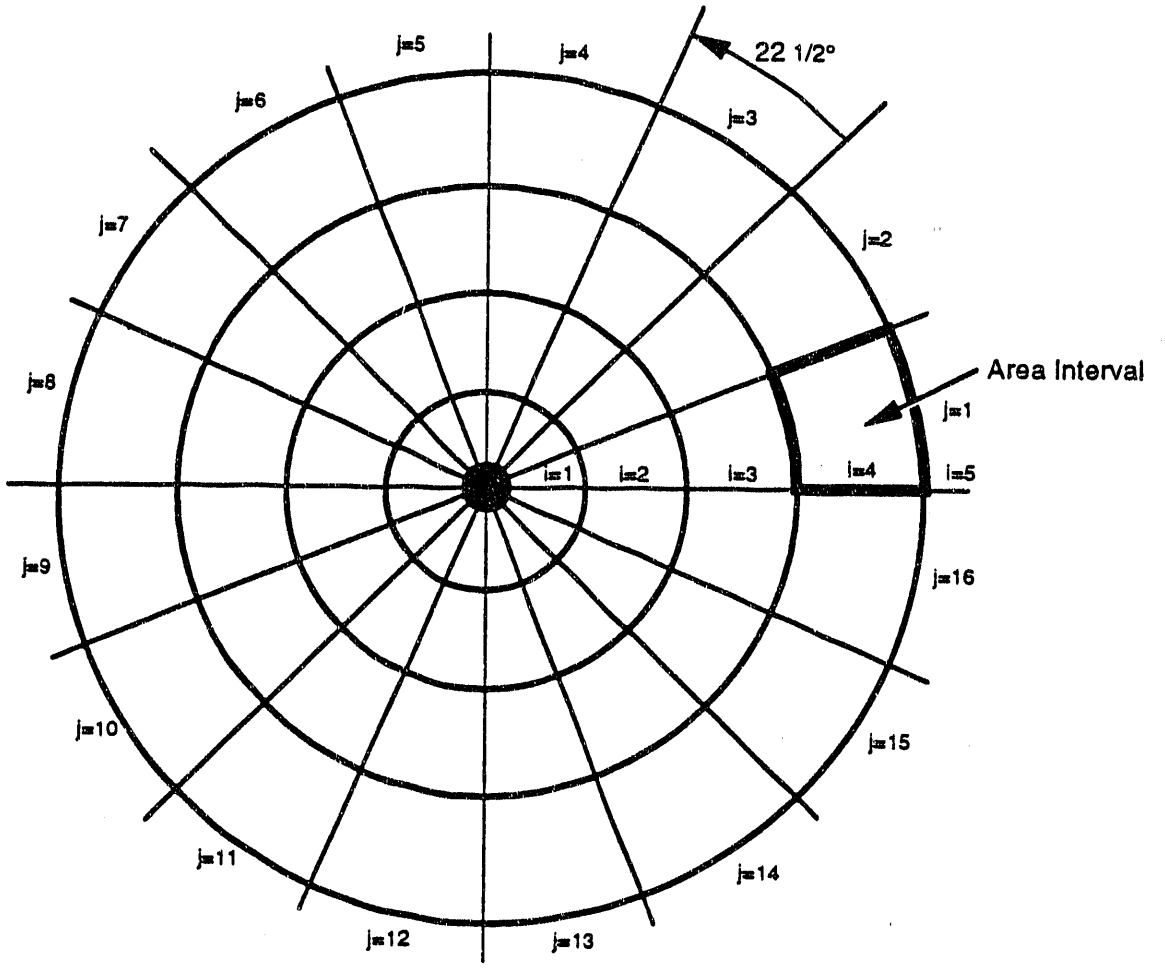

(Release at Center of Grid)

S9101075.9

FIGURE 5.2. Population Exposure Grid

$$PM(t) = \sum_{i=1}^{\text{directions}} \sum_{j=1}^{\text{distances}} P_{ij}(t)\ (\chi/Q')_{ij} \qquad (5.12)$$

where $PM(t)$ = population-exposure factor for period t, person-sec/m^3

$P_{ij}(t)$ = number of people living in the area interval in direction j at distance i in period t, persons

$(\bar{\chi}/Q')_{ij}$ = average normalized air concentration in the center of the area interval in direction j and distance i, Ci/m^3 per Ci/sec released.

As the equation indicates, the population-exposure factor is a function of time. Changes in population will be the primary cause of change in the population-exposure factor. Although climate changes may also affect the factor, such changes are difficult to predict and are not considered.

Two options that determine population-exposure factors are available for normalized air concentration values. When estimates of the total population change are provided, the population-exposure factor for the initial time may be calculated, and values for remaining time increments will then be calculated by ratio to population changes with time. If, instead, population distribution data are available as a function of time, they may be used to calculate population-exposure factors at each of the specified times, which are, in turn, interpolated for each 70-year increment.

Population-exposure factors can be specified by direct input of the factors at defined time points or by calculation from defined meteorological and population data. When population-exposure values are input, interpolations are made to determine the values at the midpoint of each 70-year increment.

5.5 WATERBORNE RELEASES

Pathways associated with waterborne releases include external exposure to contaminated water and sediment; ingestion of drinking water, farm products (via irrigation), and aquatic foods; and inhalation of resuspended material after irrigation. The release of activity to water is described by a release rate in curies per year defined at specific times. The activity released is assumed to result in exposure of a regional population. The number of people exposed to waterborne pathways is specified similarly to the definition of population for airborne pathways. The major difference is that only the total population is specified (the spatial distribution is not needed).

Two methods are available for defining population data for waterborne release. The first method is to define the population exposed during each of

the 70-year periods. The second method is to give the population present at specified times for interpolation at the midpoint of each 70-year period.

5.6 ENVIRONMENTAL CONCENTRATIONS

This section describes models used to estimate air, water, soil, sediment, and food concentrations for the important pathways. All radionuclide concentrations are expressed as time integrals over a 70-year period.

The information to be input for the pathway analysis is the total release of curies in each 70-year period. The total release is combined with population and dispersion parameters to estimate an environmental parameter for the exposure analysis. For airborne releases, the time-integrated air concentration of radionuclide i for period t, in person•Ci•yr^2/m^3, is calculated as

$$A_c(i,t) = PM(t)\frac{3.169\times10^{-8}}{\lambda_{ri}}\int_t^{t+70} a_i(s)ds \qquad (5.13)$$

where $PM(t)$ = population exposure factor for time period t, person•sec/m^3

3.169×10^{-8} = unit conversion constant, yr/sec

λ_{ri} = radiological decay constant for radionuclide i, yr^{-1}

$a_i(s)$ = instantaneous release rate to the atmosphere of radionuclide i at time s, Ci/yr.

For waterborne releases, the time-integrated water concentration of radionuclide i in period t, person•Ci•yr^2/L, is calculated as

$$W_c(i,t) = \frac{P(t)\ N\ M\ 1.119 \times 10^{-9}}{F_r\ \lambda_{ri}}\int_t^{t+70} W_i(s)ds \qquad (5.14)$$

where $P(t)$ = population exposed to water for period t, persons

N = reconcentration factor, dimensionless

M = mixing ratio, dimensionless

1.119×10^{-9} = conversion factor, $\left[\left(28.31 \frac{L}{ft^3}\right)\left(3.156 \times 10^7 \frac{sec}{yr}\right)\right]^{-1}, \frac{ft^3 \cdot yr}{L \cdot sec}$

F_r = flow rate of receiving water, ft^3/sec

$W_i(s)$ = instantaneous release rate to the receiving water, Ci/yr, at time s.

The airborne pathway analysis uses the air concentration parameter, $A_c(i,t)$, to determine several environmental concentrations:

- $S_{ca}(i,t)$, time integral of soil concentration for radionuclide i over the period t, person•Ci•yr^2/kg
- $L_{ca}(i,p,t)$, time integral of leaf concentration for radionuclide i and pathway p, from air deposition and resuspension over the period t, person•Ci•yr^2/kg
- $P_{ca}(i,p,t)$, time integral of plant concentration for radionuclide i, plant type p, and period t, person•Ci•yr^2/kg.

The soil concentration parameter is calculated from the air concentration parameter assuming deposition to be at a uniform rate over the 70-year period:

$$S_{ca}(i,t) = \frac{A_c(i,t)\ V_{di}}{7.098 \times 10^{-6}} \left(\frac{1 - e^{-\lambda_b 70}}{\lambda_b}\right) \qquad (5.15)$$

where V_{di} = deposition velocity for radionuclide i, m/sec

7.098×10^{-6} = constant, 224 kg/m^2 / 3.156×10^7 sec/yr

λ_b = environmental decay constant, yr^{-1}.

The environmental decay constant, λ_b, is calculated as the sum of a radiological decay constant, λ_{ri}, and a soil-removal constant for weathering, λ_{wi}. The soil-removal constant is a correction for long-term leaching of deposited radionuclides out of the soil's rooting and resuspension zones. The values given for λ_{wi} are calculated using the formula of Baes and Sharp (1981):

$$\lambda_{wi} = \frac{P + I - E}{d\ (1 + \rho/\theta\ kd_i)} \qquad (5.16)$$

where P = total precipitation, cm/yr

I = total irrigation, cm/yr

E = total evapotranspiration, cm/yr

d = depth of the rooting zone, cm

ρ = soil bulk density, g/cm^3

θ = soil volumetric water content, mL/cm^3

kd_i = soil-air partition coefficient for isotope i, mL/g.

For simplicity, the term P+I-E is approximated as an overwatering term, implying about 15 cm/yr of percolation through the rooting zone and into deeper soil layers. The depth, d, is defined as 15 cm to be compatible with other portions of the code. Baes and Sharp (1981) show that the term ρ/θ averages about 3. Thus the soil-removal constant for percolation can be considered as inversely proportional to the soil distribution coefficient, kd_i. The values used are based on the most conservative (i.e., largest) value of kd_i identified from a wide range of literature.

Harvest removal is simulated as a discrete process at the end of each calculational year. A quantity of each radionuclide equal to the product of the calculated vegetation concentration resulting from root uptake multiplied by the harvested yield (an input) subtracted from the soil compartments. The subtraction is normalized by the root penetration factor.

The time integral of leaf concentration is calculated from the air and soil concentration parameters, assuming a constant soil concentration equal to the value at the end of the 70-year period. This is a conservative assumption. The equation is

$$L_{ca}(i,p,t) = \frac{r V_{di}}{Y_p} \left[A_c(i,t) + 1.4933 \times 10^{-6} S_{ca}(i,t) \right] \left(\frac{1 - e^{-\lambda_{ei} T_p / 365.25}}{\lambda_{ei}} \right) 3.156 \times 10^7 \quad (5.17)$$

where r = interception fraction, dimensionless; 0.25 is used

Y_p = crop yield for food pathway p, kg/m^2

1.49×10^{-8} = conversion factor, $(1 \times 10^{-9}) \times (224/15)$, kg/m^2

λ_{ei} = effective retention rate constant for radionuclide i, yr^{-1}, or λ_{ri} + 18.0838, where 18.0838 is the rate constant for a 14-day half-life

T_p = growing period for food pathway p, days

365.25 = unit conversion constant, d/yr

3.156×10^7 = unit conversion constant, sec/yr.

The interception fraction, r, for a given vegetation type accounts for the fact that not all of the material deposited within a unit area will land on vegetation surfaces. The fraction of the total deposition that initially resides on vegetation is the interception fraction, r, such that $0 < r < 1$. The interception of materials in irrigation water has not been much studied; therefore, a default value of 0.25 is used for all materials deposited on all vegetation types by irrigation.

The factor of 1×10^{-9} (m^{-1}) represents a resuspension factor that is assumed to be constant, because that behavior is characteristic of aged deposited material (Anspaugh et al. 1975). It is assumed that the resuspended activity is deposited on plants near the soil from which it was suspended. Downwind transport of resuspended activity is not considered. The soil area density to a depth of 15 cm is assumed to be 224 kg/m^2 (soil density of 1.49 g/cm^3); 15 cm is the plowed depth through which the contamination is distributed. This value is included so that only the top centimeter of

material (1/15 of the total) is considered available for resuspension. The leaf concentration as calculated above represents the time integral over a 70-year period.

The radionuclide concentration in edible parts of the plant includes material from direct deposition plus material from root uptake:

$$P_{ca}(i,p,t) = L_{ca}(i,p,t)\ T_{vp} + S_{ca}(i,t)\ B_{iv} \qquad (5.18)$$

where T_{vp} is the translocation factor of externally deposited radionuclides to edible parts of the plant, dimensionless; and B_{iv} is the concentration ratio for plant uptake of radionuclide i, Ci/kg (plant wet weight) per Ci/kg (soil dry weight).

The concentration used for calculating uptake by the population is the animal product concentration for plant pathways. The uptake is calculated as

$$A_{ca}(i,p,t) = P_{ca}(i,p,t)\ S_{ip}\ Q_p \qquad (5.19)$$

where S_{ip} is the transfer coefficient of radionuclide i from daily intake by an animal to edible portion of animal product, Ci/L (milk) per Ci/day or Ci/kg (animal product) per Ci/day; and Q_p is the consumption rate of contaminated feed or forage by the animal for animal product p, kg/day.

The waterborne pathway analysis uses the water concentration $W_c(i,t)$ to determine the following environmental concentrations:

- $S_{cw}(i,t)$, time integral of soil concentration of radionuclide i over period t, resulting from water transport, person•Ci•yr^2/kg
- $S_{dw}(i,t)$, sediment deposition concentration for radionuclide i for period t for shoreline of contaminated water body, person•Ci•yr^2/m^2
- $L_{cw}(i,p,t)$, leaf concentrations for radionuclide i, plant type p, and period t for irrigation deposition and resuspension, person•Ci•yr^2/kg
- $P_{cw}(i,p,t)$, plant concentration for radionuclide i, plant p, and period t for deposition by irrigation and then resuspension, person•Ci•yr^2/kg.

The soil concentration at the end of the period is calculated assuming uniform deposition over the period:

$$S_{cw}(i,t) = \frac{W_c(i,t)\ I\ T_i}{224} \left(\frac{1 - e^{-\lambda_b 70}}{\lambda_b} \right) \tag{5.20}$$

where I = irrigation rate, $L/m^2 \cdot mo$

T_i = irrigation period, mo/yr

224 = soil area density, kg/m^2.

The exponential term (70) represents the integral over the 70-year period.

The concentration in the sediment is calculated similarly, as

$$S_{dw}(i,t) = W_c(i,t)\ 25300 \left(\frac{1 - e^{-\lambda_b 70}}{\lambda_b} \right) \tag{5.21}$$

where 25300 is the constant representing deposition to sediment, L/m^2 per year.

The concentration on leaves is calculated for contributions from direct irrigation deposition plus resuspension from soil:

$$L_{cw}(i,p,t) = \frac{r}{Y_p} \left\{ [W_c(i,t)\ 12\ I] + [S_{cw}(i,t)\ 0.47\ V_{di}] \right\} \left(\frac{1 - e^{-\lambda_{ei} T_p / 365.25}}{\lambda_{ei}} \right) \tag{5.22}$$

where 12 is the unit conversion constant, mo/yr; and 0.47 is the conversion factor for resuspension, $(10^{-9}\ m^{-1})$ $(3.156 \times 10^7\ sec/yr)$ $(224\ kg/m^2)$ (1/15).

The radionuclide concentration in edible parts of the plant is calculated for root uptake plus direct deposition as

$$P_{cw}(i,p,t) = L_{cw}(i,p,t)\ T_{vp} + S_{cw}(i,t)\ B_{iv} \quad (5.23)$$

The total uptake by plants during the 70-year period is given by the plant concentration parameter. For animal products, uptake from animal consumption of plants plus animal consumption of water is calculated as

$$A_{cw}(i,p,t) = S_{ip}\left[P_{cw}(i,p,t)\ Q_p + W_c(i,t)\ Q_{pw}\right] \quad (5.24)$$

where Q_{pw} is the consumption rate of water by an animal of type p, L/d.

The time-integrated concentration of radionuclide i in aquatic food p in period t, $A_{fw}(i,p,t)$, in person•Ci•yr^2/kg, is calculated from the water concentrations as

$$A_{fw}(i,p,t) = W_c(i,t)\ B_{ip} \quad (5.25)$$

where B_{ip} is the bioaccumulation factor for radionuclide i and aquatic food p, Ci/kg per Ci/L.

The time-integrated water concentration of radionuclide i in period t for the drinking water pathway, $A_{dw}(i,t)$ in person•Ci•yr^2/L, is calculated as

$$A_{dw}(i,t) = W_c(i,t)\ C_i \quad (5.26)$$

where C_i is the dimensionless water purification plant cleanup factor.

5.7 SPECIAL MODELS FOR ^{3}H AND ^{14}C

The radionuclides ^{3}H and ^{14}C are handled in a special manner. Both elements are integral to the human metabolism. Tritium (^{3}H) is assumed to be in the form of tritiated water. All tritiated water ingested or inhaled is assumed to be absorbed into the transfer compartment completely and instantaneously. Therefore at any time following intake, tritiated water is assumed to be uniformly distributed among the soft tissues, where it is retained with a

biological half-life of 10 days. In addition, exposure to an atmosphere containing ^{3}H results in intake of ^{3}H by absorption through intact skin. The total rate of intake of ^{3}H in air is assumed to be 150% of the inhalation intake rate alone.

Similarly, all intakes of ^{14}C are assumed to be absorbed into the transfer compartment completely and instantaneously. This is equivalent to assuming that inhaled material is carbon dioxide gas and that ingested materials are readily absorbed carbohydrates. Carbon is assumed to be distributed throughout the organs and tissues of the body, where it is retained with a biological half-life of 40 days. This assumption is considered by ICRP 30 (ICRP 1979-1982) to yield realistic estimates for ^{14}C-labeled metabolites and to overestimate doses for most other ^{14}C-labeled compounds.

The behavior of ^{3}H and ^{14}C in exposure pathways is handled in a special manner. The concentrations of ^{3}H or ^{14}C in environmental media (soil, plants, and animal products) are assumed to have the same specific activity (curies of radionuclide per kilogram of soluble element) as in the contaminating medium (air or water). The fractional content of hydrogen or carbon in a plant or animal product is then used to compute the concentration of ^{3}H or ^{14}C in the food product under consideration. The hydrogen contents of both the water and the dry portions of the food product are used when calculating the ^{3}H concentration. For airborne releases, it is assumed that plants obtain all of their carbon directly from airborne carbon dioxide and that animals obtain all of their carbon through ingestion of plants.

Because plants acquire most of their carbon from the air, the transfer of ^{14}C from water to plants is difficult to model for waterborne releases. Current models of ^{14}C uptake from water by plants use specific-activity models that relate the activity in the plants directly to the activity in irrigation water. This approach is extremely conservative, in that it assumes that plants receive all of their carbon from water. The interim model described here is based on the ratio of grams of ^{14}C to grams of total carbon in soil and a correction for the amount of carbon that plants obtain from soil.

In this section, the special models available in SUMO for ^{3}H are described first, followed by descriptions of the ^{14}C models. The

concentrations of ^{3}H and ^{14}C in water and air are calculated as for other nuclides, by Equations (5.13) and (5.14).

The soil concentration of ^{3}H from the water pathway is

$$S_{cw}(^{3}H,t) = 0.1\ W_c(^{3}H,t) \tag{5.27}$$

where $W_c(^{3}H,t)$ is the concentration of ^{3}H in environmental water, person•Ci•yr^2/L; and 0.1 is the soil moisture, L/kg. The plant concentration of ^{3}H in plant type p in period t, $P_{cw}(^{3}H,p,t)$ in person•Ci•yr^2/kg, is calculated as

$$P_{cw}(^{3}H,p,t) = 9\ W_c(^{3}H,t)\ F_{Hp} \tag{5.28}$$

where F_{Hp} is the fraction of hydrogen in total vegetation. The coefficient 9 converts ^{3}H concentration in environmental water to concentration in hydrogen. The fractions of hydrogen in various food types are given in Table 5.4.

For an airborne release, the concentration of ^{3}H in environmental water is calculated from the air concentration and the absolute humidity, as follows:

$$W_c(^{3}H,t) = 9A_c(^{3}H,t)/H \tag{5.27}$$

where H is the absolute humidity, L/m^3, assumed to be 0.008 L/m^3. (This value is based on humidity at the arid Hanford Site in southeastern Washington.)

The concentration of ^{3}H in the animal product is

$$A_{cw}(^{3}H,p,t) = \frac{P_{cw}(^{3}H,p,t)Q_f + W_c(^{3}H,t)Q_w}{F_{Hf}Q_f + Q_w/9}\ F_{Hp} \tag{5.30}$$

where $A_{ow}(^{3}H,p,t)$ = concentration of ^{3}H in animal product p, Ci/kg or Ci/L

$P_{cw}(^{3}H,p,t)$ = concentration of ^{3}H in crop used for animal feed, Ci/kg

TABLE 5.4. Fractions of Hydrogen and Carbon in Environmental Media, Vegetation, and Animal Products

Food or Fodder	Water (f_w)	Carbon (dry) (f_c)	Hydrogen (dry) (f_h)	Carbon[a] (wet) (F_{cv} or F_{ca})	Hydrogen[b] (wet) (F_{hv} or F_{ha})
Fresh fruits, vegetables, and grass	0.80	0.45	0.062	0.090	0.10
Grain and stored animal feed	0.12	0.45	0.062	0.40	0.068
Eggs	0.75	0.60	0.092	0.15	0.11
Milk	0.88	0.58	0.083	0.070	0.11
Beef	0.60	0.60	0.094	0.24	0.10
Poultry	0.70	0.67	0.087	0.20	0.10

Absolute humidity . . . . . 0.008 L/m^3

Concentration of carbon in water . . . . . 2.0×10^{-5} kg/L[c]

Concentration of carbon in air . . . . . 1.6×10^{-4} kg/m^3[d]

Fraction of soil that is carbon 0.03

Soil moisture . . . . . 0.1 L/kg

(a) F_{cv} or $F_{ca} = f_c (1 - f_w)$.
(b) F_{hv} or $F_{ha} = f_w/9 \ [f_h(1 - f_w)]$.
(c) Assumes a typical bicarbonate concentration of 100 mg/L.
(d) Assumes a typical atmospheric CO_2 concentration of 320 ppm_v.

$W_c(^3H,t)$ = concentration of ^3H in animal drinking water, Ci/L

F_{Hf} = fraction of hydrogen in animal feed, dimensionless

F_{Hp} = fraction of hydrogen in animal product p, dimensionless.

The models for ^{14}C are similar to those for ^3H. The concentration of ^{14}C in vegetation from irrigation is

$$P_{cw}(^{14}C,p,t) = W_c(^{14}C,t)\ I\ te_p \frac{0.1}{0.01\ \rho\lambda s_C}\left[1 - \exp\left(-\lambda s_C\ te_p\right)\right] \qquad (5.31)$$

where $P_{cw}(^{14}C,p,t)$ = concentration of ^{14}C in plant type p, person•Ci•yr^2/kg

$W_c(^{14}C,t)$ = concentration of ^{14}C in irrigation water, Ci/L

te_p = length of growing period for plant type p, sec

ρ = soil density of 15-cm surface (rooting) layer, kg/m^2

0.1 = the assumed uptake of 10% of plant carbon from soil

0.01 = the average fraction of soil that is carbon

λs_C = effective removal rate constant for ^{13}C in soil, sec^{-1}.

The concentration of ^{14}C in crops from atmospheric contamination is calculated as

$$P_{ca}(^{14}C,p,t) = A_c(^{14}C,t)\frac{F_{cp}}{P_c} \tag{5.32}$$

where $A_c(^{14}C,t)$ = concentration of ^{14}C in air, person•Ci•yr^2/m^3

F_{Cp} = fraction of carbon in plant type p, dimensionless

P_c = concentration of carbon in air, kg/m^3.

The concentration of ^{14}C in animal products resulting from water pathways is calculated as

$$A_{cw}(^{14}C,p,t) = \frac{P_{cw}(^{14}C,p,t)\ Q_f + W_c(^{14}C,t)\ Q_w}{F_{Cf}Q_f + F_{Cw}Q_w}\ F_{Cp} \tag{5.33}$$

where $A_{cw}(^{14}C,p,t)$ = concentration of ^{14}C in animal product p, Ci/kg or Ci/L

$P_{cw}(^{14}C,p,t)$ = concentration of ^{14}C in crop used for animal feed, Ci/kg

$W_c(^{14}C,t)$ = concentration of ^{14}C in animal drinking water, Ci/L

F_{Cf} = fraction of carbon in animal feed, dimensionless

F_{Cw} = fraction of carbon in animal drinking water, dimensionless

F_{Cp} = fraction of carbon in animal product p, dimensionless.

This expression can be simplified for airborne releases by noting that the water concentration [$W_c(^{14}C,t)$] is zero and that the carbon content is much higher in plants than in water ($F_{Cf} >> F_{Cw}$). The animal product concentration then becomes

$$A_{ca}(^{14}C,p,t) = P_{ca}(^{14}C,p,t)\frac{F_{Cm}}{F_{Cf}} \quad (5.34)$$

5.8 GENERAL CONSIDERATIONS FOR THE DOSE MODEL

Additional considerations in the dose model include handling of decay chains and generation of dose conversion factors.

5.8.1 Decay Chains

Radioactive nuclei sometimes decay through a number of unstable products before reaching a stable (or very long-lived) end state. These decay chains are important in that the decay energies of the products contribute to the total dose received from intake of the original material. The data on radionuclide half-lives, decay chains, and various fractional branching ratios within chains are largely taken from the DRALIST data of Kocher (1981). These data are obtained from the GENII standard library (Napier et al. 1988).

Radionuclides with half-lives of less than 10 min are of little importance in environmental calculations and in terms of internal dose, unless they are members of longer decay chains. All decay data in the standard library represent radionuclides with half-lives longer than 10 min and less than 2×10^6 years. These points of truncation were chosen because radionuclides with very short half-lives will decay to a negligible amount quickly (presenting little exposure) and those with extremely long half-lives are virtually inactive within any given 70-year period. For chains with products with very short half-lives, the decay energy associated with the short-lived products has been assigned to the original material. The appropriate branching ratios have been considered.

The SUMO program includes a generalized chain decay processor that can give the activity of any member of a decay chain as a function of time from any initializing condition. The chain processor operates on a recursive application of the Bateman (1910) equations modified to include branching. This implementation of the Bateman equations provides a simple means of solving the differential equations describing chain decay. The general form of the decay equation for the jth member of a decay chain is as follows:

$$Q_j(t) = \sum_{m=1}^{j} C_{j,m}\, e^{-\lambda_m T} \qquad (5.35)$$

where $Q_j(t)$ = quantity of chain member j at time t, atoms

λ_m = decay constant of radionuclide m, d^{-1}

$C_{j,m}$ = coefficient for term m of chain member j, atoms.

The amount of each radionuclide is expressed in units proportional to the number of atoms present. The units are related to the activity as

$$Q_j(t) = \frac{k\, Y_j}{\lambda_j} \qquad (5.36)$$

where k is the proportionality constant, equal for all radionuclides (k = 1 where activity is given in Bq and λ_j is given in inverse seconds).

Evaluation of the coefficients begins with the first member and proceeds downward through the chain. The number of coefficients needed for a given chain member is equal to the position of the member in the chain. Thus, for example, the third chain member requires three coefficients. The coefficient for the first chain member is just the amount present at the start of the decay period:

$$C_{1,1} = Q_1(0) \qquad (5.37)$$

The coefficients for other chain members are evaluated using the following formulas and previously evaluated coefficients:

$$C_{j,m} = \left[\sum_{i=m}^{j-1} f_{i,j}\ \lambda_i\ C_{i,m}\right] / \prod_{j=1}^{m-1} (\lambda_j - \lambda_m) \text{ for } m<j \qquad (5.38)$$

and

$$C_{j,j} = Q_j(0) - \sum_{i=1}^{j-1} C_{i,i} \qquad (5.39)$$

where $f_{i,j}$ is the fraction of radionuclide i decays that results in production of radionuclide j, dimensionless. This generic representation of the Bateman equation allows decay and branching from any chain member to any member lower in the chain. In practice it is only necessary to include terms in the equation for which the branching fractions ($f_{i,j}$) are greater than zero. The subroutine that implements the decay calculation contains logic to include only those branches that are defined as present. With the exception of the expression for leaf concentration, all equations reflect chain decays. Chain decays for concentrations on leaves are not justifiable because the leaves of the types of plants considered are only short-term sources of exposure.

5.8.2 Special Assumptions for Dose Conversion Factors

The SUMO code uses dose conversion factors that are generated by external research codes. Some unusual assumptions have been made (see Napier et al. 1988):

- All xenon decay products of iodine are assumed to escape the body before further decaying.
- All iodine produced in the body by the decay of tellurium is translocated instantaneously to the iodine inorganic transfer compartment.

- All ^{222}Rn produced by the decay of ^{226}Ra is assumed to diffuse entirely out of soft tissues of the body before decaying, and 30% is retained in mineral bone tissues. Products of radon are allowed to continue to accumulate in the bone compartments.

The SUMO code will issue warning messages concerning these assumptions for some input data configurations.

6.0 MATHEMATICAL STRATEGY FOR GENERATING RANDOM VARIABLES

This section presents random-number-generation theory and algorithms for statistical distributions implemented in the SUMO code. The topics addressed are probability concepts, including generation of uniform random numbers, the concept of stratified sampling, and algorithms for random-number generation.

6.1 PROBABILITY CONCEPTS

The distribution of a continuous random variable X (the term "continuous" indicates that the random variable is defined over a continuum of values) is completely described by its probability density function f(x) (referred to as a PDF), such as those given in Figure 6.1. The interpretation of the PDF is that the area under f(x), for an interval $a < x < b$, equals the probability that the random variable, X, will fall in the interval (a,b), denoted P[a<X<b]. One cannot make the statement P[X=t], because at any single point t there is no area under the PDF. An axiom of probability theory states that the probability of any event is between 0 and 1, so the integral of the PDF over the entire support (the interval [L,U]) of X equals 1 (Strait 1989, p. 24). The integral of the PDF from the lower bound L to some value x (that is less than the upper bound U) represents the probability that X will be observed in the interval (L,x). This integral operation defines the cumulative distribution function (CDF) for the random variable X. The CDF is denoted by F(x) and is represented mathematically by the equation

$$F(x) = \int_L^x f(s)\, ds \qquad (6.1)$$

The inverse CDF, $[F^{-1}(\bullet)]$, is single-valued if x is in the interval (L,U). Hence if $p' = F(x')$ is known, in theory $x' = F^{-1}(p')$ exists. In practice there are situations for which no analytic expressions for F(x) or $F^{-1}(p)$ are available, so approximate numerical expressions are used instead.

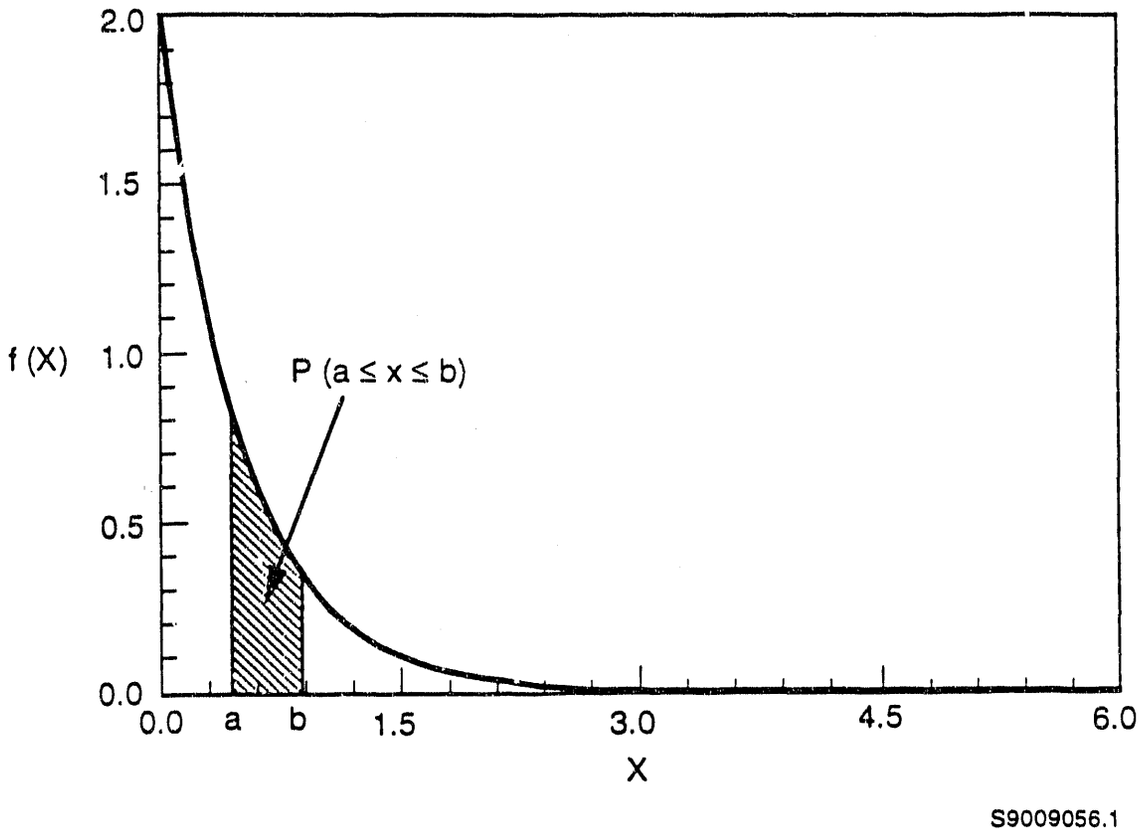

FIGURE 6.1. Example of Probability Density Functions

6.1.1 Random-Number Generation by the Probability Integral Transform Method

Generation of a random variable from a given distribution typically involves the use of information about either f or F. There are two philosophical approaches to generating random numbers: exact methods and approximate methods. The algorithms embedded in SUMO employ exact methods. Exact methods can be further categorized as probability integral transform (PIT) methods or functional methods (Bratley et al. 1983). The PIT method is employed in the SUMO code.

In the PIT method, the random variable of interest is expressed as a function of a U(0,1) random variable, where U(0,1) denotes the continuous random variable ranging uniformly over the interval (0,1). The PDF of the uniform random variable is $g(u) = 1$ if $u \epsilon (0,1)$ and is zero elsewhere. The CDF for this random variable takes the simple form $G(u) = u$. It can be shown that any CDF evaluated at a random value X (instead of being evaluated at a known

value x as in the previous discussion) is distributed uniformly over the interval (0,1) (Mood et al. 1974, p. 202). Therefore, given a realization u of the U(0,1) random variable and a known statistical distribution, one can set $u = F(x)$ and solve to obtain $x = F^{-1}(u)$. The value x thus obtained is a realization from the statistical distribution.

In principle, one can obtain an exact solution for x given any specific CDF and value u. In reality, there are some PDFs (e.g., the normal distribution) for which no closed-form analytical expression for F^{-1} exists, and hence approximation methods must be applied. The PDFs are nonetheless exact in the sense that they are derived from the exact equation $x = F^{-1}(u)$ rather than an approximate equation.

The PIT method allows efficient sampling from a subregion of the interval (L,U), such as (c,d) where $L < c < d < U$ (e.g., sampling from a subregion of the selected distribution). In this case, one would find the corresponding interval in the uniform domain, say (c',d'), and sample uniformly over that interval, by sampling from the rescaled uniform distribution [i.e., $u' = (d-c)u+c$] and then obtaining x as usual using $x = F^{-1}(u')$. The rescaled uniform distribution takes the form $g(u) = 1/(d'-c')$ for $u \in (c',d')$ and is zero elsewhere. For any distribution with PDF f(x), the PDF truncated to the interval (c,d) is $f_T(x) = f(x)/[F(d)-F(c)]$. The divisor ensures that $f_T(x)$ integrates to unity.

6.1.2 Dependence on the Uniform Random-Number Generator

Desirable attributes of a random-number generator are ease and portability of implementation, independence between generated deviates, and long cycles between recurrence of values. However, the occurrences should be in accordance with the shape of the distribution, not uniformly distributed over the interval of nonzero probability density. Using the PIT method, the degree of each of these features is determined by the extent to which they are associated with the uniform random-number generator selected (this relationship is guaranteed by the monotonicity of F^{-1}). The use of a suitable uniform random-number generator is central to the successful use of the PIT method.

6.1.3 Stratified Sampling

Stratified sampling can easily be implemented when random deviates are generated using the PIT method. This is accomplished by dividing the uniform interval (0,1), into subintervals, or strata, and sampling a specified number of times within each stratum, each time obtaining the corresponding value of x. Within the SUMO code, the stratum intervals are assigned equal probability, so their sample sizes are also (approximately) equal. The total number of draws, k, of the random variable is given as a control input. Equal numbers of draws are made within each stratum, except for a single additional realization in some strata as a result of k's not being evenly divisible by the number of strata. The method generates samples from each stratum, then randomly "shuffles" the entire set of realizations using a variation of the Quicksort algorithm (Singleton 1969). The primary purpose of stratified sampling is to ensure more evenly spaced (in a probability sense) samples from the distribution of a random variable than might result from randomly sampling over the whole range of the distribution.

6.2 STATISTICAL ALGORITHMS IMPLEMENTED IN THE SUMO CODE

The statistical distributions available for use in the SUMO code are summarized in Table 6.1. The distributions are indexed as required in an input control file to the SUMO code.

6.2.1 Algorithm for the Uniform Distribution

Algorithms that generate truly random uniform numbers do not exist, although many algorithms generate pseudo-random deviates (hereafter loosely referred to as random numbers). The selection of a random-number generator is based on four considerations: 1) computer implementability, 2) degree of independence within a sequence of deviates, 3) periodicity or cyclic length of a sequence, and 4) uniform coverage of sequences (occurrence) over the interval (0,1), the square (0,1) X (0,1), and so on, up to the hypercube $(0,1)^k$.

Commonly used random-number-generation techniques on digital computers involve feedback shift register (FSR) and linear congruential methods (Kennedy and Gentle 1980, pp. 136, 150). The SUMO code uses a linear congruential random-number generator.

TABLE 6.1. Statistical Distributions Implemented in the SUMO Code

Index	Distribution
0	Constant
1	Uniform
2	Loguniform (base 10)
3	Loguniform (base e)
4	Normal
5	Lognormal (base 10)
6	Lognormal (base e)
7	Exponential
8	Triangular
9	Gamma
10	Beta
11	Weibull
12	Logistic
13	Cauchy
14	User-supplied table of values

6.2.1.1 Generation Algorithm

The linear congruential generator generates "random" integers from an algorithm of the form

$$R_i = \left(A \cdot R_{i-1} + C\right) \bmod M \tag{6.2}$$

where R_i is the ith random integer to be generated between 1 and M-1, A and C are constants, M is the modules of the generated integers, and mod denotes the remainder function. These integers are converted to approximate U(0,1) numbers by the division

$$U_i = R_i / M \tag{6.3}$$

The period of a sequence (U_i) of generated deviates is the minimal value k such that $U_i = U_{i+k}$ (this occurs independent of i for linear congruential generators). It can be shown that the period of any congruential generator does not exceed M. Therefore, if one is generating many uniform deviates, it is desirable that M be large. The performance of each congruential generator (each choice of A, C, and M) can thus be examined with respect to criteria

proceeding from the four considerations given above. The SUMO implementation uses A = 16,807 and M = 2,147,483,647. These choices of A and M yield a sequence (U_i) that 1) is implementable on a 32-bit computer without machine language coding, 2) is sufficiently independent on an element-by-element basis, 3) possesses a long cycle (period), and 4) has a reasonable degree of coverage over all hypercubes of dimension less than k. These attributes are identified from results of tests described by Fishman and Moore (1986).

Any value x generated from the uniform (a,b) distribution in the SUMO code makes use of a value y from the U(0,1) distribution. The value y is generated first, then x is evaluated as x = a+(b-a)y. The uniform (a,b) distribution will be denoted by U(a,b).

6.2.2 Algorithm for the Loguniform Distribution

6.2.2.1 Definition of the PDF

The PDF for a loguniform random variable of base b is

$$f(x) = I(b^c<x<b^d) \,/\, [x(d-c)\ \ln(b)] \tag{6.4}$$

for $-\infty < c < d < \infty$, where I is an indicator function (0 if false, 1 if true), b is the logarithm base (either 10 or the natural constant e), and ln(b) denotes the natural logarithm of b.

6.2.2.2 CDF and Inverse CDF Algorithms

The CDF algorithm for the loguniform distribution is

$$F(x) = 0 \qquad \text{if } x \le b^d \tag{6.5a}$$

$$F(x) = [\ln(x) - c\ \ln(b)] \,/\, [(d-c)]\ \ln(b)] \qquad \text{if } b^c \le x \le b^d \tag{6.5b}$$

$$F(x) = 1 \qquad \text{if } x \le b^d \tag{6.5c}$$

The logarithm base b can be chosen to be either e (the natural constant) or 10.

The inverse CDF algorithm used to generate a value x from the loguniform distribution first generates a value y from the U(c,d) distribution and then evaluates the expression $x = b^u$.

6.2.3 Algorithms for the Normal Distribution

6.2.3.1 Definition of the PDF

A normally distributed random variable with mean μ and variance σ^2, denoted as $N(\mu,\sigma)$, has the PDF

$$f(x) = \left(\sigma\ (2\pi)^{0.5}\right)^{-1} \exp[-0.5(x-\mu)^2/\sigma^2] \qquad (6.6)$$

for $-\infty < x < \infty$, $-\infty < \mu < \infty$, and $\sigma^2 > 0$. The CDF has no closed-form expression.

6.2.3.2 CDF Algorithm

An $N(\mu,\sigma^2)$ random deviate, y, is obtained by generating a N(0,1) deviate, x, then transforming as $y = \mu+\sigma x$. This description of the generation of normal random variables will therefore focus on the N(0,1) parameterization.

The first step in the algorithm for the CDF of the standard normal distribution is to compute the area in the smallest "tail," evaluated from x to the lower or upper limit of the range of x, depending on the sign of x. Let T(x) be that area defined as T(x) = Prob[X<s] for $s < 0$, or Prob[X>s] for $s \geq 0$. Thus F(x) = T(x) for $x < 0$ and F(x) = 1-T(x) for $x \geq 0$. The approximation used for T(x) is that of Adams (1969) and is given by

$$T(x) = 0.5 - z\left((a_1+a_2y) \,/\, \left\{(y+a_3+a_4) \,/\, [(y+a_5+a_6) \,/\, (y+a_7)]\right\}\right) \qquad (6.7a)$$

for $|x| \leq 1.28$,

$$T(x) = b_1 \exp(-y) \Big/ \left\{(z+b_2+b_3) \Big/ \left[(z+b_4+b_5) \Big/ \left((z+b_6+b_7) \Big/ \left\{(z+b_8+b_9) \Big/ [(z+b_{10}+b_{11}) \Big/ (z+b_{12})]\right\}\right)\right]\right\} \tag{6.7b}$$

for $1.28 < x \leq$ UTZERO or $1.28 < -x \leq$ LTONE, and

$$T(x) = 0.0 \tag{6.7c}$$

for $x >$ UTZERO or $x <$ -LTONE. The algorithm uses $z = |x|$ and $y = z^2/2$. Values for the coefficients a_i and b_i are given in Table 6.2.

A FORTRAN implementation of this algorithm was taken from Hill (1985). The values UTZERO and LTONE are machine-dependent. The variable UTZERO represents the upper tail limit of the statistical density such that P[X>UTZERO] = 0 at machine accuracy, and LTONE represents the lower tail limit such that P[X>LTONE] = 1 at machine accuracy. If n denotes the decimal length of real numbers for the machine being used, and w denotes the smallest allowable positive real number, LTONE = (n+9)/3 and UTZERO = $-0.3+[-2\ln(w)-2]^{0.5}$.

6.2.3.3 Inverse CDF Algorithm

The inverse CDF for the N(0,1) random variable is approximated by

$$F^{-1}(p) = \begin{cases} q\, A(q^2)/B(q^2) & \text{if } |q| < 0.42 \\ \text{sgn}(q)\, C(r)/D(r) & \text{if } |q| \geq 0.42 \end{cases} \tag{6.8}$$

where $q = p - 0.5$, and $r = [\ln(0.5-|q|)]^{0.5}$. The quantity $(0.5-|q|)$ is formed as p or, to avoid cancellation if p is small, as (1-p). The letters A, B, C, and D represent polynomials of order 3, 4, 3, and 2, respectively, whose coefficients are given by Beasley and Springer (1985), and sgn(q) equals 1 if $q > 0$ and -1 if $q < 0$.

6.2.3.4 Precision

The approximation for the normal CDF is accurate to 9 decimal digits on a machine with that accuracy (Hill 1985). The algorithm is implemented in

TABLE 6.2. Coefficients in the Normal CDF Algorithm

i	a_i	b_i
1	0.398942280444	0.398942280385
2	-0.399903438504	-3.8052E-8
3	5.75885480458	1.00000615302
4	-29.8213557808	3.98064794E-4
5	2.62433121679	1.98615381364
6	48.6959930692	-0.151679116635
7	5.92885724438	5.29330324926
8	--	4.8385912808
9	--	-15.1508972451
10	--	0.742380924027
11	--	30.789933034
12	--	3.99019417011

double precision, so it achieves the desired accuracy on a machine with a 32-bit word length.

The polynomial approximation for the inverse normal CDF is accurate up to 2^{-31} in the domain of p [e.g., $|p'-p| < 2^{-31}$, where p' is the actual value of $F(x_{p'})$]. Consideration of roundoff error brings the accuracy to the order of 20 times the least significant bit in the machine's mantissa (in the domain of p). The actual accuracy of x_p is of concern, however, and is linearly approximated by

$$x_{p'} - x_p = (p'-p)\ \exp(0.5x_{p'}^2)\ (2\pi)^{0.5} \qquad (6.9)$$

This error approximation is identical (up to a constant) for the truncated distribution.

6.2.4 Algorithm for the Lognormal Distribution

6.2.4.1 Definition of the PDF

The logarithm of a random variable being distributed as a normal $N(\mu,\sigma^2)$ random variable is a lognormal random variable. The PDF of the lognormal distribution is

$$f(x) = \frac{A}{x\sigma(2\pi)^{0.5}} \exp\left\{-0.5[\log(x)-\mu]^2/\sigma^2\right\} I(0,<x,<\infty) \qquad (6.10)$$

Because this distribution is available in both base 10 and natural logarithm base form, the constant A is $1/\log_e 10$ or 1, respectively.

6.2.4.2 Generation Algorithms

In the SUMO code, a lognormal random variable x is obtained by transforming an $N(\mu,\sigma^2)$, y, using the expression $x = b^y$, where the base b is either 10 or the natural constant e. The loguniform CDF is evaluated for a value x by computing $y = \log_b(x)$ and using y in the algorithm for the $N(\mu,\sigma^2)$ algorithm.

Truncation limits specified for the lognormal distribution are converted to limits in the normal domain, then further converted to appropriate limits in the U(0,1) domain as described in the section on the normal distribution. Thus, the generation algorithm for the truncated distribution uses a subset of the U(0,1) distribution in the algorithm for the untruncated distribution.

6.2.4.3 Precision

The precision of the lognormal generation algorithm can be obtained by approximated using the first two terms of the equation

$$b^{y_{p'}} = \left[(p'-p)\,\sigma \exp\left(y_{p'}^2/2\right) \ln(b)\,(2\pi)^{0.5}\right] + \left\{0.5(p'-p)^2\pi\,\sigma \ln(b) \exp\left(y_{p'}^2\right)\left[y_{p'} + 2\sigma \ln(b)\right]\right\} + o\left[(p'-p)^2\right] \qquad (6.11)$$

where o(s) is a collection of terms in s such that $\lim_{s\to 0} o(s)/s = 0$, y_p is the theoretical realization from the normal $N(\mu,\sigma^2)$ distribution associated with uniform realization p, and $y_{p'}$ is the value actually obtained ($y_{p'}$ is exact for the value p', which did not occur). Thus $y_{p'}-y_p$ is the error (in the normal domain) caused by the algorithm approximation and computer implementation of

the algorithm, and $b^{y_{p'}}-b^{y_p}$ is the error of the lognormal deviate. (Recall that the bound on $|p'-p|$ is given in the description of the normal deviate generation.)

6.2.5 Algorithm for the Exponential Distribution

6.2.5.1 Definition of the PDF

The exponential distribution has PDF

$$f(x) = \theta\, e^{-\theta x}\, I(0<X<\infty) \tag{6.12}$$

for $\theta > 0$.

6.2.5.2 Generation Algorithms

Random variables from the exponential distribution are easily generated, because there is a closed-form analytic expression for $F^{-1}(p)$. The CDF for the exponential distribution is

$$F(x) = 1 - e^{-\theta x} \tag{6.13}$$

After obtaining a value, u, from the U(0,1) distribution, the CDF is inverted to obtain the generation algorithm

$$x = -\theta^{-1} \ln(1 - u) \tag{(6.14)}$$

6.2.6 Algorithm for the Triangular Distribution

6.2.6.1 Definition of the PDF

The triangular distribution has PDF

$$f(x) = \begin{cases} 2(x-a)/[(b-a)(c-a)] & a < x \le b \\ 2(c-x)/[(c-b)(c-a)] & b \le x < c \\ 0 & a > x \text{ or } x > c \end{cases} \tag{6.15}$$

6.2.6.2 CDF Algorithm

The CDF algorithm for the triangular distribution takes the form

$$F(x) = \begin{cases} 0 & x \le a \\ (x-a)^2/[(c-a)(b-a)] & a \le x \le b \\ 1-(x-c)^2/[(c-a)(c-b)] & b \le x \le c \\ 1 & x \ge c \end{cases} \qquad (6.16)$$

6.2.6.3 Inverse CDF Algorithm

The algorithm for generating values from the triangular distribution depends on the value u chosen from the U(0,1) distribution. The expressions for $F^{-1}(u)$ are

$$F^{-1}(u) = x = \begin{cases} a + [u(c-a)(b-a)]^{0.5} & 0 \le u \le (b-a)/(c-a) \\ c - [(1-u)(c-a)(c-b)]^{0.5} & (b-a)/(c-a) \le u \le 1 \end{cases} \qquad (6.17)$$

6.2.7 Algorithm for the Gamma Distribution

6.2.7.1 Definition of the PDF

The PDF for the gamma distribution has the form

$$f(x) = \beta^{\alpha} x^{\alpha-1} e^{-\beta x} / G(\alpha) \; I(0<x<\infty) \qquad (6.18)$$

for $\alpha, \beta > 0$, where

$$G(s) = \int_0^{\infty} x^{s-1} e^{-x} dx \qquad (6.19)$$

is the gamma function.

6.2.7.2 CDF Algorithm

There is no general analytic expression for either F(x) or its inverse, and hence a numerical approximation is required for evaluating them. The CDF can be written as,

$$F(x) = \int_0^x \beta^{\alpha} s^{\alpha-1} e^{-\beta s} ds \; / \; G(\alpha) \qquad (6.20)$$

where $G(\alpha)$ denotes the gamma function. With a change of variable, the CDF can be expressed as

$$F(x) = \int_0^{x\beta} s^{\alpha-1} e^{-s} ds \; / \; G(\alpha) \qquad (6.21)$$

The CDF algorithm given below is valid for $\beta = 1$. If $\beta \neq 1$, then the CDF can be evaluated using $y = x\beta$ instead of x. The approximation implemented by the SUMO code for F(x) is that of Bhattacharjee (1970):

$$F(x) = e^{-x} x^{\alpha} \left[1 + \sum_{j=1}^{\infty} x^j \; / \; G(\alpha+j+1) \right] \qquad x\epsilon(0,1) \text{ or } x < \alpha \qquad (6.22a)$$

$$F(x) = \frac{1 - [e^{-x} x^{\alpha} \; / \; G(\alpha)]}{[x + (1-\alpha)/(1 + 1/\{x + (2-\alpha)/[1 + 2/(x + \ldots)]\})]} \qquad \text{otherwise} \qquad (6.22b)$$

In each case, evaluation continues until the absolute difference in the approximations to F is less than a specified number (which is 1E-8 in the SUMO code). The value for $G(\alpha)$ is obtained from the FORTRAN algorithm of Macleod (1989) for $\ln[G(\alpha)]$. MacLeod's implementation uses algorithms by Cody and Hillstrom (1967) and Hart et al. (1968).

6.2.7.3 Inverse CDF Algorithm

Deviates from the gamma distribution are generated by obtaining a realization u from the uniform U(0,1) distribution and solving the equation

$F(x)-u = 0$ for x via a bisection search method. The precision of this method is determined by the number of iterations in the bisection search and the precision of the approximation F. The SUMO code iterates 22 times and thus obtains a level of precision of at least 1.0E-6.

Two steps are required when generating a random deviate x from the general gamma distribution. First, generate a value y from the distribution in Equation (6.21). Second, set $x = y/\beta$.

6.2.8 Algorithm for the Beta Distribution

6.2.8.1 Definition of the PDF

The beta random variable is described by the PDF

$$f(x) = x^{p-1}(1-x)^{q-1}/B(p,q) \qquad I(0<x<1) \tag{6.23}$$

or

$$f(y) = (b-a)^{-(p+q-1)}(y-a)^{p-1}(b-y)^{q-1}/B(p,q) \qquad I(a<y<b) \tag{6.24}$$

for $p,q > 0$, where $B(p,q) = G(p+q)/[G(p)G(q)]$, and G denotes the gamma function. The second expression for the PDF can be obtained from the first by the changing variable y to the quantity $(b-a)(x+a)$.

6.2.8.2 CDF Algorithm

A general analytic expression for F(x) does not exist; hence the SUMO code employs a recursion formula of Majumder and Bhattacharjee (1985, p.117). The recursion operates with two steps. First, one calculates

$$H(x) = \sum_{i=1}^{\min(k,s)} x^{p}(1-x)^{q-1}G(p+q+1) \;/\; [G(p+j)G(q-j)] \tag{6.25}$$

for $p \geq (p+q)x$ and $s = [q+(1-x)(p+q)] > 0$, and then calculates

$$F(x) = H(x)\,I(s>0) + \sum_{j=1}^{k} x^{p+s}(1-x)^{q-s}G(p+q+j) \;/\; [G(p+q+j)G(q-s)] \qquad (6.26)$$

The index k is the (final) iteration, such that the absolute value of an additional term is less than a specified level of precision (set to 1.0E-6 in the SUMO code). The square brackets in the expression for s denote the greatest integer portion of the argument, and min(a,b) selects the minimum of a and b.

6.2.8.3 Inverse CDF Algorithm

As with the inverse CDF for the gamma distribution, the SUMO code uses the bisection method to generate a beta deviate x by solving F(x)-u = 0 for x [u is a realization from the U(0,1) distribution] at precision level 1.0E-6. The value ln{G(•)} is obtained via the method described in subsection 6.2.7.2 for the gamma distribution. The logarithm values are added or subtracted, depending on whether the function G is in the numerator or denominator, and the result is exponentiated.

6.2.9 Algorithm for the Weibull Distribution

6.2.9.1 Definition of the PDF

The Weibull distribution has PDF

$$f(x) = a\,b\,x^{b-1}\,e^{-ax^{b}}\;\; I(0<x<\infty) \qquad (6.27)$$

for a,b > 0.

6.2.9.2 CDF Algorithm

The CDF for the Weibull distribution can be written as

$$F(x) = \begin{cases} 0 & \text{for } x \le 0 \\ 1 - e^{-ax^{b}} & \text{for } x > 0 \end{cases} \qquad (6.28)$$

6.2.9.3 Inverse CDF Algorithm

The deviates x from the Weibull distribution are generated using the equation

$$x = F^{-1}(u) = [-\ln(1-u)/a]^{1/b} \tag{6.29}$$

given a value u from the U(0,1) distribution.

6.2.10 Algorithm for the Cauchy Distribution

6.2.10.1 Definition of the PDF

The Cauchy distribution has PDF

$$f(x) = \left(\pi\beta\{1 + [(x-a)/\beta]^2\}\right)^{-1} \qquad I(-\infty<x<\infty) \tag{6.30}$$

for $-\infty < \alpha < \infty$ and $\beta > 0$.

6.2.10.2 CDF and Inverse CDF Algorithms

The CDF for the Cauchy distribution is

$$F(x) = \{\tan^{-1}[(x-\alpha)/\beta] + \pi/2\} / \pi \tag{6.31}$$

Deviates x from the Cauchy distribution are generated using the equation

$$x = F^{-1}(u) = \alpha + \beta\tan[\pi(u - 0.5)] \tag{6.32}$$

given a value u from the U(0,1) distribution.

6.2.11 Algorithm for the Logistic Distribution

6.2.11.1 Definition of the PDF

The logistic distribution has PDF

$$f(x) = x\, e^{-(x-\alpha)/\beta} \Big/ \left[\beta\left\{1 + e^{-(x-\alpha)/\beta}\right\}^2\right] \qquad I(-\infty<x<\infty) \tag{6.33}$$

for $-\infty < \alpha < \infty$ and $\beta > 0$.

6.2.11.2 CDF Algorithm

The algorithm for the CDF for the logistic distribution is

$$F(x) = \left[1 + e^{-(x-\alpha)/\beta}\right]^{-1} \tag{6.34}$$

6.2.11.3 Inverse CDF Algorithm

Deviates x from the logistic distribution are generated using the equation

$$x = F^{-1}(u) = \alpha - \beta \ln[(1-u)/u] \tag{6.35}$$

given a value u from the U(0,1) distribution.

6.2.12 User-Specified Distribution

In addition to selecting from the foregoing families of distributions, the user may implement any other distribution by supplying a table of data pairs corresponding to [x,F(x)]. Thus, the user can provide the SUMO code with discrete evaluations of the CDF. The SUMO code linearly interpolates between these points to solve for F^{-1} when generating a deviate or determining truncation limits in the domain of the uniform U(0,1) distribution.

7.0 REFERENCES

Abriola, L. M. 1984. Multiphase Migration of Organic Compounds in a Porous Medium, A Mathematical Model. Springer-Verlag, New York.

Adams, A. G. 1969. "Areas under the Normal Curve." Algorithm 39, Computer Journal 12:197-198.

Altenhofen, M. K., and P. W. Eslinger. 1990. "Evaluation of Near-Field Thermal Environmental Conditions for a Spent Fuel Repository in Tuff." In The 1st International Topical Meeting on High-Level Radioactive Waste Management Conference, pp. 402-409. American Nuclear Society, La Grange Park, Illinois.

Altenhofen, M. K. 1981. Waste Package Heat-Transfer Analysis: Model Development and Temperature Estimates for Waste Packages in a Repository Located in Basalt. RHO-BWI-ST-18, Rockwell Hanford Operations, Richland, Washington.

Amter, S., E. Behl, and B. Ross. 1988. Carbon-14 Travel Time at Yucca Mountain. Disposal Safety Incorporated, Washington, D.C.

Anspaugh, L. R., J. H. Shinn, P. L. Phelps, and N. C. Kennedy. 1975. "Resuspension and Redistribution of Plutonium in Soils." Health Physics 29:571-582.

Averjanov, S. F. 1950. "About Permeability of Subsurface Soils in Case of Incomplete Saturation." Eng. Collect. 7.

Baes, C. F., and R. D. Sharp. 1981. Predicting Radionuclide Leaching from Root Zone Soil from Assessment Applications. CONF-810606-44, Oak Ridge National Laboratory, Oak Ridge, Tennessee.

Bain, G. A., W. A. McInteer, and T. P. Papazoglou. 1985. "Release and Migration of Fission Products in High Burnup Fuel." In Proceedings of the ANS Topical Meeting on Light Water Reactor Fuel Performance, pp. 4-1 to 4-18. American Nuclear Society, La Grange Park, Illinois.

Barner, J. O. 1984. LWR Spent Fuel Approved Testing Materials for Radionuclide Release Studies. PNL-4686, Pacific Northwest Laboratory, Richland, Washington.

Bateman, H. 1910. "Solution of a System of Differential Equations Occurring in the Theory of Radioactive Transformations." In Proceedings of the Cambridge Philosophical Society 15:423-427.

Bear, J. 1972. Dynamics of Fluids in Porous Media. American Elsevier Publishing Co., New York.

Beasley, J. D., and S. G. Springer. 1985. "The Percentage Points of the Normal Distribution." Algorithm AS 111 in Applied Statistics Algorithms, eds. P. Griffiths and I. D. Hill. Ellis Horwood Limited, Chichester, United Kingdom.

Bhattacharjee, G. P. 1970. "The Incomplete Gamma Integral." Algorithm AS 32, Applied Statistics 19:285-287.

Bonano, E. J., S. C. Hora, R. L. Keeney, and D. von Winterfeldt. 1990. Elicitation and Use of Expert Judgement in Performance Assessment for High-Level Radioactive Waste Repositories. NUREG/CR-5411, U.S. Nuclear Regulatory Commission, Washington, D.C.

Bratley, P., B. L. Fox, and L. E. Schrage. 1983. A Guide to Simulation. Springer-Verlag, New York.

Brooks, R. H., and A. T. Corey. 1966. "Properties of Porous Media Affecting Fluid Flow." Journal of the Irrigation and Drainage Division 92(IR2):61-88.

Brutsaert, W. 1967. "Some Methods of Calculating Unsaturated Permeability." Transactions of American Society of Agricultural Engineers 10:400-404.

Burdine, N. T. 1953. "Relative Permeability Calculations from Pore-Size Distribution Data." Petroleum Transactions, AIME 198:71-77.

Chambré, P. L., C. H. Kang, W. W.-L. Lee, and T. H. Pigford. 1988. "The Role of Chemical Reaction in Waste-Form Performance." In Scientific Basis for Nuclear Waste Management IX, Materials Research Society Symposium Proceedings, Vol. 112, eds. M. J. Apted and R. E. Westerman, pp. 285-291. Materials Research Society, Pittsburgh.

Chambré, P. L., T. H. Pigford, W. W.-L. Lee, J. Ahn, S. Kajiwara, C. L. Kim, H. Kimura, J. Lung, W. J. Williams, and S. J. Zavoshy. 1985. Mass Transfer and Transport in a Geologic Environment. LBL-19430, Lawrence Berkeley Laboratory, Berkeley, California.

Cheng, P. 1978. Heat Transfer in Geothermal Systems, Advances in Heat Transfer, Vol. 14, pp. 1-105. Academic Press, New York.

Childs, E. C., and N. Collis-George. 1950. "The Permeability of Porous Materials." In Proceedings of Royal Society, Series A, 201:392-405.

Cody, W. J., and K. E. Hillstrom. 1967. "Chebyshev Approximations for the Natural Logarithm of Gamma Function." Math. Comput. 21:198-203.

Droppo, J. G., Jr., D. L. Strenge, J. W. Buck, B. L. Hoopes, R. D. Brockhaus, M. B. Walter, and G. Whelan. 1989. Multimedia Environmental Pollutant Assessment System (MEPAS) Application Guide: Volume 1 - User's Guide. PNL-7216 Vol. 1, Pacific Northwest Laboratory, Richland, Washington.

Edwards, A. L. 1969. TRUMP: A Computer Program for Transient and Steady-State Temperature Distributions in Multidimensional Systems. UCRL-14754, Rev. II, National Technical Information, Service Springfield, Virginia.

Engel, D. W., A. M. Liebetrau, G. C. Nakamura, B. M. Thronton, and M. J. Apted. 1989. The AREST Code: User's Guide for the Analytical Repository Source-Term Model. PNL-6645, Pacific Northwest Laboratory, Richland, Washington.

Ferguson, T. S. 1967. Mathematical Statistics: A Decision Theoretic Approach. Academic Press, New York.

Fishman, G. S., and L. R. Moore. 1986. "An Exhaustive Analysis of Multiplicative Congruential Random Number Generators with Modulus 2^{31}-1." SIAM Journal of Scientific and Statistical Computing 7(1):24-44.

Ford, F. P. 1982. Mechanisms of Environmental Cracking in Systems Peculiar to the Power Generation Industry. EPRI NP-2589, Electric Power Research Institute, Palo Alto, California.

Freeze, R. A., and J. A. Cherry. 1979. Groundwater. Prentice-Hall, Engelwood Cliffs, New Jersey.

Garisto, F., and N. Garisto. 1985. "A UO_2 Solubility Function for the Assessment of Used Nuclear Fuel Disposal." Nuclear Science and Engineering 90:103-110.

Goltz, M. N., and P. Roberts. 1988. "Simulations of Physical Nonequilibrium Solute Transport Models: Application to a Large-Scale Experiment." Journal of Contaminant Hydrology 3:37-63.

Gosman, A., W. Pun, A. K. Runchal, D. B. Spalding, and M. Wolfshtein. 1969. Heat and Mass Transfer in Recirculating Flows. Academic Press, London.

Gray, W. J., and G. L. McVay. 1984. "Comparison of Spent Fuel and UO^2 Release in Salt Brines." In Proceedings of the 3rd Spent Fuel Workshop, ed. L. Werme. SKBF/KBS-83-76, Stockholm.

Hart, J. F., E. W. Cheney, C. L. Lawson, H. J. Machly, C. K. Mesztenyi, J. R. Rice, J. R. Thacher, M. C. Pike, and C. Witzgall. 1968. Computer Approximations. John Wiley and Sons, New York.

Hassanizadeh, S. M. 1986a. "Derivation of Basic Equations of Mass Transport in Porous Media, Part 1. Macroscopic Balance Laws." Advances in Water Resources 9:196-206.

Hassanizadeh, S. M. 1986b. "Derivation of Basic Equations of Mass Transport in Porous Media, Part 2. Generalized Darcy's and Fick's Law." Advances in Water Resources 9:207-222.

Hill, I. D. 1985. "The Normal Integral." Algorithm AS 66 in Applied Statistics Algorithms, eds. P. Griffiths and I. D. Hill. Ellis Horwood Limited, Chichester, United Kingdom.

Hayakorn, P. S., and G. F. Pinder. 1983. Computational Methods in Subsurface Flow. Academic Press, New York.

ICRP. 1979a. "ICRP Publication 30, Part 1, Limits for Intakes of Radionuclides by Workers." Annals of the ICRP, Vol. 2, No. 3-4. International Commission on Radiological Protection, Pergamon Press, New York.

ICRP. 1979b. "ICRP Publication 30, Supplement to Part 1, Limits for Intakes of Radionuclides by Workers." Annals of the ICRP, Vol. 3, No. 1-4. International Commission on Radiological Protection, Pergamon Press, New York.

ICRP. 1979c. Radionuclide Release into the Environment: Assessment of Doses to Man. ICRP Publication 29, International Commission on Radiological Protection, Pergamon Press, New York.

ICRP. 1980. "ICRP Publication 30, Part 2, Limits for Intakes of Radionuclides by Workers." Annals of the ICRP, Vol. 4, No. 3-4. International Commission on Radiological Protection, Pergamon Press, New York.

ICRP. 1981a. "ICRP Publication 30, Supplement to Part 2, Limits for Intakes of Radionuclides by Workers." Annals of the ICRP, Vol. 5, No. 1-6. International Commission on Radiological Protection, Pergamon Press, New York.

ICRP. 1981b. "ICRP Publication 30, Part 3 Including Addendum to Parts 1 and 2, Limits for Intakes of Radionuclides by Workers." Annals of the ICRP, Vol. 6, No. 2-3. International Commission on Radiological Protection, Pergamon Press, New York.

ICRP. 1982a. "ICRP Publication 30, Supplement A to Part 3, Limits for Intakes of Radionuclides by Workers." Annals of the ICRP, Vol. 7, No. 1-3. International Commission on Radiological Protection, Pergamon Press, New York.

ICRP. 1982b. "ICRP Publication 30, Supplement B to Part 3 Including Addendum to Supplements to Parts 1 and 2, Limits for Intakes of Radionuclides by Workers." Annals of the ICRP, Vol. 8, No. 1-3. International Commission on Radiological Protection, Pergamon Press, New York.

Johnson, L., N. Garisto, and S. Stroes-Gascoyne. 1985. "Used-Fuel Dissolution Studies in Canada." In Waste Management '85 Proceedings of the 1985 Symposium on Waste Management, ed. R. G. Post, pp. 479-482. University of Arizona, Tucson, Arizona.

Kang, C.-H. 1990. Mass Transfer and Transport Through Backfill in a Geologic Nuclear Waste Repository. Ph.D. Dissertation, University of California, Berkeley, California.

Katayama, Y. B., D. J. Bradley, and C. O. Harvey. 1980. Status Report on the LWR Spent Fuel IAEA Leach Tests. PNL-3173, Pacific Northwest Laboratory, Richland, Washington.

Kennedy, W. J., Jr., and J. E. Gentle. 1980. Statistical Computing. Marcel Dekker, New York.

Kim, C., P. L. Chambré, and T. H. Pigford. 1986. Mass-Transfer-Limited Release of a Soluble Waste Species. LBL-20899, Lawrence Berkeley Laboratory, Berkeley, California.

Kocher, D. C. 1981. Dose-Rate Conversion Factors for External Exposure to Photons and Electrons. NUREG/CR-1918, U.S. Nuclear Regulatory Commission, Washington, D.C.

Liebetrau, A. M., M. J. Apted, D. W. Engel, M. K. Altenhofen, D. M. Strachan, C. R. Reid, C. F. Windisch, R. L. Erikson, and K. I. Johnson. 1987. The Analytical Repository Source-Term (AREST) Model: Description and Documentation. PNL-6346, Pacific Northwest Laboratory, Richland, Washington.

Macleod, A. J. 1989. "A Robust and Reliable Algorithm for the Logarithm of the Gamma Function." Algorithm AS 245, Applied Statistics 38(2):397-423.

Majumder, K. L., and G. P. Bhattacharjee. 1985. "The Incomplete Beta Integral." Algorithm AS 63 in Applied Statistics Algorithms, eds. P. Griffiths and I. D. Hills. Ellis Horwood Limited, Chichester, United Kingdom.

Marsh, G. P. 1983. "Carbon Steel Canister for the Containment of Nuclear Wastes." Transactions of the American Nuclear Society 45:292 (Abstract).

Mood, A. M., F. A. Graybill, and D. C. Boes. 1974. Introduction to the Theory of Statistics, 3rd ed. McGraw-Hill, New York.

Mualem, Y. 1976. "A New Model for Predicting the Hydraulic Conductivity of Unsaturated Porous Media." Water Resources Research 12(3):513-522.

Napier, B. A., R. A. Peloquin, D. L. Strenge, and J. V. Ramsdell, Jr. 1988. GENII - The Hanford Environmental Radiation Dosimetry Software System. PNL-6584, Pacific Northwest Laboratory, Richland, Washington.

Narasimhan, T. N., and P. A. Witherspoon. 1976. "An Integrated Finite Difference Method for Analyzing Fluid Flow in Porous Media." Water Resources Research 12(1):57-64.

Newman, J. F. 1981. "The Stress Corrosion of Steel in Sodium Hydroxide Solution: A Film Rupture Model." Corrosion Science 21(7):487-503.

Nuclear Waste Policy Act (NWPA) of 1982. 42 USC 10101 et seq.

Ouderkirk, S. J. 1988. WASTES II: Waste System Transportation and Economic Simulation - Release 24. User's Guide. PNL-5714 Rev. 1, Pacific Northwest Laboratory, Richland, Washington.

Patankar, S. V. 1980. Numerical Heat Transfer and Fluid Flow. McGraw-Hill, New York.

Pigford, T. H., and P. L. Chambré. 1986. "Reliable Predictions of Waste Performance in a Geologic Repository." In High-Level Waste Disposal, ed. H. C. Burkholder, pp. 163-186. Battelle Press, Columbus, Ohio.

Posey, F. A., and A. A. Palko. 1979. "Corrosivity of Carbon Steel in Concentrated Chloride Solution." Corrosion 35(1):38-43.

Postlethwaite, J., and M. Onofrei. 1979. "Hydrogen Evolution and Anodic Disintegration During Electrochemical Pitting of Zirconium in Alkaline-Chloride Solutions." Corrosion 35(4):185-189.

Reimus, P. W., A. M. Liebetrau, M. J. Apted, and D. W. Engel. 1988. "Performance Assessment for Spent Fuel Waste Packages in Hydrologically Unsaturated Geologic Media," Presented at SPECTRUM '88, International Topical Meeting on Nuclear and Hazardous Waste Management, Pasco, Washington. PNL-SA-15624, Pacific Northwest Laboratory, Richland, Washington.

Runchal, A. K. 1969. Transfer Processes in Steady Two-Dimensional Separated Flows. Ph.D. Dissertation, London University, London.

Runchal, A. K. 1972. "Convergence and Accuracy of Three Finite Difference Schemes for a Two-Dimensional Conduction and Convection Problem." International Journal of Numverical Methods in Engineering 4:541-550.

Runchal, A. K., and B. Sagar. 1989. PORFLO-3: A Mathematical Model for Fluid Flow, Heat, and Mass Transport in Variably Saturated Geologic Media - Theory and Numerical Methods, Version 1.0. WHC-EP-0042, Westinghouse Hanford Company, Richland, Washington.

Sastre, C., C. Pescatore, and T. Sullivan. 1986. Waste Package Reliability. BNW-NUREG-51953, Brookhaven National Laboratory, Upton, New York.

Scheidegger, A. E. 1961. "General Theory of Dispersion in Porous Media." Journal of Geophysical Research 66:3273-3278.

Singleton, R. C. 1969. "An Efficient Algorithm for Sorting with Minimal Storage." Algorithm 347, Communications of the Association for Computing Machinery 12(3):185-187.

Spalding, D. B. 1972. "A Novel Finite-Difference Formulation for Differential Expressions Involving Both First and Second Derivatives." International Journal for Numerical Methods in Engineering 4:551-559.

Sudicky, E. A., and E. O. Frind. 1982. "Contaminant Transport in Fractured Porous Media: Analytic Solutions for a System of Parallel Fractures." Water Resources Research 18(6):808-820.

Stahl, D., and N. E. Miller, compilers. 1985. Long-Term Performance of Materials Used for High-Level Waste Packaging, Volume 4. NUREG/CR-3900, Vol. 4, U.S. Nuclear Regulatory Commission, Washington, D.C.

Stegun, I. A., and R. Zucker. 1970. "Automatic Computing Methods for Special Functions." Journal of Research of the National Bureau of Standards-B. Mathematics Sciences 74B(3):211-224.

Strait, P. T. 1989. A First Course in Probability and Statistics with Applications, 2nd ed. Harcourt Brace Jovanovich, New York.

Swanson Analysis Systems, Inc. 1986. ANSYS--Engineering Analysis System, Revision 4.2. Swanson Analysis Systems, Houston, Pennsylvania.

Trent, D. S., L. L. Eyler, and M. J. Budden. 1983. A Three-Dimensional Time-Dependent Computer Program for Hydrothermal Analysis, Volume 1: Numerical Methods and Input Instructions. PNL-4348, Vol. 1, Rev. 1, Pacific Northwest Laboratory, Richland, Washington.

van Genuchten, R. 1978. Calculating the Unsaturated Hydraulic Conductivity with a New Closed-Form Analytical Model. Report 78-WR-08, Water Resources Program, Department of Civil Engineering, Princeton University, Princeton, New Jersey.

Van Konynenburg, R., C. Smith, H. Culham, and C. Otto, Jr. 1985. "Behavior of Carbon-14 in Waste Packages for Spent Fuel in a Repository in Tuff." In Scientific Basis for Nuclear Waste Management VIII, eds. C. Jantzen, J. Stone, and R. Ewing, pp. 405-412. Elsevier, Amsterdam.

Vetter, K., and H. Strehblow. 1974. "Pitting Corrosion in an Early Stage and its Theoretical Implications." Localized Corrosion 3:240-251.

Werme, L., and R. S. Forsyth. 1985. "Spent Fuel as a Wasteform--The Swedish Program for Studies and Evaluation of Spent Fuel for Direct Disposal." In Waste Management 85: Proceedings of the 1985 Symposium on Waste Management, ed. R. G. Post, pp. 483-488. University of Arizona, Tucson, Arizona.

Westerman, R. E., J. H. Haberman, S. G. Pitman, B. A. Pulsipher, and L. A. Sigalla. 1986. Annual Report--FY 1984. Corrosion and Environment--Mechanical Characterization of Iron-Base Nuclear Waste Package Structural Barrier Materials. PNL-5426, Pacific Northwest Laboratory, Richland, Washington.

Wilson, C. N. 1985. Results from NNWSI Series 1 Spent Fuel Leach Tests. HEDL-TME 84-30, Westinghouse Hanford Company, Richland, Washington.

Wilson, C. N. 1986. Results from NNWSI Series 2 Spent Fuel Dissolution Tests, Cycles 1 and 2. HEDL-TME 85-22, Westinghouse Hanford Company, Richland, Washington.

Wilson, C. N., and V. Oversby. 1985. "Radionuclide Release from PWR Fuels in a Reference Tuff Repository Groundwater." In Waste Management 85: Proceedings of the 1985 Symposium on Waste Management, ed. R. G. Post, p. 497. University of Arizona, Tucson, Arizona.

Zavoshy, S. J., P. L. Chambré, and T. H. Pigford. 1985. "Mass Transfer in a Geologic Environment." In Scientific Basis for Nuclear Waste Management VIII, eds. C. Jantzen, J. Stone, and R. Ewing, pp. 311-322. Elsevier, Amsterdam.

10 CFR 60. 1991. U.S. Nuclear Regulatory Commission, "Disposal of High-Level Radioactive Waste in Geologic Repositories." U.S. Code of Federal Regulations.

40 CFR 191. 1991. U.S. Environmental Protection Agency, "Environmental Radiation Protection Standards for Management and Disposal of Spent Nuclear Fuel, High-Level and Transuranic Radioactive Wastes: Final Rules." U.S. Code of Federal Regulations.

DISTRIBUTION

No. of Copies

OFFSITE

12 DOE Office of Scientific and Technical Information

2 Agency for Nuclear Projects
State of Nevada
C. H. Johnson
R. R. Loux
Evergreen Center, Suite 252
1802 N. Carson St.
Carson City, NV 89710

D. A. Beck
Water Resources Division
U.S. Geological Survey
6770 S. Paradise Road
Las Vegas, NV 89119

C. G. Bell, Jr.
Civil and Mechanical Engineering
University of Nevada
4505 S. Maryland Parkway
Las Vegas, NV 89154

E. P. Binnall
Lawrence Berkeley Laboratory
Building 50B/4235
Berkeley, CA 94720

J. A. Blink
Lawrence Livermore National Laboratory
101 Convention Center Drive
Suite 280, M.S. 527
Las Vegas, NV 89109

S. Bradhurst
P.O. Box 1510
Reno, NV 89505

L. Bradshaw
P.O. Box 593
Tonopah, NV 89049

No. of Copies

R. L. Bullock
Raytheon Services Nevada
P.O. Box 95487, M.S. 403
Las Vegas, NV 89193-5487

4 J. A. Canepa
Los Alamos National Laboratory
P.O. Box 1663
Los Alamos, NM 87545

City of Las Vegas
Economic Development Department
400 E. Stewart Ave.
Las Vegas, NV 89101

City of North Las Vegas
Community Development and Planning
P.O. Box 4086
North Las Vegas, NV 89030

Clark County
Comprehensive Planning Dept.
225 Bridger Ave., 7th Floor
Las Vegas, NV 89155

Commission of the European Communities
200 Rue de la Loi
B-1049 Brussells
BELGIUM

2 Desert Research Institute
John Fordham
David Rhode
P.O. Box 60220
Reno, NV 89506

P. A. Domenico
Geology Department
Texas A & M University
College Station, TX 77843

No. of
Copies

D. R. Elle
Environmental Protection
Division
U.S. Department of Energy
Nevada Field Office
P.O. Box 98518
Las Vegas, NV 89193-8518

P. K. Fitzsimmons
U.S. Department of Energy
Nevada Field Office
P.O. Box 98518
Las Vegas, NV 89193-8518

A. L. Flint
U.S. Geological Survey
P.O. Box 327, M.S. 721
Mercury, NV 89023

L. D. Foust
TRW Environmental Safety
Systems
101 Convention Center Drive
Suite 540, M.S. 423
Las Vegas, NV 89109

B. Hastings
TRW Environmental Safety
Systems
2650 Park Tower Drive
Suite 800
Vienna, VA 22180

T. Hay
Office of the Governor
State of Nevada
Capitol Complex
Carson City, NV 89710

D. Hedges
Roy F. Weston, Inc.
4425 Spring Mountain Road
Suite 300
Las Vegas, Nevada 89102

No. of
Copies

D. Hoxie
U.S. Geological Survey
Denver Federal Center
P.O. Box 25046
Denver, CO 80225

2 INTERA, Inc.
R. W. Nelson
A. E. Van Luik
101 Convention Center Drive
Phase II, Suite 540
Las Vegas, NV 89193

3 Lawrence Livermore National
Laboratory
W. L. Clarke
W. J. O'Connell
W. Halsey
University of California
P.O. Box 808
Livermore, CA 94550

Los Alamos National Laboratory
Exploratory Shaft Test Manager
101 Convention Center Drive,
Suite 820, M.S. 527
Las Vegas, NV 89101

J. J. McKetta, Jr.
Department of Chemical
Engineering
CPE Building 1.450
Austin, TX 78712

I. Miller
Golder Associates
4104 184th Avenue N.E.
Redmond, WA 98052

D. Warner North
Decision Focus, Inc.
4984 El Camino Real
Los Altos, CA 94062

Nuclear Waste Technical Review
Board
1011 Evergreen Way
Blacksburg, VA 24060

No. of Copies

NRC Document Control Desk
Division of Waste Management
Nuclear Regulatory Commission
Washington, DC 20555

ONWI Library
Battelle Columbus Laboratory
Office of Nuclear Waste Isolation
505 King Avenue
Columbus, OH 43201

T. H. Pigford
Department of Nuclear Engineering
University of California
Berkeley, CA 94720

Nye County
Planning Department
P.O. Box 153
Tonopah, NV 89049

V. Poe
P.O. Box 1026
Hawthorne, NV 89415

P. T. Prestholt
301 E. Stewart Ave.
Room 203
Las Vegas, NV 89101

M. Reeves
INTERA, Inc.
6850 Austin Center Blvd.
Suite 300
Austin, TX 78731

Repository Licensing & Quality Assurance-Project Directorate
Division of Waste Management
Nuclear Regulatory Commission
Washington, DC 20555

No. of Copies

Senior Project Manager
Repository Project Branch
Nuclear Regulatory Commission
Washington, DC 20555

G. Van Roekel
City of Caliente
P.O. Box 158
Caliente, NV 89008

2 Roy F. Weston, Inc.
E. L. Snow
Technical Info. Center
955 L'Enfant Plaza, S.W.
Washington, D.C. 20024

2 Sandia National Laboratory
H. A. Dockery
M. A. Wilson
Division 6312
Albuquerque, NM 87185

4 Sandia National Laboratory
R. W. Barnard
T. E. Blejwas (2)
T. O. Hunter
Division 6313
Albuquerque, NM 87185

3 Science Applications International Corporation
A. Brandstetter
P. L. Cloke
M. D. Voegele
101 Convention Center Drive
Suite 450
Las Vegas, NV 89109

B. Selinder
190 W. First St.
Fallon, NV 89406

2 S.W. Research Institute
B. Sagar
J. Walton
622 Culebra Road
San Antonio, TX 78228

No. of Copies

A. T. Tamura
Office of Scientific and Technical Information
U.S. Department of Energy
P.O. Box 62
Oak Ridge, TN 37831

12 Technical Information Officer
U.S. Department of Energy
Nevada Field Office
P.O. Box 98518
Las Vegas, NV 89193-8518

5 U.S. Department of Energy
Yucca Mountain Site Characterization Project Office
J. M. Boak
J. R. Dyer
C. P. Gertz (2)
J. J. Lorenz
P.O. Box 98608
Las Vegas, NV 89193-8608

7 U.S. Department of Energy
S. J. Brocoum, RW-22
R. A. Milner, RW-332
G. J. Parker, RW-322
J. Roberts, RW-30
J. Roberts, RW-33
S. Rousso, RW-50
T. Wood, RW-52
1000 Independence Avenue, S.W.
Washington, DC 20585

2 U.S. Geological Survey
J. H. Sass
S. C. Wu
2255 N. Gemini Drive
Flagstaff, AZ 86001

No. of Copies

6 U.S. Geological Survey
D. H. Appel
G. L. Ducret
L. R. Hayes
W. R. Keefer
J. M. LaMonaca
J. S. Stuckless
P.O. Box 25046
Denver, CO 80225

2 U.S. Geological Survey
R. W. Craig
D. Zesiger
101 Convention Center Drive
Suite 860, M.S. 509
Las Vegas, NV 89109

2 U.S. Nuclear Regulatory Commission
Division of Engineering Safety
R. Codell
S. Coplan, NLS-260
Washington, DC 20555

P. J. Weeden
Environmental Monitoring Systems Laboratory
P.O. Box 93478
Las Vegas, NV 89193-3478

C. L. West
Office of External Affairs
U.S. Department of Energy
Nevada Field Office
P.O. Box 98518
Las Vegas, NV 89193-8518

ONSITE

DOE Richland Field Office

D. C. Langstaff

No. of Copies

2 Westinghouse Hanford Company

D. W. Langford
S. J. Ouderkirk

22 Pacific Northwest Laboratory

P. J. Chamberlain
P. G. Doctor
L. A. Doremus
D. M. Elwood
D. W. Engel
P. W. Eslinger (5)
L. K. Grove

No. of Copies

C. K. Hastings
M. R. Kreiter
T. B. Miley
W. E. Nichols
Publishing Coordination
Technical Report Files (5)

Routing

R. M. Ecker
J. W. Falco
P. M. Irving
R. L. Skaggs
C. S. Sloane
P. C. Hays (last)

END

DATE FILMED

11/13/92